Universidade do Minho
Escola de Medicina

Isabella França Santos de Oliveira

Interneuron characterization in Rett Syndrome: insights from mice prefrontal cortex

outubro de 2023

Interneuron characterization in Rett Syndrome: insights from mice prefrontal cortex

Isabella França Santos de Oliveira

UMinho | 2023

Universidade do Minho
Escola de Medicina

Isabella França Santos de Oliveira

Interneuron characterization in Rett Syndrome: insights from mice prefrontal cortex

Dissertação de Mestrado
Mestrado em Ciências da Saúde

Trabalho efetuado sob a orientação da
Doutora Patrícia Espinheira Sá Maciel
e da
Doutora Sara Carina Duarte da Silva

outubro de 2023

DIREITOS DE AUTOR E CONDIÇÕES DE UTILIZAÇÃO DO TRABALHO POR TERCEIROS

Este é um trabalho académico que pode ser utilizado por terceiros desde que respeitadas as regras e boas práticas internacionalmente aceites, no que concerne aos direitos de autor e direitos conexos.

Assim, o presente trabalho pode ser utilizado nos termos previstos na licença abaixo indicada.

Caso o utilizador necessite de permissão para poder fazer um uso do trabalho em condições não previstas no licenciamento indicado, deverá contactar o autor, através do RepositóriUM da Universidade do Minho.

Licença concedida aos utilizadores deste trabalho



Atribuição CC BY

https://creativecommons.org/licenses/by/4.0

ACKNOWLEDGEMENTS

Ao Doutor Jorge Correia Pinto, Presidente da Escola de Medicina da Universidade do Minho, à Doutora Patrícia Maciel, Presidente do Instituto de Investigação em Ciências da Vida e Saúde (ICVS) e Diretora do Mestrado em Ciências da Saúde.

À professora Doutora Patrícia Maciel, Diretora do Mestrado em Ciências da Saúde, expresso a minha gratidão pelo voto de confiança para fazer parte da sua equipa. Agradeço à Doutora Sara Silva, pela orientação, compreensão demonstrada em tempos desafiadores. Expresso um agradecimento especial a Daniela M. por sua orientação, colaboração neste trabalho e por sua paciência, juntamente com a Sara G., durante as buscas por anticorpos que, por vezes, pareciam desaparecidos. Sou grata pela oportunidade de fazer parte da equipe do TransNeuro e compartilhar o laboratório com cientistas incrivelmente apaixonados por ciência: Daniela G., Daniela C., Cármen, Rita, Joana, Jorge F., Stephanie, Marta e Bruna.

Um agradecimento a todas as pessoas que tiveram nesses dois últimos anos a compartilhar os sucessos e desafios, consequentemente contribuíram para o meu crescimento. À Jonas, pela significativa contribuição para o meu desenvolvimento como pesquisadora. Agradeço a disponibilidade em auxiliar-me a aprimorar a minha pesquisa e pela colaboração valiosa na realização deste projeto. À Leandro, agradeço o incentivo e apoio na conclusão desse projeto. Sua companhia na realização das minhas imunos tornaram essa jornada mais memorável. Um agradecimento aos colegas de licenciatura (Natan, Marta e Mayara) que mesmo longe estiveram a torcer por mim. Aos meus colegas de curso (Joana, Rúben, Maria, Mariaguilia, Anabela, Rui, Thiago e Bruno) a quais pude compartilhar imensas discussões científicas intermináveis. À Silva, agradeço as palavras de sabedoria e apoio fundamental para minha determinação e o sucesso empreendido. À Yara agradeço as nossas pausas de estudo e pelas conversas entre períodos de incubação. A Claudia, le agradezco la amistad que hemos construido durante estos años¡ ¡Gracias por el cariño, hermana!

Aos meus pais e meu irmão, agradeço com especial carinho todo suporte e paciência para comigo nesse empreendimento. Por cuidarem de mim, pelo afeto diário e pela curiosidade em compreender o meu trabalho. ‘Por vocês eu dançaria tango no teto/ Eu iria a pé do Rio a Salvador.’

The work presented in this thesis was performed in the Life and Health Sciences Research Institute (ICVS), University of Minho. Financial support was provided by National funds, through the Foundation for Science and Technology (FCT) - project UIDB/50026/2020 and UIDP/50026/2020

STATEMENT OF INTEGRITY

I hereby affirm that I have conducted this academic work with integrity. I certify that I have refrained from any form of plagiarism, unethical use of information, or manipulation of results throughout the entire process of its development.

Furthermore, I explicitly acknowledge my adherence to the University of Minho's Code of Ethical Conduct, following it guidelines in every aspect of this work.

RESUMO (Caracterização de interneurônios na Síndrome de Rett: insights do córtex pré-frontal de ratinhos)

O córtex pré-frontal (CPF) é a região do cérebro responsável por funções cognitivas e executivas especializadas. Por sua vez, o CPF medial é a sub-região que desempenha um papel crucial na realização de tarefas essenciais necessárias para o pensamento humano, sendo composta por áreas com uma citoarquitetura e funções distintas. Cada unidade funcional e por sua vez a rede cortical de neurónios são controlados por um equilíbrio entre estímulos excitatórios e inibitórios (E/I), que estabelecem uma relação dinâmica fundamental para manter a atividade neuronal adequada. O desequilíbrio da rede E/I tem sido associada a síndromes neurocomportamentais e doenças com características semelhantes ao autismo. A Síndrome de Rett (RTT) é uma síndrome do neurodesenvolvimento que afeta principalmente meninas, dado a sua transmissão ligada ao cromossoma X e é causada pela perda da função da proteína de ligação metil-CpG 2 (MeCP2), codificada pelo gene *MECP2*. Estudos anteriores demonstraram que a proteína MeCP2 desempenha papéis diversos em diferentes regiões do cérebro e contribui para funções cognitivas e sociais. Além disso, o mosaicismo somático associado à expressão da MeCP2, poderá estar na base das alterações observadas dentro dos interneurónios (IN), sendo uns mais afetados do que outros pela ausência do gene. Apesar de ser um distúrbio com graves deficiências cognitivas e uma distribuição sexual bem definida, a maioria dos estudos sobre a RTT ignora a caracterização fenotípica em modelos fêmea, bem como as alterações na rede cortical no CPF, que, como mencionado, é uma região com um papel central na cognição. Assim, o principal objetivo deste estudo foi avaliar as alterações dos vários tipos de IN corticais que expressam parvalbumina (PV+) e péptido intestinal vasoativo (VIP+) dentro das várias subregiões do CPF, utilizando para isso um modelo de ratinho (fêmeas heterozigóticas) bem caracterizado e amplamente utilizado, o *Mecp2*$^{tm1.1Bird}$. Os nossos resultados demonstram uma tendência para a redução da imunorreatividade de IN PV+ em ratinhos fêmea Mecp2$^{+/-}$ (em estadio adulto), sendo que estas alterações foram encontradas maioritariamente na região dorsomedial de infralímbica do CPF. Considerando o mosaicismo somático observado para MeCP2, avaliamos a expressão de VIP em células que expressam/não expressam MeCP2 nas fêmeas *Mecp2*$^{+/-}$, tendo observado uma redução de células VIP+ em IN que não expressam MeCP2. Este resultado poderá estar associado a fenótipos comumentemente observado em ratinhos *Mecp2*$^{+/-}$, nomeadamente defeitos na locomoção e perturbações na respiração, e também suportam o efeito específico em diferentes classes de INs corticais. Em suma, os IN corticais podem desempenhar um papel importante na patogénese da Síndrome de Rett, levando a uma possível sobreinibição de redes corticais específicas em regiões cruciais envolvidas nos processos motores e cognitivos. Os resultados obtidos neste estudo apontam para novas pistas para compreender os componentes celulares da deficiência de MeCP2 e, consequentemente, identificar novos alvos farmacológicos.

PALAVRAS-CHAVE: córtex pré-frontal, E/I balanço, interneurônios corticais, MeCP2 e Síndrome de Rett.

ABSTRACT
(Interneuron characterization in Rett Syndrome: insights from mice prefrontal cortex)

The Prefrontal cortex (PFC) is the brain region responsible for higher-order cognitive and executive functions. The medial PFC is the subregion that plays a crucial role in enabling essential tasks necessary for human thinking. The region is composed of cytoarchitecture and functionally distinct areas, in which at the single neuron level and each cortical network are controlled by excitatory and inhibitory (E/I) inputs that establish a dynamic ratio fundamental to maintain proper brain activity. Disbalance in E/I network has been associated with neurobehavioral syndromes and autistic-like features. Rett Syndrome (RTT) is a neurodevelopment disorder affecting mostly females. It is inherited in an X-linked manner and caused by the loss of function of methyl-Cp G binding protein 2 (MeCP2), encoded by the *MECP2* gene. Previous research has shown that MeCP2 plays diverse roles in different brain regions and contributes to cognitive and social functions. Moreover, MeCP2 expression seems to have a class-specific effect upon which some types of interneurons (IN) are more affected than others by the absence of the gene. Despite being a disorder with severe cognitive impairments and well-defined sex distribution, most RTT studies disregard phenotypic characterization in female mice as well as the alterations of the cortical network in the PFC, which, as stated, is a region with a central role in cognition. Our primary aim was to assess alterations of distinct cortical IN expressing parvalbumin (PV+) and vasoactive intestinal peptide (VIP+) within the PFC, with a particular focus on female heterozygous mice *Mecp2*$^{tm1.1Bird}$ *mice* —a widely accepted model of RTT by immunofluorescence assay and a semi-automated 2D fluorescence-based workflows for analysis. Our findings at the 12-week-old mark revealed a trend towards reduced PV immunoreactivity in female *Mecp2*$^{+/-}$ mice, especially pronounced in the dorsomedial PFC (dmPFC) and infralimbic cortex (IL). Additionally, we also observed decreased expression of VIP in MeCP2 null cells in *Mecp2*$^{+/-}$ mice, suggesting a potential link between loss of MeCP2. These differences may underlie the phenotype seen in *Mecp2*$^{+/-}$ mice, which often exhibit motor impairments and breathing disturbances, as well as support the class-specific effect of MeCP2 expression in cortical IN.

Overall, cortical IN may play an important role in the pathogenesis of Rett Syndrome, leading to potential over-inhibition of specific cortical networks in crucial regions involved in motor and cognitive process. This elucidation is a crucial step toward understanding the cellular components of MeCP2 deficiency and, consequently, identifying novel pharmacological targets.

KEYWORDS: Cortical Interneurons, E/I balance, MeCP2, Prefrontal cortex and Rett Syndrome

TABLE OF CONTENTS

DIREITOS DE AUTOR E CONDIÇÕES DE UTILIZAÇÃO DO TRABALHO POR TERCEIROS ii

ACKNOWLEDGEMENTS..... iii

STATEMENT OF INTEGRITY iv

RESUMO v

ABSTRACT vi

LIST OF ABREVIATIONS..... ix

LIST OF FIGURES xi

LIST OF TABLES xiii

CHAPTER 1: INTRODUCTION 1

1.THE PREFRONTAL CORTEX.....2

1.1. EVOLUTIONARY HISTORY.....2

1.2. THE PFC STRUCTURAL ANATOMY IN RODENTS.....4

1.3. FUNCTIONS OF PFC 5

1.4. NEURONAL CORTICAL CYTOARCHITECTURE 7

1.5. AFFERENT AND EFFERENT PROJECTIONS OF mPFC 8

2.INTERNEURONS 10

2.1. CLASSIFICATION AND GROUPS 11

2.1.1. PARVALBUMIN POSITIVE CELLS 11

2.1.2. SOMATOSTATIN POSITIVE CELLS.....12

2.1.3. SEROTONIN RECEPTOR 3A POSITIVE CELLS.....13

2.2. EMERGENCE OF CORTICAL INTERNEURON: ORIGIN AND DIVERSITY.....13

3.RETT SYNDROME 16

3.1. RTT-LIKE CLINICAL FEATURES.....16

3.2. GENETIC BASIS 18

3.3. MeCP2 AS A TRANSCRIPTIONAL REGULATOR.....19

3.4. *MECP2* MUTANT MOUSE MODELS 20

3.5. E/I CORTICAL DISBALANCE IN RETT SYNDROME 21

CHAPTER 2: AIMS.....23

CHAPTER 3: MATERIALS AND METHODS.....25

1.ETHICS STATEMENTS....26
2.THE MOUSE MODEL....26
2.1 MAINTENANCE....26
2.2. GENOTYPING....27
2.3. MOUSE EUTHANASIA....27
3.IMMUNOHISTOCHEMISTRY....28
3.1. SAMPLE PROCESSING....28
3.2. IMMUNOFLUORESCENCE....28
3.3. IMAGING....29
3.4. ANALYSIS....30
4. STATISTICAL ANALYSES....31
CHAPTER 4: RESULTS....32
1.DIFFERENTIAL PATTERNS OF MeCP2 EXPRESSION IN FEMALE *Mecp2*$^{+/-}$ MICE....33
2.REGION-SPECIFIC VARIATIONS OF PV+ CELL DENSITY IN SYMPTOMATIC *Mecp2*$^{+/-}$ MICE....37
3.DECREASED CORTICAL DENSITY OF VIP+ IN IN FEMALE *Mecp2*$^{+/-}$ MICE....45
CHAPTER 5: DISCUSSION....47
CHAPTER 6: CONCLUSION....52
REFERENCES....546
SUPPLEMENTARY INFORMATION....71

LIST OF ABREVIATIONS

A	ACA	Anterior Cingulate Area
	ARA	Allen Reference Atlas
	ASD	Autism spectrum disorder
B	BLA	Basolateral amygdalar nucleus
C	CB	Calbindin
	CCK	Cholecystokinin
	CGE	Caudal Ganglionic Eminences
	CR	Calretinin
D	dmPFC	Dorsomedial Prefrontal Cortex
	DAPI	4′,6-diamidino-2-phenylindole
E	EF	Executive functions
	E/I	Excitatory and inhibitory
G	GABA	γ-aminobutyric acid
I	IF	Infralimbic
	IF	Immunofluorescence
	IN	Interneurons
L	LGE	Lateral Ganglionic Eminences
	lORB	Lateral Orbital area
M	M1	Primary motor cortex
	MC	Martinotti cells
	MD	Mediodorsal nucleus of the thalamus
	MECP2	Methyl-CpG binding protein 2
	MGE	Medial Ganglionic Eminences
	MOs	Secondary Motor cortex
	mORB	Medial Orbital area
N	NDDs	Neurodevelopmental disorders
	NGS	Normal Serum Goat
	NPY	Neuropeptide Y
O	O/N	Overnight
	OCT	Optimal Cut Temperature medium
P	PBS	Phosphate Buffer Saline
	PBS-T	PBS 1x supplemented with Triton X-100
	PFA	Paraformaldehyde
	PFC	Prefrontal Cortex
	PL	Prelimbic
	PN	Pyramidal Neurons
	POA	Preoptic area
	PV	Parvalbumin
R	RELN	Reelin
	RT	Room temperature
	RTT	Rett Syndrome
S	S1	Primary Somatosensory cortex

	SD	Standard deviation
	SST	Somatostatin
	SVZ	Subventricular zone
	$5HTr_{3A}$	Serotonin receptor 3A
V	VIP	Vaso-Active Intestinal Peptide
	vlPFC	Ventrolateral Prefrontal Cortex
	vlORB	Ventrolateral Orbital area
	vmPFC	Ventromedial Prefrontal Cortex
	VZ	Ventricular zone
W	WT	Wild type

UNITS	°C	Degree Celsius
	h	Hour
	min	Minute
	M	Molar
	mL	Milliliter
	µL	Microliter
	µm	Micrometer

OTHERS	3D	Three-dimensional

LIST OF FIGURES

Figure 1. Anatomical organization of the PFC and its subregions in the rodent brain.....5

Figure 2. GABAergic IN subtypes and embryonic origin......15

Figure 3. Schematic representation of stages and symptoms of RT-like clinical features......17

Figure 4. Schematic representation of the *MECP2* gene locus, transcript isoforms and proteins domains.....20

Figure 5. Schematic representation of semi-automated 2D fluorescence-based workflow for quantifying positive cells in IF assays.....30

Figure 6. PFC subdivision of *Mecp2*$^{+/-}$ mice have comparable area size percentages to WT and less MeCP2+ expression 34

Figure 7. Hierarchical clustering analysis of MeCP2 immunoreactivity indicates differential expression patterns in the same genotype of *Mecp2*$^{+/-}$ mice.....35

Figure 8. Cluster groups comparison of IN+ cell density with WT.....36

Figure 9. Atypical high-PV expression in the dmPFC cortex of *Mecp2*$^{+/-}$. 38

Figure 10. PV expression in the vlPFC cortex of *Mecp2*$^{+/-}$ shows similar tendency of increase.....39

Figure 11. Altered PV expression in the vmPFC cortex of *Mecp2*$^{+/-}$.....40

Figure 12. Increased high PV cell fraction in the IL cortex of *Mecp2*$^{+/-}$ mice underlying the observed intensity differences within vmPFC. 42

Figure 13. *Mecp2*$^{+/-}$ have an overall slight enhance in high PV cell fraction in the mORB and PL cortex. .43

Figure 14. MeCP2-expressing cells exhibit an increase in VIP+ immunoreactivity 45

Supplementary Figure 1. Representative images of negative control of immunofluorescence validates the assay.. 71

Supplementary Figure 2. Analysis of confocal microscopy images has comparable values of PV+ cells from photos obtained in bright field microscope.....71

Supplementary Figure 3. Hierarchical cluster output analysis based on z-score values of Mecp2 immunolabeled cells 72

LIST OF TABLES

Table 1. Detailed list of primary and secondary antibodies used in the immunofluorescence staining 29

Table 2. Detailed list of acquisition parameters for each fluorochrome used in the immunofluorescence staining assay 29

Table 3. Report on the hierarchical clustering analysis of three PFC subregions and fold change percentage of MeCP2 density 36

Table 4. Statistical report on the PV+ IN analysis of tree PFC subregions. 41

Table 5. Statistical report on the PV+ IN analysis of vmPFC divisions 44

Table 6. Statistical report on the VIP+ IN analysis of tree PFC subregions 46

CHAPTER 1

INTRODUCTION

INTRODUCTION

1. THE PREFRONTAL CORTEX

Historically, the field of neuropsychology has made significant progress in unraveling the relationship between brain structures and behavior. Early studies, using animals, were based on the experimental ablation of brain areas to test for sensorial and motor deficits. These initial studies highlighted the critical role of specific brain structures in neurophysiology, including the PFC. However, the (first/most notorious) clinical report to validate the hypothesis of the relevance of the PFC for cognition was the case of Phineas Gage, an American constructor who had his skull pierced by an iron pipe, destroying his frontal lobe. After surviving the accident, the man exhibited severe cognitive deficits, and descriptions of his behavior provided early hints of the involvement of the PFC in cognitive processes, leading researchers to investigate deeper into its structure and function (Squire et al., 2008, Chapter 52).

Nowadays, the PFC is seen as having the role of a maestro, orchestrating a synchronized symphony of cognitive processes, by integrating information from various sensory sources, to create a unified and comprehensive understanding of the world around us. The PFC shapes our cognitive control, long-term memory, decision-making, and problem-solving (Le Merre et al., 2021). Thus, when the delicate balance between excitation and inhibition within the PFC becomes disrupted, the cognitive processes can descend into disarray (Schubert et al., 2015). Therefore, desynchronization on this complex of the human brain can underly several neurological disorders.

1.1. EVOLUTIONARY HISTORY

One of the evolutionary hallmarks in mammals is the emergence of the neocortex, a structure that is developed from the telencephalon, and is the so-called ‘new part of the brain’. Its Latin name refers to the relatively new appearance in the vertebrate evolution scale (Rakic, 2009; Squire et al., 2008). The neocortex comprises several anatomically different substructures that are responsible for the most diverse and complex functionalities such as sensory processing and high-order cognitive abilities (Lui et al., 2011; Molnár et al., 2019).

At the core of the neocortex and situated in the front of the brain, lies the PFC, a region considered to play the central role in cognitive functioning. As the process of evolution unfolds, the PFC demonstrates a notable enlargement in size and complexity, reaching its maximum area percentage in humans – almost

30% of total cortical area (Brodman, 1909). This developmental trajectory reflects the growing demands of sophisticated cognitive processes in our species

The knowledge about the brain cortex structure has immensely been explored since the groundwork of Korbinian Brodmann. Brodmann's descriptions of cerebral cortex from primates and non-primates was one of the milestones in the neurological world, as it paved the way for consistent localization of structures by the segmentation of regions based on similar cellular and laminar structure (Brodman, 1909; Marie Carlén, 2017). His description of a distinct granular layer (L5) in primate's frontal lobe was for a long time adopted to identify the PFC structure and has inspired other suitable nomenclatures for the region, such as frontal granular cortex. As consequence, the distinctive anatomical differences in non-primates has led to adherence to another nomenclature for rodents, the orbitofrontal lobe (Preuss, 1995; Ongur, 2000).

Following Broadman's descriptions, one of the first attempts to consensually describe the structure, the absence of a granular area in non-primates awakened a need to adopt another criterion on top of the cytoarchitecture features (Preuss, 1995). Therefore, analyses of retrograde degeneration of non-primates frontal lobe have led to the identification of a common thalamo-cortical relationship (Leonard, 1969, 2016). Based on its connectivity pattern, the PFC has been described as to be the part of the cortex that receives projections from the mediodorsal nucleus of the thalamus (MD) (Rose & Woolsey, 1948). Studies on MD-projection of the cortex have added on the definition by distinguishing the main types of projections, considering the PFC to be richly innervated by dopaminergic projections (Berger et al., 1991; Björklund et al., 1978). These descriptions, for a long time, have fulfilled the identification of the PFC. However, scientific evidences were raised against it, mostly concerning the unprecise overlap of thalamus projections and the agranular layer, as well as the indistinctiveness of the named characteristics (Leonard, 2016; Preuss, 1995; Wise, 2008).

Despite the different terminologies to reference this single unit on the frontal cortical region in the brain, the main challenges surrounding the PFC primarily revolve around defining its subdivisions and their nomenclature, as well as establishing criteria for inferring homology across different species (Briscoe & Ragsdale, 2018).

In that perspective, parcellation of the brain cortex is better described considering the combination of function, architecture, connectivity, and topography criteria (Essen & Glasser, 2018). In the following sections of this thesis, the cortex anatomy, its cytoarchitecture, and its physiology will be explored to set

ground for further topics approached in this work and to set a better a correlation of it with the studies developed in mice.

1.2. THE PFC STRUCTURAL ANATOMY IN RODENTS

The PFC comprises the cortical structure of the anterior pole, just after to the olfactory bulb, highly interconnected with other neocortical areas that send and receive projections from other subcortical structures (Gabbott et al., 2005). Many brain regions converge external and internal information into the PFC and, therefore, it physically concentrates information processing and carries out executive functions (EF), such as attention focusing, working memory, and decision-making (Friedman & Robbins, 2022). On that account, parcellation of the PFC in rodents has been grossly based on connectivity patters, which support the presence of three prefrontal categories named by anatomical orientation and further subdivided upon cytoarchitectural criteria that adhere to the Allen Reference Atlas (ARA) (Wilson et al., 2010; Kamigaki, 2019).

The dorsal part of the medial PFC (dmPFC) comprises the Secondary Motor cortex (MOs) and Anterior Cingulate Area (ACA). Its main feature in terms of connectivity corresponds to its reciprocal interaction with cortical regions that are associated with sensory (visual, auditory and somatosensory regions) and motor (Primary Motor area and thalamic sources) information processing (Zingg et al., 2014; Barthas & Kwan, 2017)

The ventral part of the medial PFC (vmPFC) is constituted by the infralimbic (IL), prelimbic (PL) and medial orbital area (mORB). Anatomically close to the central commissure, this region is distinguished by its connection to the limbic system in which inputs from ventral hippocampus mediate social behavior and memory (Parent et al., 2010; Phillips et al., 2019).

The ventral part of the lateral PFC (vlPFC), also called lateral orbitofrontal (lOFC), mainly consists of the lateral and ventrolateral orbital area (lORB and vlORB, respectively). Being one of the least investigated regions, it is associated with limbic and primary somatosensory cortex (S1) inputs (Aronoff et al., 2010), as well as inputs from other sensory regions (C.-F. F. Chen et al., 2014; Winkowski et al., 2018).

Parcellation and segmentation of brain areas can be helpful to understand the complexity underlying information processing, however, the PFC is a highly integrated network that converges synaptic inputs from the whole brain as well as from itself. The regions are considered to be interdependent and not to have any clear functional or hierarchical organization (Wilson et al., 2010).

Taking into consideration the named areas from the rodent's PFC, the only segments that have homologues with primates in terms of cytoarchitectures, connectivity and topology aspects are the infralimbic (IL), prelimbic (PL), agranular orbital area (aORB), and anterior cingulate area (ACA) (Wise, 2008).

In the context of this thesis, the rodent's cortical anatomy and nomenclature will be used unless otherwise stated, in accordance with ARA nomenclature and ontology (Wang et al., 2020).

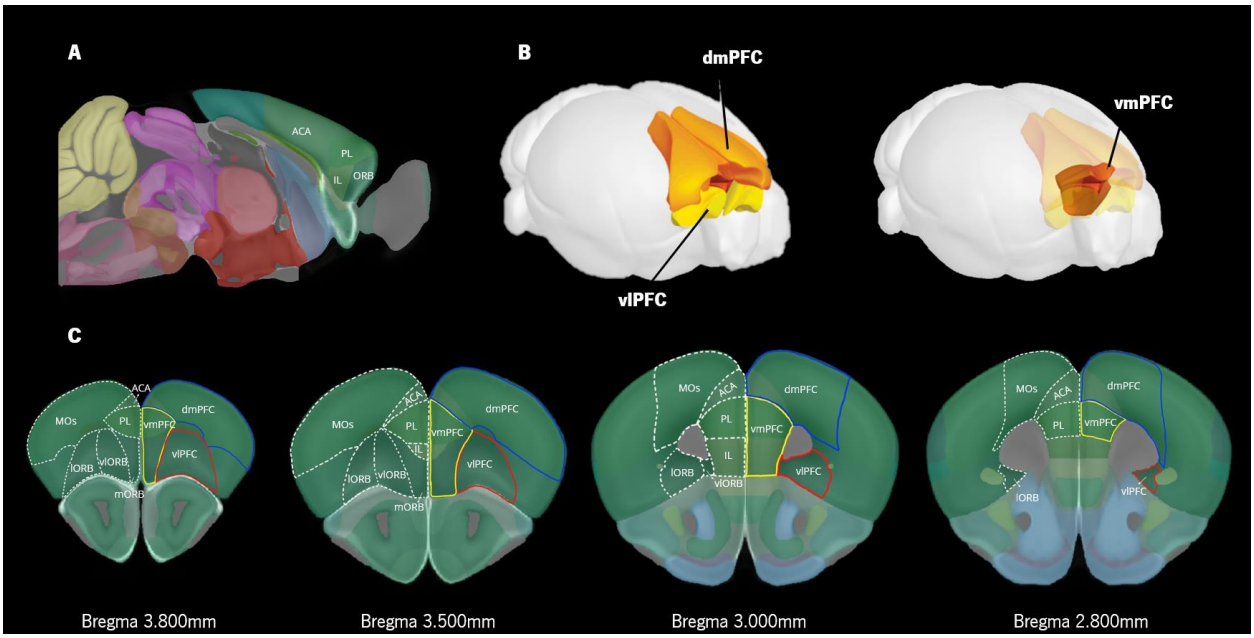


Figure 1. Anatomical organization of the PFC and its subregions in the rodent brain. **(A)** Sagittal sections showing most peripheral subregions of the PFC. **(B)** 3D view of the PFC subdivisions in the mouse's brain (Kamigaki, 2019). **(C)** Coronal sections showing PFC's organization. On the left, subregions according to the ARA terminologies and their location in the suggested PFC division. On the right, connectivity classification illustrating three main PFC regions... Credit: EBRAINS Knowledge Graph, "https://kg.ebrains.eu" (ACA: anterior cingulate area; dmPFC: dorsomedial; IL: infralimbic; lORB: lateral orbital area; mORB: medial orbital area; MOs: Secondary Motor cortex; PL: prelimbic; vlORB: ventrolateral orbital area; vlPFC: ventrolateral and vmPFC: ventromedial).

1.3. FUNCTIONS OF PFC

While the physiological role of the PFC in cognitive control has been extensively acknowledged, it is essential to clarify the fundamental concept of cognition and what that means in simpler terms. Cognition is defined as the mental process of acquiring knowledge and understanding through thoughts, experiences, and the senses. It is normally categorized by functional domains that ranges from basic sensory process to elements of executive function (Harvey, 2019; Friedman & Robbins, 2022)

From that starting point, proposal theories of functionality normally associate PFC activity with executive functions that can be generally summarized in attention, memory, working memory, decision-

making, and inhibitory behavior (Manes et al., 2002; D. A. Lewis et al., 2004; Rossi et al., 2009; Navawongse & Eichenbaum, 2013; Rae et al., 2015). These terms, despite their seemingly intuitive names, can often be subject to varied interpretations, leading to potential confusion and ambiguity. Therefore, in simple terms they all stand for the top-down control that the PFC has on behavior. Communication of the region with several other cortical and subcortical nuclei will enabling factor for processing sensory and motor information when behavior must be guided by internal intentions, instead of stereotyped reactions that are executed automatically and rapidly (Miller & Cohen, 2001).

Upon closer examination, the *modus operandi* of the PFC relies on activity patterns that serve as operating signals for other interconnected brain regions. With a goal-directed approach, the emitted signals shape the neuronal pathways by considering the internal state, inputs, and desired outputs, all within the context of a specific task (Miller & Cohen, 2001). On that account, most functions depend on the anatomical and functional integrity of the PFC (Holmes & Wellman, 2009; Czéh et al., 2018). In that perspective, the neuronal network in this region must be highly efficient, flexible, and plastic to generate correct and timely responses (Bortz et al., 2023).

Looking for the localized functions, previous studies past research has consistently theorized brain functions by examining perturbational studies, which involve linking the area affected by a lesion with observed disruptions in task performance. A research synthesis of the PFC functions in rodents reviewed more than 100 recent publications on the field to correlate with anatomical regions the sensory modality (i.e. auditory, visual, somatosensory, olfactory, or multisensory) perturbed with the type of task evaluated (i.e. sensorimotor transformation, delay/memory or rule/context) to precisely define localized functions (Le Merre et al., 2021). The research analysis identified that most of the studies targeting the dmPFC identified it to have impact on sensorimotor task and considered that the subregion is essential for planning and executing goal-directed behavior normally required to produce accurate motor response. Meanwhile, studies evaluating the function of the vmPFC have primarily centered on assessing behavioral changes related to the generation of internal information, such as emotions and memory, and how these factors influence future decision-making in animals. In contrast, the mouse vlPFC has received considerably less attention in research compared to the other two subdivisions. Consequently, it has not yet been established a consolidate correlation between this region area and cognitive functions, due to the lack of studies exploring the delay/memory tasks. However, it is suggested that the area is involved in processing reward-related information and plays a role in addictive behavior, due to its projections towards the striatum.

This functional categorization is in accordance with each subdivision and their brain anatomical connectivity. However, it is important to highlight that the PFC is a highly integrative region in which any dysfunction in some subarea will likely influence the unity itself (Zingg et al., 2014). Hence, this significant level of functional specialization elicits a sense of curiosity on understanding what are the differences across these areas. In the following sections, the cortical cytoarchitecture and connectivity patterns will be explored, in the attempt to provide a basis for these variances in functionality, focusing on the vmPFC.

1.4. NEURONAL CORTICAL CYTOARCHITECTURE

In the cerebral cortex, each region's neuronal network exhibits a distinctive cytoarchitecture, consisting of six organized cortical layers and vertically arrayed columns (Mountcastle, 1997). These networks are characterized by their remarkable diversity in morphology and connectivity patterns, which contribute to their varying roles in facilitating efficient and effective information processing (Zingg et al., 2014). Consequently, the circuitry organization may be categorized as comprising multiple types of long-range projecting excitatory neurons and locally connecting inhibitory neurons, respectively called glutamatergic pyramidal neurons (PN) and GABA (γ-aminobutyric acid)-ergic interneurons (IN) (DeFelipe et al., 2013; Llorca & Deogracias, 2022; Marín, 2012). The dynamic interaction between these two antagonist types of cells creates and maintains neuronal organization necessary for functional brain activity and the balance of excitatory and inhibitory (E/I) information processing (Marín, 2012; Rubenstein & Merzenich, 2003; Sohal & Rubenstein, 2019).

PN are excitatory pyramidal-shaped cell body neurons with an apical dendritic tree; this cell type accounts for more than 70–80% of all neocortical neurons (Lodato & Arlotta, 2015). These cells secrete glutamate and interact with themselves as well as with other physically distant neurons, as this interaction is mediated by their long projections (Catapano et al., 2008). This is one of the morphological features that allow information exchange and the high interconnection across brain regions (Molyneaux et al., 2007). The remaining ±15% correspond to GABAergic-IN, a diversified group of neurons, with over 20 subtypes listed (Beaulieu, 1993). Considering the prominent role of GABA as a major inhibitory neurotransmitter, IN cells predominantly influence the circuitry through processes of inhibition or disinhibition achieved by the inhibition of other inhibitory neurons. Hence, circuitry flexibility in the information process is mostly given by them, due their different functional specializations (Czéh et al., 2018).

Collective evidence suggests a particular involvement of the PFC network in social dysfunctional behavior, normally observed in autism spectrum disorders (ASD). GABAergic signaling pathway is found to be important to the correct performance of many of the high-level executive functions controlled by the PFC in which alterations of excitatory/inhibitory (E/I) balance and synaptic dysfunction are considered to underly the pathophysiology of many ASD (Yan & Rein, 2022). Postmortem brain examination of children with autism, a focal disruption of prefrontal cortex cytoarchitecture was found to have a abnormal laminar organization of neurons, but not from glia cells (Stoner et al., 2014; Trutzer et al., 2019). In adults and in individuals, the density of excitatory neurons in the PFC of postmortem brain of ASD individuals was found to be reduce, suggesting a likely excitatory signal disorganization (Liu et al., 2020).

In mice model, a design optogenetics tool to sample neuronal activity in medial PFC mediated by activation of excitatory neurons have shown that modulation of activity in awake animals by the shift of E/I ratio led to significant impairments during novel object exploration (Yizhar et al., 2011). Importantly, these impairments were unique to the mPFC, as by increasing of the ratio in primary visual cortex did not elicit such impairments in behavior, that in the case of PFC were able to ameliorated by lowering the ratio towards an increase in inhibition (Han et al., 2014; Selimbeyoglu et al., 2017).

Despite accounting for less than 20% of the neocortical cells, it is critical to consider key facets of GABAergic inhibition system in normal brains and its specification for each PFC subregion to understand what gives information coding flexibility and how behavior impairments are impacted by the local circuitry E/I ratio. This topic will be one of the main focuses on the following section.

1.5. AFFERENT AND EFFERENT PROJECTIONS OF mPFC

The mPFC network is known for its extensive interconnections with both cortical and subcortical structures, receiving incoming (afferent) and carrying outgoing (efferent) projections of different brain structures (Hoover & Vertes, 2007). By examining the connectivity patterns of each of the three subdivisions, it is possible to understand the functional specialization within this network.

In mice, the vmPFC region distinguishes from the dmPFC by an intense afferent connection with core structures of the limbic system (i.e., ventral tegmental area (VTA) and basolateral amygdala nucleus (BLA) (Beier et al., 2015) and by a lack of inputs from non-limbic cortex (i.e., motor, somatosensory and associational regions in the cortex) (Van Eden et al., 1992) common in the dmPFC (Dixsaut & Gräff, 2021;

Le Merre et al., 2021). Moreover, hippocampal interactions are one of the most enhanced pathways associated to the mPFC, afferents projections are present in the vmPFC and dmPFC, but considerably more intense on the ventral part then on the dorsal one (Cruikshank et al., 2012). This pattern of interaction is what elicits the vmPFC control in behavior flexibility and working memory (Bolkan et al., 2017). The vlPFC, appear be a combination of projections of the other two areas, as it receives inputs from sensory areas such as auditory cortex (Mori et al., 2013; Winkowski et al., 2018) and limbic system by BLA and MD association mediating fear-related memories (Mátyás et al., 2014).

2. INTERNEURONS

As standard definition, cortical interneurons (IN) are neurons with short axons that do not leave the neocortex and the remaining body soma present in the cerebral cortex (DeFelipe et al., 2013). Additionally, most of them does not resemble the typical PN morphology, by these means they have been subdivided into two groups based on their dendrite structure: (I) spiny non-pyramidal neurons and (II) aspiny or sparsely spiny non-pyramidal neurons (Ascoli et al., 2008). The first group comprises mostly the glutamatergic neurons, located in L4, conversely the other group concerns local GABA producing cells, present in all cortical layers, hereon called GABAergic IN, which present an inhibitory activity (Scala et al., 2019).

The heterogeneous population of GABAergic IN can be further subdivided into subgroups that acquire specific features during development that are determinant to define their functional function (Tremblay et al., 2016). Over the past years, several studies have been investigating the functional role of each GABAergic IN subtype in brain circuitry. However, the results are sometimes contradictory and conclusions are hampered by the difficulty in comparing the data obtained in different laboratories (DeFelipe et al., 2013).

To facilitate GABAergic IN classification, Petillas' terminology (Ascoli et al., 2008) was created as a neuronal classification system that defines criteria to unify parameters in order to correctly identify cortical IN based on their morphological, molecular and electrophysiological features. The creation of this IN nomenclature allowed the identification of different subtypes by observational methods as well as and quantifiable measurements, reducing the unreliability of results.

Briefly, morphological features comprise the shape, size, and orientation of the body cell, dendrites, and axons. These are important features to establish circuit connectivity and understand the functional role in brain circuitry (Zilberter et al., 1999). The molecular features consist of several specific molecular markers that have already been identified to distinguish IN subtypes such as transcription factors, neurotransmitter receptors, structural proteins, and ion channels (Cauli et al., 1997; Paul et al., 2017). This molecular identification is crucial for understanding the complexity of synaptic communication within the brain circuitry. Finally, the electrophysiological properties of the cell are the most reliable aspect to distinguish IN, considering that they dictate IN functionality into the circuitry (Beierlein et al., 2003).

Considering all the above-mentioned distinguishing features, IN can be classified in subtypes, however, despite the generalized adherence to this classification, some of the terms population still lack consistent definition, due to their divergent morphological descriptions. All things considered, the

development of microscopy, electrophysiological methods, as well as single-cell analysis greatly contributed for the exponential expansion of what is known about IN population thanks to identification of novel unique specific features (Kawaguchi, 1993).

In this thesis, for the sake of simplicity and time available to perform the analysis we will consider a broader classification in three main categories of cortical IN, based on the expression of different non-overlapping markers: parvalbumin (PV), somatostatin (SST), and serotonin receptor 3A ($5HTr_{3A}$) (Cowan et al., 1990; Gozlan et al., 1983; Vincent et al., 1983) (**Figure 2A**). Further on, each of these classes can be subdivided into different IN subtypes, given their specific common features and specializations, as well as the co-expression of other molecular markers such as calbindin (CB), calretinin (CR), cholecystokinin (CCK), neuropeptide Y (NPY), reelin (RELN) and vaso-active intestinal peptide (VIP) (Kawaguchi & Kubota, 1993; Bennett & Bolam, 1993; Takagi et al., 1984; Vuillet et al., 1989; Theriault & Landis, 1987; Pohlkamp et al., 2014)

2.1. CLASSIFICATION AND GROUPS

2.1.1. PARVALBUMIN POSITIVE CELLS

The largest class of cortical IN express the calcium binding protein parvalbumin (PV)+ positive cells and have a fast-spiking electrophysiological profile (Hu et al., 2014). PV+ cells are morphologically distinguishable from other IN subtypes by their extensive arborization (20- to 24-mm length), and their aspiny dendrites, which facilitates the generation of fast excitatory postsynaptic potentials (EPSPs) (Geiger et al., 1997). These cells are highly interconnected with PN by synapses localized at different cell compartment and receive inputs from other PV+ cells as well as other IN subtypes, namely vasoactive intestinal peptide (Hioki et al., 2013) (**Figure 2B**).

PV+ cells can be further subcategorized into three groups: the axo-axonic chandelier cells, the soma-targeting basket cells, and the translaminar cells (Ascoli et al., 2008; Lim et al., 2018; Llorca & Deogracias, 2022). The axo-axonic chandelier cells have the lowest level of PV expression in comparison with the rest of the group (Taniguchi et al., 2013) and exhibit an elaborated dendritic arborization that targets the initial segment of PN axons (Somogyi et al., 1982). They are mainly distributed throughout L6 and in the borders of L1 and L2 and their its input modulates PN according to cell specific structural properties. However, their contribution for network function is still unclear (Lim et al., 2018; Schneider-Mizell et al., 2021). The soma-

targeting basket cells are one of the most abundant subtypes of neocortical IN and they are evenly distributed throughout the six cortical layers (Lim et al., 2018). Their complex axonal arbor synapses mainly with the soma and dendrites of PN and other IN, and they are associated with the enhancement of the spike synchrony of networks (Kriener et al., 2022). Finally, the translaminar cells, as their name indicates, are IN whose cell body is deeply located throughout L5 and L6; conversely, their axons are distributed across more superficial layers (Bortone et al., 2014; Lim et al., 2018).

2.1.2. SOMATOSTATIN POSITIVE CELLS

Another class of IN is characterized by the expression of somatostatin (SST), a neuropeptide with several signaling roles within and outside the central nervous system (Liguz-Lecznar et al., 2022). The molecule itself has an inhibitory effect, as the activation of its receptors leads to membrane hyperpolarization and inhibition of Ca2+ influx induced by depolarization (Yang et al., 2005). At the functional level, SST+ IN are associated with the facilitation of inhibitory inputs into apical dendrites of PN, but they can as well mediate disinhibition by targeting PV+ neurons (Liguz-Lecznar et al., 2022; Silberberg & Markram, 2007).

SST+ IN are divided in two vast categories of cells, the Martinotti cells (MC) and non-Martinotti cells (non-MC) (Lim et al., 2018; Llorca & Deogracias, 2022). The first one is predominantly present in L5 as well as in L2/3, and their ascending arbor axon is distributed throughout L1, targeting the dendrites of PN or other IN subtypes mediating synaptic inhibition of PN (Hilscher et al., 2017). MC correspond to almost 60% of all SST+ cells, however, as a highly diverse category, MC can be distinguished from one another by their co-expression of CR, CB, RELN and NPY, as well as by their functional specialization, depending on the cortical layer they are immersed (Ma et al., 2006; Tremblay et al., 2016; Muñoz et al., 2017). Locally present in L5, MC co-expressing CR or CB are called fanning-out MC and T-shaped MC, respectively. The SST/CR+ IN has an axonal branch towards L2/3 and adapting neurons firing patterns. Contrarily, as for the SST/CB+ IN, have axonal branching targeting L1 and have an adapting neurons firing patterns (Ma et al., 2006; Nigro et al., 2018).

The other 40% of SST+ cells are non-MC and lack projections to L1, which means that they are locally targeting neurons with axons confined to the same layer where the cell body is located. Additionally, their abundance in L4 and similar firing pattern as fast spiking neurons make these cells functionally distinct from the rest of SST+ cells (Tremblay et al., 2016).

2.1.3. SEROTONIN RECEPTOR 3A POSITIVE CELLS

Lastly, the most heterogeneous IN family is known for the expression of serotonin 5-hydroxytryptamine 3A receptor ($5HTr_{3a}$), an ionotropic serotonergic receptor (Chameau & van Hooft, 2006; Lee et al., 2010). Inside this category, there are IN that co-express the vaso-intestinal peptide (VIP), dividing this family in VIP+ and non-VIP+ IN. Accounting for almost 13% GABAergic neurons, VIP+ neurons are a transcriptionally and morphologically diverse group of cells distributed throughout the six cortical layers, oppositely to the non-VIP IN, which are predominantly present in L1 (Prönneke et al., 2015)

Among the VIP+ cells, there are the bipolar and the multipolar cells (Lee et al., 2010). The bipolar cells are abundantly present in L2/3 and have mainly vertically orientated axons that target other IN, mainly the SST+ subtype (Porter et al., 1998; Rozov et al., 2001). Molecularly, they can be distinguished from other VIP+ IN by the co-expression of CR (Caputi et al., 2009). Conversely, the multipolar cells are predominantly present in superficial cortical layers and co-express the neuropeptide CCK. They are also named as basket cells considering their morphological characteristics, namely the small soma with multiple long primary dendrites (Férézou et al., 2002).

2.2. EMERGENCE OF CORTICAL INTERNEURON: ORIGIN AND DIVERSITY

Several genetic fate-mapping studies have been dedicated to understand the relation between IN subtypes and birth place of progenitor cells (Anderson et al., 2001; Nery et al., 2002; Butt et al., 2005) Initially, PN and GABAergic-IN were thought to originate from the same progenitor cells on the ventricular zone of the dorsal pallium of the telencephalon due to their tight integration and network organization. Nowadays, it is considered that GABAergic IN originate from distinct embryonic structures, mainly rising from progenitor cells in the ventral of the telencephalon (subpallium) (Anderson et al., 1997; Wichterle et al., 2001; Letinic et al., 2002; Wonders & Anderson, 2006).

The subpallium is divided in the preoptic area (POA) and ganglionic eminences which is further subdivided in lateral, medial, and caudal (LGE, MGE and CGE, respectively) (**Figure 2C**). Moreover, these three regions are highly associated to specific classes of IN due to the exposure to genetic programs most expressed in each region (Lavdas et al., 1999; Butt et al., 2008; Xu et al., 2010). Specifically, The MGE gives rise to PV+ and SST+ IN while the CGE mostly generates VIP+ IN (Xu et al., 2004). Together, these two regions generate nearly 90% of cortical IN while the remaining GABAergic population is suggested to originate

in the POA, without specific subtype distinction (Gelman et al., 2011). Nevertheless, it is only during the migration process to the cortex that the different IN populations appear, as they acquire their distinguishing features (Llorca & Deogracias, 2022).

In mice, IN start a tangential migration to reach invade the cortex whereby radial migration they start to allocate vertical in laminar organization. Reaching its final destination, IN start to establish synapses on different subcellular compartments of PN or other IN (Lim et al., 2018). Indeed, it is throughout these migratory routes that the different populations of IN acquire their biochemical markers by exposure to a succession of different transcription factors programs (Kessaris et al., 2014). However, other key differentiating aspects like morphology and synaptic connections are only acquired later in development, some even during postnatal ages (Rymar & Sadikot, 2007).

Considering the high heterogeneity within IN groups and their diverse functional specializations, it becomes evident that the source of circuitry flexibility in information processing can be traced back to these variations (Kvitsiani et al., 2013; K. Jung et al., 2023). Consequently, disturbances in GABAergic neuronal circuitry have been strongly linked to implications in the pathophysiology of neurodevelopmental disorders (Chao et al., 2010).

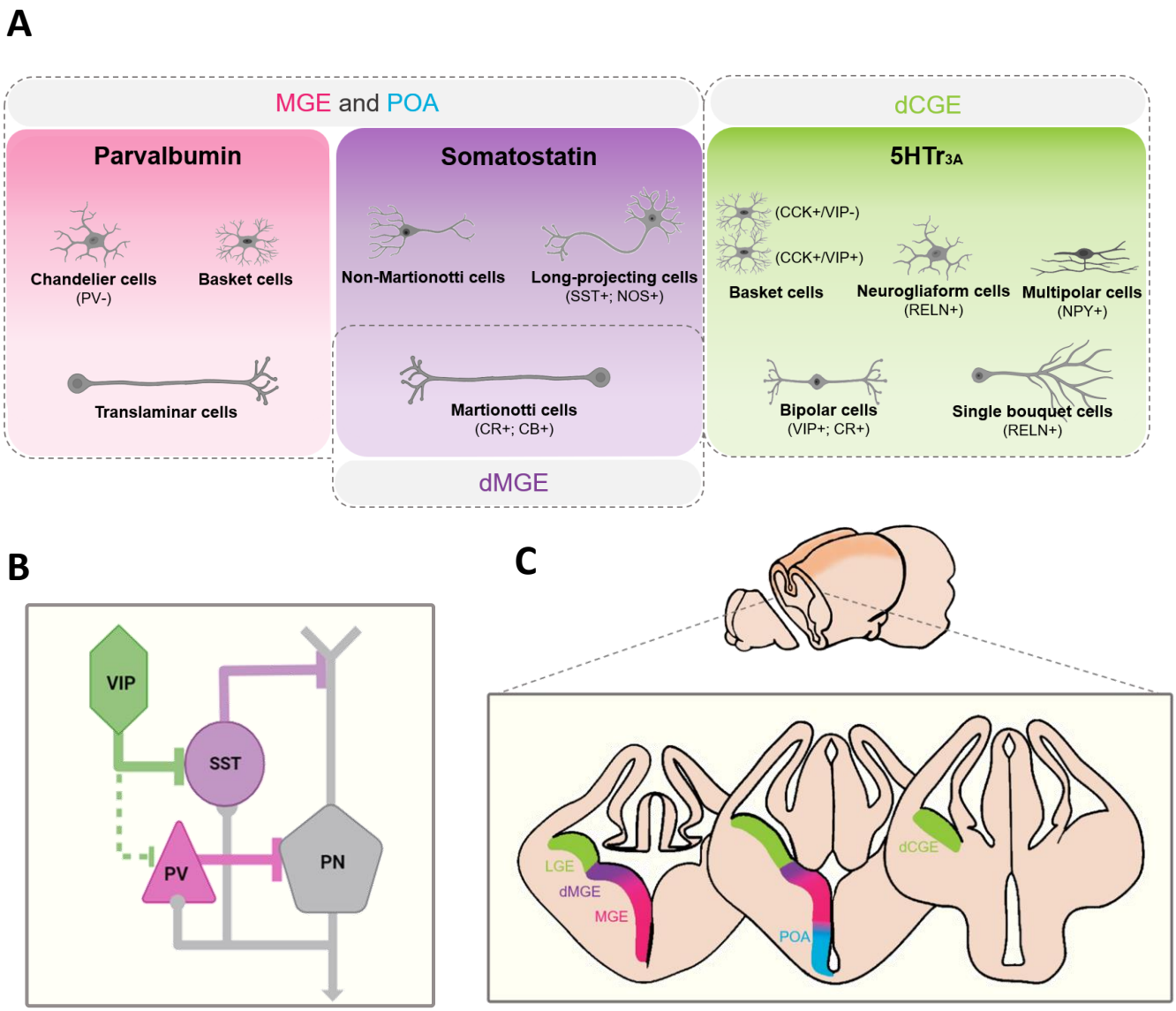


Figure 2. GABAergic IN subtypes and embryonic origin. (**A**) Representation of the three major cortical IN groups that are considered to originate from specific division of embryonic telencephalon. Each IN subtype is correlated by an origin site within the divisions. (PV: parvalbumin; SST: somatostatin; $5HTr_{3A}$: serotonin receptor 3A; CB: calbindin ; CR: calretinin; CCK: cholecystokinin; NPY: neuropeptide Y ; RELN: reelin and VIP: vaso-active intestinal peptide) (**B**) Schematic of cortical inhibitory circuitry between major IN subtypes and PN. (**C**) Schematic representation of embryonic subcortical telencephalon divisions and association with mature IN subtype origin. (CGE: caudal ganglionic eminence; dCGE: dorsal part of the CGE; MGE: medial ganglionic eminence; dMGE: dorsal MGE and POA: preoptic area)

3. RETT SYNDROME

Recognized more than thirty years ago, Rett Syndrome was reported as a unique clinical entity by Dr. Andreas Rett, a neurologist who observed two girls with development delay making the same repetitive hand-washing motions (Rett, 1966). The atypical hand movements from both girls were one of the things that drew Rett's attention, alongside with their cognitive impairments. The condition was only recognized by the medical community after the reports of more than 35 similar cases (Hagberg et al., 1983; Santos et al., 2009).

The understanding of the underlying genetic cause of the syndrome was only achieved in the 90s, when mutations in the X chromosome-linked gene methyl-Cp G binding protein 2 (MECP2) were found to be associated with more than 95% of 'classic' RTT cases (Sirianni et al., 1998; Amir et al., 1999). Later, the syndrome was also associated with mutations in other X-linked genes, the cyclin-dependent kinase-like 5 (CDKL5) (Grosso et al., 2007) or Forkhead box G1 (FOXG1) (Mencarelli et al., 2010), adding another layer of complexity to the variability of the syndrome (Ehrhart et al., 2016; Kyle et al., 2018). In the past years, other pathogenic gene variants, whether in novel genes or in genes already recognized for their association with neurodevelopmental disorders, were identified as suitable candidates to be disease-causing in patients tested negative for MECP2, CDKL5 and FOXG1 mutations (Lopes et al., 2016), expanding the genetic basis of the disease.

Rett Syndrome is characterized by a neurological regression during postnatal development, occurring in 1:10.000 girls worldwide (May et al., 2023). Despite the strong correlation between pathogenic variants in the *MECP2* gene and Rett syndrome, mutations in MECP2 are not required for the diagnosis of RTT. Therefore, the clinical diagnosis is still based on clinical presentation and the corresponding clinical criteria (Neul et al., 2010; Petriti et al., 2023).

3.1. RTT-LIKE CLINICAL FEATURES

The syndrome onset and progression can be summarized in a cycle of normal development followed by a period of regression and skill loss between the age of 1 to 4 years of age (**Figure 3**). Divided into four stages, the key clinical features of RTT appear across the different phases (Chahrour & Zoghbi, 2007; Kyle et al., 2018). Stage I, known as stagnation stage, starts around 6 and 18 months of age, where children with a normal development start to no longer meet cognitive and motor milestones expected for their age. Following this initial development slowdown, the Stage II - rapid regression phase is dramatically

characterized by developmental regression with deceleration of head growth, loss of acquired skills, such as hand movements and speech, along with development of autistic features like social withdrawal, disinterest in the surrounding and lack of eye contact. Throughout the mental deterioration stage, patients with RTT tend to experience also autonomic dysfunction, which impacts on heart rate and body temperature regulation. These clinical conditions appear throughout the years and persist until the *Stage III* - plateau stage, which is normally reached in between 2- to 10-years of age. During this period there may be slight improvements in motor and communication skills, and stereotypic hand movements might decrease. However, seizures and breathing anomalies such as hyperventilation during wakefulness and apneas continue to be a concern for the patients' overall health. Stage IV, known as late motor deterioration, is one of the final phases of Rett syndrome. Typically affecting patients around the age of 10, this stage is marked by a significant decline in motor function, characterized by severe muscle weakness. This weakening ultimately culminates in loss of mobility, often involving the necessity of a wheelchair throughout the teenage years (Hagberg, 2005; Chahrour & Zoghbi, 2007; Kyle et al., 2018; May et al., 2023).

Despite these broad spectra of clinical manifestations, affected children experience until puberty a severe debilitated physical condition, marked by the loss of essential motor skills and the necessity of specialized care and assistance in their daily lives. Some of these patients can also develop Parkinsonism features at advancing stages of the disease (Roze et al., 2007; Chahrour & Zoghbi, 2007). The clinical diagnosis takes mostly into account four main motor criteria: loss of purposeful hand skills, loss of spoken language, gait abnormalities, and stereotypic hand movements (Neul et al., 2010; Petriti et al., 2023).

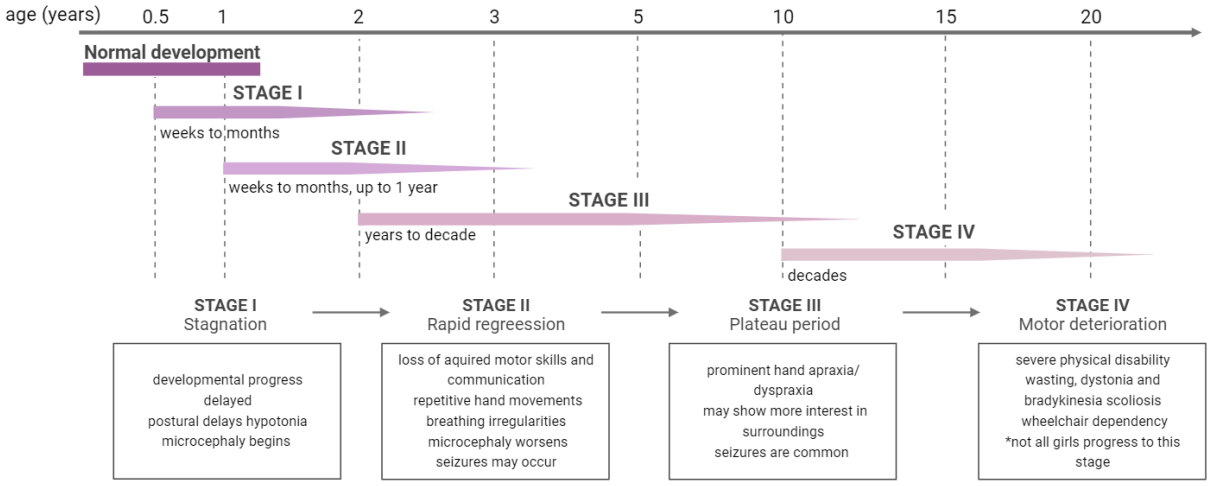


Figure 3. Schematic representation of stages and symptoms of RT-like clinical features. Individuals with

Rett syndrome experience an initial period of normal development, but between 6 and 18 months of age (Stage I), they begin to exhibit signs of developmental arrest, marked by the loss of speech, purposeful hand use, and decelerating head growth. In Stage II, from 1 to 4 years of age the children experience a rapid regression and exhibit an autistic behavior, irritability, and disturbance sleep pattern for a period of moths to a year. Between 2 to 10 years of age, they reach a plateau stage (Stage III) in which they exhibit a partial improvement in behavior and motor skills. In the last stage (Stage IV), individuals present a late motor deterioration characterized by reduced mobility, dystonia and hypomimia. However, cognitive functions are stable and autistic features often show improvement.

3.2. GENETIC BASIS

RTT is a rare genetic neurological disorder in which more than 95% of cases are associated with mutations in the *MECP2* gene, located in the chromosome X (Chahrour & Zoghbi, 2007). In a minority percentage of cases, mutations on the gene are inherited usually in the maternal side, whereas for the large percentage, they are associated with a sporadic *de novo* mutation in the genome derived from the paternal germline (Wan et al., 1999; Trappe et al., 2001; Good et al., 2021).

The RTT phenotype can be derived by a wide spectrum of mutations in the MeCP2 protein, ranging from missense variants that impact its folding, leading to instability in DNA binding, or nonsense, frameshift variants or the eraser whole exon deletions that lead to full loss of expression and function (null variants) (Chahrour & Zoghbi, 2007). Yet, mutation sites are primarily concentrated on specific gene regions, which can be classified into three categories (Good et al., 2021). The first two occur on the initial segments of the protein, (I) the NTD and (II) the MBD, and both have impact on the protein ability bind to the DNA (Saunders et al., 2009; Martínez de Paz et al., 2019). Specifically, missense mutations in the MBD domain exhibit the highest rates among patients, and are associated with impact on protein folding and DNA interaction (Spiga et al., 2019). The final category (III) displays a wide spectrum of occurrence, with a higher frequency of mutations found in the C-terminal domain (CTD), although they can be distributed throughout the rest of the protein. Mutations on the CTD have been linked to alterations in protein-protein interactions with repressors or other transcription factors regulation, and are associated with the manifestation of a milder phenotype (Bebbington et al., 2010; Good et al., 2021).

Other key determinant that contributes for phenotypic spectrum of the syndrome is the process of X-chromosome inactivation (XCI). This natural gene silencing process specific of the X chromosome plays a significant role in the phenotypic variability of impairments experienced by the affected individuals (Amir et al., 2000; Hoffbuhr et al., 2002). Being a general random process and inherent to females, the XCI results

in differential expression levels of the wild-type vs. mutant version of the *MECP2* gene at the cellular level, but with an overall 50:50 ratio at tissue level (Wan et al., 1999; Augui et al., 2011). When, however, the process occurs in a non-random manner, preferential inactivation of one X chromosome over the other, a situation known as XCI skewing this leads to an unbalanced and may impact the expression of the phenotype. Often this occurs by a preferential inactivation of the chromosome with the mutant allele (Fang et al., 2022),but this is not always the case.

3.3. MeCP2 AS A TRANSCRIPTIONAL REGULATOR

The *MECP2* gene encodes for the methyl-CpG binding protein 2 (MeCP2) which as the own name suggests is known to bind to methyl-CpG sites in the DNA (Meehan et al., 1992). The CpG sites correspond to a part of the genome with a high content of dinucleotides of cytosine and guanine that are separated by a phosphate group (M. Jung & Pfeifer, 2013). These regions are known to be important for epigenetic regulation, as DNA methylations on these sites were discovered to enhance repression of gene expression. This repression is mainly mediated by proteins that bind to these methyl-CpG, such as MECP2 (J. D. Lewis et al., 1992; Nan et al., 1997), and being to that location other proteins that either modify the chromatin structure or otherwise alter the predicting of recruitment of the transcription machinery.

Consistent with its functional role, MeCP2 is a nuclear protein, expressed in all tissues, predominantly expressed in mature neurons, but not in astroglia or immature neuroblasts (Kishi & Macklis, 2005). Encoded by four exons, the MeCP2 protein has four primary functional domains that provide its ability to bind to methylated DNA (**Figure 4A**) (Kyle et al., 2018). As a methyl-DNA binding protein, it features two important domains: the methyl binding domain (MBD), responsible for the association with methyl-CpG binding sites, and the transcriptional repression domain (TRD), which interacts with various protein complexes, including histone deacetylases and transcriptional corepressors (Jones et al., 1998; Adkins & Georgel, 2011). The activation of these protein complexes' enhances the DNA-histone interaction, leading to DNA compaction and, ultimately, transcriptional repression (Nan et al., 1997; Kishi & Macklis, 2005). The protein exists in two primary isoforms, MeCP2-E1 and MeCP2-E2, characterized by slight variations in their N-terminal domain (NTD) amino acid residues (**Figure 4B**) (Good et al., 2021). It is estimated that more than half of the RTT cases are explained by the eight more frequent recurrent point mutations (R106W, R133C, T158M, R168X, R255X, R270X, R294X, R306C) or by C-terminal truncations (**Figure 4C**) (Kyle et al., 2018). Given the numerous CpG sites located near promoter regions in human genes and their changing

methylation patterns over time, MeCP2 plays a crucial role as an epigenetic regulator. Its influence on long-term cellular changes is substantial, significantly impacting cellular differentiation and the establishment of tissue-specific gene expression profiles (Ehrhart et al., 2016).

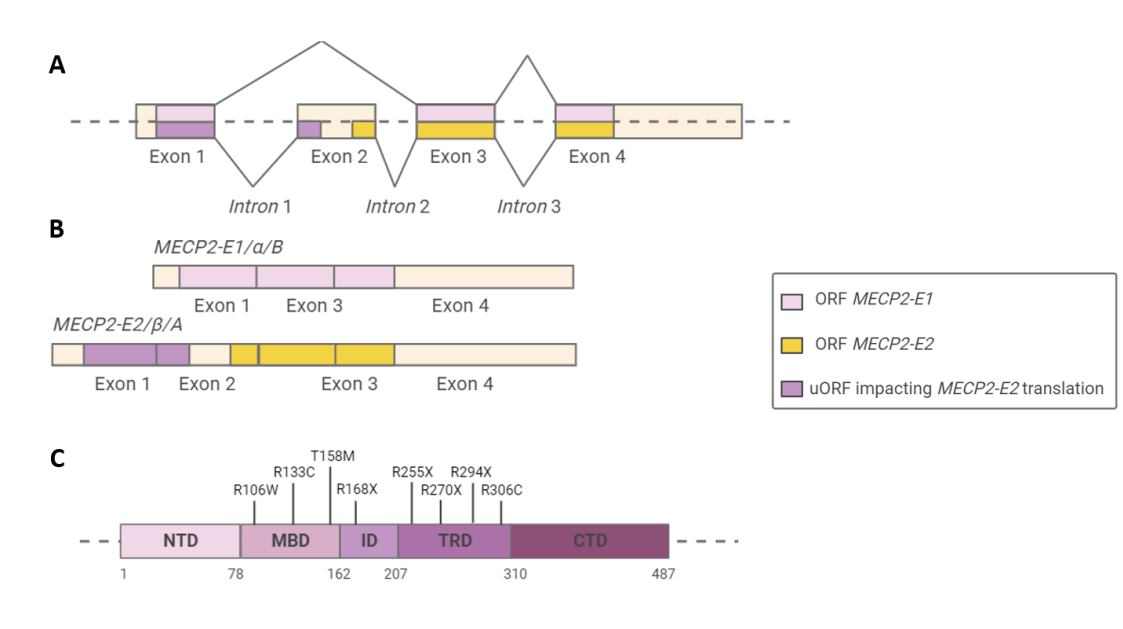


Figure 4. Schematic representation of the MECP2 gene locus, transcript isoforms and proteins domains. (**A**) *MEPC2* gene is composed of four exons and three introns which can generate two transcript isoform, MeCP2-E1 and MeCP-E2. (**B**) The MeCP2-E2 isoform includes all four exons, while the MeCP2-E1 isoform lacks exon 2. (**C**) Simplified representation of proteins domains and most common site of main point mutations associated with RTT-like phenotype. (NTD: N-terminal region; MBD: Methyl-CpG-binding domain; ID: Intervening domain; TRD: Transcriptional repression domain and CTD: C-terminal domain).

3.4. *MECP2* MUTANT MOUSE MODELS

The identification of the causative gene and mutations have allowed the creation of various mutant mouse models for RTT, effectively recapitulating distinct aspects of the human condition, within the wide range of phenotypes associated with the syndrome. Until nowadays, *Mecp2*$^{tm1.1Bird}$ (Guy et al., 2001) and *Mecp2*$^{tm1.1Jae}$ (R. Z. Chen et al., 2001) mice are one of the most common models used and investigated. Several other mouse models, based on a specific exon deletion, nonsense or missense variant have been created, as well as by the use of gene silencing approach (Guy et al., 2007) or conditional deletion (Chao et al., 2010; Ezeonwuka & Rastegar, 2014).

The *Mecp2*$^{tm1.1Bird}$ mice bear a deletion of exon 3 and 4 of the *MECP2* gene (Guy et al., 2001). In his model, it was possible to recapitulate the somatic mosaicism of the X inactivation and many phenotypic characteristics of the human disorder (Braunschweig et al., 2004; Santos et al., 2010). Despite the similar

phenotypic deficits observed in both genders within this model, the *Mecp2*$^{tm1.1Bird}$ females present a slower progression and a milder phenotype, and thus a greater longevity than males. Recent work from our lab (Monteiro et al., in preparation) and others (Samaco et al., 2013; Matagne et al., 2021; Urbinati et al., 2021; Villani et al., 2021; Flores Gutiérrez et al., 2022; Urbinati et al., 2023) confirms the relevance of female heterozygous animals as a RTT model. Their symptoms appear considerably later, at 3-4 months of age and comprise hypoactivity, ataxic gait, hindlimb clasping, and breathing abnormalities. This contrasts with the shorter lifespan observed in null males, that present a more severe phenotype with an early onset (Ribeiro & MacDonald, 2020).

Additionally, 12-week-old heterozygous female mice are known to exhibit impairments in sensory perception, especially in the texture and social interactions tasks, which suggest a hyposensitivity considering that the RTT mice spent more time investigating and longer time per interaction with texture than a control adult mice (Mykins, Layo-Carris, et al., 2023). Recently reported data about performance regression in adult mice, suggest two different behavioral phenotypes in the *Mecp2*$^{-/-}$ mice based on goal-directed performance during pup retrieval tasks (Mykins, Bridges, et al., 2023).

Alternatively, the *Mecp2*$^{tm1.1Jae}$ model lacks only the exon 3 allele, which compromises most of the MBD domain and NTD (Stuss et al., 2013; Ribeiro & MacDonald, 2020). These deletion results mostly to N-terminal truncation of the protein resulting in alterations in sites that are critical for DNA and protein interaction (R. Z. Chen et al., 2001). The male mice of this model experience similar physical deficiencies, however as opposed to the heterozygous females of *Mecp2*$^{tm1.1Bird}$ model, these females appear to be asymptomatic for the first four months of life subsequently acquiring the abnormal features (Ribeiro & MacDonald, 2020).

3.5. E/I CORTICAL DISBALANCE IN RETT SYNDROME

The functional role of the excitation/inhibition (E/I) imbalance within the context of Rett Syndrome is supported by numerous lines of research (Sohal & Rubenstein, 2019; Li, 2022; Banerjee et al., 2016). In mouse studies, correct expression of MeCP2 levels reveal to be an important contribution to the proper organization of the cortex network (McGraw et al., 2011). Indeed, in the absence of functional MeCP2 protein synaptic abnormalities culminate in an unfunctional neural circuitry that is thought to that underlie the RTT neurological symptoms such as the profound cognitive impairments, but also the social behavior abnormalities and the loss of motor skills (Wood et al., 2009; Morello et al., 2018; Ip et al., 2018).

Considering the increased interest in the hypo- and hyperactivity of cortical networks as factors underlying the dysfunction seen in neurodevelopment disorders, prior research provided evidence suggesting that the loss or mutation of MeCP2 can influence the E/I balance within specific brain regions, resulting in distinct ratio shifts occurring in each neocortical region (Chahrour & Zoghbi, 2007; Li, 2022). At the neuronal cell level, it has been unveiled that MeCP2 expression exerts a class-specific impact in neocortical regions, certain types of inhibitory neurons being more profoundly affected by the loss of MeCP2 function than others (Mossner et al., 2020). Consequently, the loss of MeCP2 function significantly disrupts the proper development of the inhibitory system within the somatosensory and motor cortex.

At the S1 and M1 cortices of *Mecp2*$^{tm1.1Jae}$ mice (R. Z. Chen et al., 2001), the E/I ratio has opposite shift tendencies, and a dual adjustment of both forces appears to underlie somatosensory processing and motor control impairments (Li, 2022). In the S1 region, the pyramidal neurons appears to exhibit a general hypoactivity, that results from a reduced glutamatergic excitation and increased GABAergic inhibition (Dani et al., 2005). Conversely, in the M1 region, there is a shift towards hyperactivity, which suggests an underlying dysfunctional GABAergic activity (Tropea et al., 2009). In both cortices, studies on PV+ populations of symptomatic male *Mecp2* null mice revealed elevated expression levels of PV as well as excessive excitatory inputs (Morello et al., 2018). Moreover, specific deletion of *Mecp2* from PV+ IN shows to recapitulate effects of global deletion of *MECP2* on PN (Banerjee et al., 2016). This evidence suggests that PV+ cells' developmental organization as well as the correct level of PN inputs are affected by *Mecp2* expression. Additionally, it has been observed that in female heterozygous *Mecp2* mice exhibited a high level of PV expression in S1 and M1 cortices, correlated with the severity of their motor impairments (Donato et al., 2013; Morello et al., 2018).

In the PFC, recent studies indicated that synaptic activity of pyramidal neurons was shifted towards a reduced excitation rather than an increase on inhibitory activity (C. James Howell et al., 2017; Li, 2022). Additionally, this hypoactivity has been associated with increased rates of targeting of PV+ coming from hippocampal projections towards the PFC (Phillips et al., 2019). At the cellular level, abnormalities observed in this region are associated with structural synaptic changes of PN as well as reduced levels of NMDA/AMPA currents which sustain an hypothesis of an overall reduction in excitatory synaptic activity (Sceniak et al., 2016). Although the link between the RTT phenotype and the PFC seems to be obvious, considering that frontal cortical dysfunctions are found to contribute to ASD features, the specific components of the neuronal circuitry affected in that region and involved in the disease are still unclear.

CHAPTER 2

OBJECTIVES

AIMS

Previous studies point to the existence of an imbalance in E/I ratio related to the loss of MeCP2 function in the context of RTT. Considering the increased interest in over-inhibition of cortical networks in the context of the intellectual disability of RTT subjects, we hypothesize that specific alterations of distinct inhibitory GABAergic-IN circuits in the PFC may be contributing to the pathophysiology cognitive and sociability deficits in Rett Syndrome.

This research aims to characterize the GABAergic-IN population and their possible perturbations in RTT female mice model. To tackle these, our objectives were:

I. **Characterize the profile of key IN subtypes within distinct subregions of the prefrontal cortex,** through immunofluorescence analysis.

II. **Establish a relationship between differential patterns of MECP2 expression and IN profiles in the context of Rett syndrome,** by examination of immunoreactivity MECP2 levels.

CHAPTER 3

MATERIAL AND METHODS

MATERIALS AND METHODS

1. ETHICS STATEMENTS

All animal procedures were conducted in accordance with the European Community Council (EEC Union Directive 2010/63/EU.) for experimental animals; animal protocols were approved by the Animal Welfare Body of ICVS-I3Bs from the University of Minho (reference: ORBEA EM/ICVS-I3Bs/3Bs_012-2021). Mouse health monitoring was performed according to FELASA guidelines. The Specified Pathogen Free status of the facility was confirmed using sentinel mice housed in the same room. Humane endpoints were considered if necessary, including a 20% reduction of the body weight, incapacity to reach food and/or water, presence of wounds in the body or signs of dehydration. The animal facility and the people that worked directly in animal procedures were certified by the Portuguese regulatory – Direção Geral de Alimentação e Veterinária (DGAV).

2. THE MOUSE MODEL

Experiments were performed in 12-week-old (P(90)) *Mecp2*$^{tm1.1Bird}$ KO mouse line (Guy et al., 2001). *Mecp2* heterozygous female (*Mecp2*$^{+/-}$) mice and WT littermates were obtained of 3 months P(90) from our local mice colony. *Mecp2*$^{+/-}$ mice exhibit mobility problems starting at about 3 months, considered an early developmental stage for symptoms onset in comparison to other models. This RTT model (Guy et al., 2001) was originally obtained from the Jackson Laboratory (ME, USA). Each animal was individually genotyped to confirm identity accordingly to the protocol described below.

2.1 MAINTENANCE

All animals were kept in typical laboratory settings, which included a 12-hour artificial light cycle (lights on from 8:00 to 20:00), a temperature of 21°C, and relative humidity levels of 50–60%. All experiments were conducted following the guidelines of Portuguese national authority for animal experimentation, Direção Geral de Veterinária (ID: DGV9457)) and the Directive 2010/63/EU of the European Parliament and Council.

2.2. GENOTYPING

At weaning, animals were identified using ear clipping and a tail biopsy (~2mm) was collected for further genotyping. DNA was isolated from this tissue using a commercial DNA isolation kit (Citogene, Portugal). Briefly, mouse samples were incubated overnight (O/N), at 55°C, with 300 µl of cell lysis solution and 1µl of Proteinase K (Thermo Scientific, USA). On the following day, 100 µL of protein precipitation was added to the samples and they were vigorously vortexed. After, the samples were centrifuged at 13 000 rpm for 8 min. The supernatant, which contained the DNA, was collected, and precipitated by the addition of 300 µl of 100% (v/v) isopropanol and centrifugation at 13 000 rpm for 8 min. After the removal of the supernatant, 300 µl of 70 % (v/v) ethanol was added for a final centrifugation at 13 000 rpm for 5 min and the supernatant discarded. Finally, the remaining pellet was resuspended in 30 µl of DNA hydration solution until further processing.

Tail DNA samples were genotyped for *Mecp2* according to the protocol provided by The Jackson Laboratory (Guy et al., 2001; Samaco et al., 2013). The protocol involves the use of two sets of primers for each animal. Both sets contain three common primers (OIMR 1436: 5'GGT AAA GAC CCA TGT GAC CC'3; oIMR 042: 5'CTA GGC CAC AGA ATT GAA AGA TCT'3; and oIMR 043: 5'GTA GGT GGA AAT TCT AGC CAT CAT'3). The sets are distinguished by the presence of one unique primer each (oIMR 1437: 5' TCC ACC TAG CCT GCC TGT AC'3; oIMR 1438: 5'GGC TTG CCA CAT GAC AA'3) by polymerase chain reaction (PCR). The amplification conditions were set as follows: 5 min at 94°C, followed by 35 cycles of 1 min denaturation at 95°C, 1 min annealing at 64°C, 1 min extension at 72°C, and a final extension for 5 min at 72°C. The amplification products were loaded in 1.5 % (w/v) agarose gel using standard electrophoretic conditions.

2.3. MOUSE EUTHANASIA

Animals were anesthetized with an intraperitoneal injection of mixture of ketamine hydrochloride (150 mg/kg) and medetomidine (0.3 mg/kg) and withdrawal reflexes were assessed by toe pinching and, when absent, animals were transcardially perfused with NaCl 0.9% followed by ice-cold paraformaldehyde [4% in 0.1 M phosphate buffer (PB), pH 7.4]. Brains were harvested and were kept in PFA 4% for 2h, at room temperature (RT) with agitation. After this period, the brains were embedded in 30% sucrose at 4°C, until further slicing in the cryostat.

3. IMMUNOHISTOCHEMISTRY

3.1. SAMPLE PROCESSING

Following sample collection and preparation, the brain hemispheres were segmented in left and right side and both parts were then rapidly frozen in optimal cut temperature compound (OCT, Sakura Finitek, USA) and stored at -20℃. The PFCs were sectioned using a cryostat (CM1900, Leica Biosystems), at -20℃, into 30 μm free-floating coronal sections. Free-floating sections were later rinsed in PBS 1x to remove OCT debris and stored in 0.2 % (v/v) sodium azide in PBS 1x (pH 7.4) and stored at -20℃.

3.2. IMMUNOFLUORESCENCE

Brain tissue sections were rinsed 3 times in PBS for 10min and then placed in a 6-well plate containing heated citrate buffer 1x (#251275, Sigma-Aldrich, Germany) and incubated in a warm bath for 5min. The slices were permeabilized in PBS 1x supplemented with 0.5% Triton X-100 (PBS-T) 3 times 10min each, followed by 1h blocking with 10% (v/v) Normal Goat Serum (NGS) in 0.5% PBS-T, at RT. Sections were then simultaneously incubated O/N, at 4℃, with the primary antibodies prepared in 4% NGS in 0.3% PBS-T: rabbit anti-parvalbumin (detailed information on antibodies can be found in **Table 1**), under gentle agitation. On the following day, sections were washed 3 times for 10min with 0.3% PBS-T and probed for 2h with the respective secondary antibodies (**Table 1**) prepared in 4% NGS in 0.3% PBS-T, at RT. After 3 rinses with PBS 1x for 10 min, the slices were counterstained with 4′,6-diamidino-2-phenylindole (DAPI) (1:1000, D1306, Thermo Scientific) for 10min, followed by 2 rinses with PBS 1x for 10min.

For double immunofluorescence, following the antigen retrieval, the slices were permeabilized with 0.1% PBS-T for 15min and washed 3 times with 1x PBS to the blocking step in 0.3% PBS-T solution and 10% NGS by 1h, at RT. Sections were incubated continuously with the one of primary antibody prepared in 4% NGS in 0.3% PBS-T (**Table 1**), under gentle agitation O/N, at 4℃. On the following day, sections were washed 3 times for 10 min with 0.3% PBS-T and probed for 2h with the respective secondary antibodies (**Table 1**) prepared in 4% NGS in 0.3% PBS-T, at RT. After 3 rinses with PBS 1x for 10min, the slices were counterstained with DAPI (1:1000, D1306, Thermo Scientific) for 10min, followed by 2 rinses with PBS 1x for 10min.

Lastly, for both types of immunoassay protocols, all sections were mounted with (Thermo Scientific) onto microscope slides and then stored at 4°C, protected from the light. A negative control was also performed by omitting the primary antibodies.

Table 1. Detailed list of primary and secondary antibodies used in the immunofluorescence staining.

	Target	Host species	Working dilution	Reference	Supplier (country)
PRIMARY ANTIBODIES	Parvalbumin	Rabbit	1:500	PA1-933	Invitrogen (USA)
	MeCP2	Rabbit	1:500	D4F3	Cell signaling
	VIP	Guineapig	1:500	443 005	Synaptic Systems (Germany)
SECONDARY ANTIBODIES	Alexa-Fluor 488 anti-rabbit	Goat	1:1000	A-11034	Invitrogen (USA)
	Alexa-Fluor 647 anti-guineapig	Goat	1:1000	A-21450	Invitrogen (USA)

3.3. IMAGING

Images of immunostained cortical slices were acquired using an Olympus Widefield Inverted Microscope IX81 (Olympus, USA). Mosaic images were taken of each animal coronal slice (n=6 animals/genotype; 4 to 7 slices/animal). with a 20x objective. Acquisition parameters (detailed in **Table 2**) were maintained constant for each set of conditions. All photos were acquired with a resolution of 1316 x 1038.

Table 2. Detailed list of acquisition parameters for each fluorochrome used in the immunofluorescence staining assay.

	Target	Excitation and Emission	Exposure time	Gain
PV immunolabel assay	Alexa-Fluor 488 anti-rabbit	495-519 nm	199.90 ms	18 dB
	DAPI	358-461 nm	14.51ms	18 dB
VIP and MeCP2 immunolabel assay	Alexa-Fluor 488 anti-rabbit	495-519 nm	126.03 ms	18 dB
	Alexa-Fluor 647 anti-guineapig	663-690 nm	462.60 ms	18 dB
	DAPI	358-461 nm	18.00ms	18 dB

3.4. ANALYSIS

2D Image analyses were conducted in the FIJI software (Schindelin et al., 2012). The DAPI signal from brain coronal sections was used for registration against the Allen CCFv3 reference atlas (Wang et al., 2020) with the Aligning Big Brains and Atlases (ABBA) plugin in Fiji (Chiaruttini et al., 2022). Integrated tools in the ABBA software (manual affine transformation and spline transformation) were used to manually adjust brain alignment to the reference atlas The segmented brain regions were then imported into QuPath software (Bankhead et al., 2017) and used to quantify the number of positive cells in each brain region (**Figure 5**).

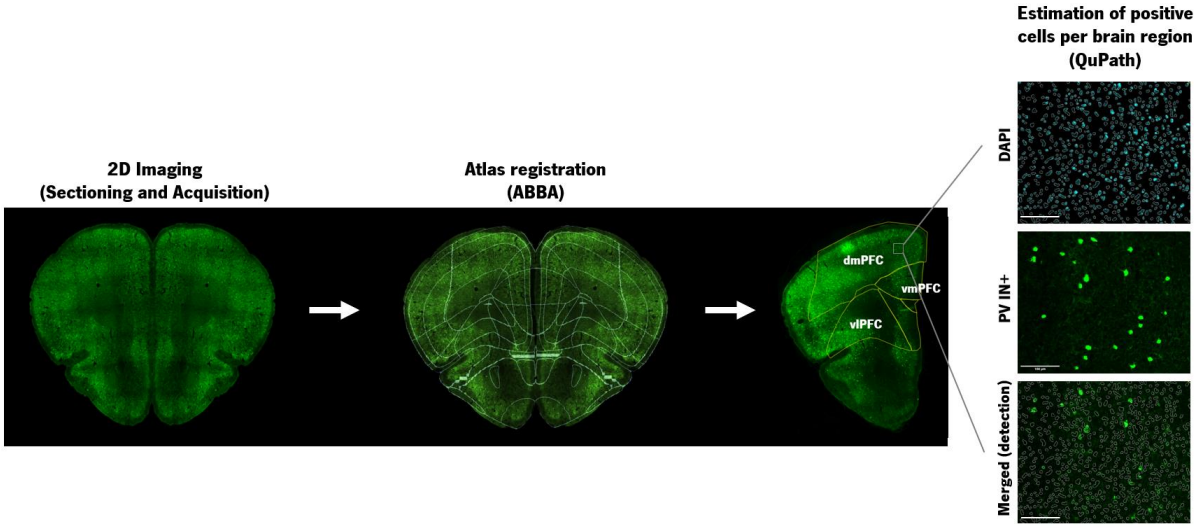


Figure 5. Schematic representation of semi-automated 2D fluorescence-based workflow for quantifying positive cells in IF assays. Coronal brain sections were aligned with the Allen CCFv3 reference atlas with the ABBA plugin in Fiji. The QuPath software was then used to identify and quantify positive signals. Scale bar = 100 µm.

The PV immunoreactivity analysis took into account images acquired from at least 4 coronal brain animal sections from female Mecp2$^{+/-}$ KO and WT mice littermates of 12-week-old. In QuPath, using the cell detection tool, PV+ cells were identify and measurements of each puncta in FITC channel retrieved (i.e.mean intensity, soma size and circularity). Based on the mean soma size extract of the PV+ puncta, only puncta with a minimum area of 40 µm^2 were included.

For each cortical area, we assessed the total density of PV+ immunolabeled cells, the mean fluorescence intensity, measured as average pixel intensity in each cell body and cumulative frequency distributions data per cell puncta. Additionally, histograms were also built by classifying PV+ cells into four subclasses, based on PV fluorescence intensity per soma size. The classification was done in IBM SPSS

Statistics 26.0 (IBM Inc, USA) with the z-score binning method, which calculates lower (l) and higher (h) PV intensity values based on the Mean ± Standard Deviation. The range of intensities was divided into four subclasses of PV+ INs as follows: low-PV; medium-low PV; medium-high PV and high-PV. Data were expressed as fraction (%) of PV+ INs.

For VIP immunoreactivity, the number of puncta was quantified, and the intensity of fluorescence retrieved. For each area, the number of VIP positive puncta was normalized for the defined area of interest.

Regarding MeCP2 immunoreactivity, puncta were counted and the mean intensity on 647 channels (secondary antibody for VIP) inside the MeCP2+ puncta extracted for each animal. To evaluate differential gene expression patterns, MeCP2 cell density values of *Mecp2*$^{-/y}$ mice were normalized for the WT based on a z-score process, in which values below the mean were represented as negative and those above the mean as positive. Analysis is represented on an heatmap. Hierarchical clustering analysis was performed on the normalized datasets to identify different groups through cluster-based quantification of *Mecp2* null cells. This is a statistical method that groups data into distinct clusters based on how similar they are. The Python programming language's SciPy library was used for clustering. The 'single' linkage method, which links clusters based on the smallest pairwise distance between each of their members, was used in the clustering process. The level of dissimilarity between data points was measured using the 'Euclidean' distance metric. The code used for this analysis is provided on supplementary information section.

4. STATISTICAL ANALYSES

All statistical analyses were performed using SPSS Statistics software, unless otherwise mentioned. Graphical representations were generated using GraphPad Prism 10 (GraphPad Software, USA). Data is presented in the format of mean ± SEM. To assess normality, we employed the Shapiro-Wilk test, and normality was presumed when $p > 0.05$. When normality was met, we employed parametric statistical tests; conversely, non-parametric tests were utilized when normality was not observed. Levene's test was employed to evaluate the equality of variances, assuming equality when $p > 0.05$. IF data was statistically analyzed using a two-tailed independent samples t-test comparing the mean between genotypes. Frequency distribution of PV+ cells was performed with a non-parametric test with mean intensity values of detected cells within each region. Probability values lower than 0.05 were considered statistically significant. In regard of the significance of effect size, Cohen's d was computed as an effect size measure whenever applicable.

CHAPTER 4

RESULTS

RESULTS

1. DIFFERENTIAL PATTERNS OF MeCP2 EXPRESSION IN FEMALE *Mecp2*$^{+/-}$ MICE

Recent reports have highlighted increased phenotypic heterogeneity among adult *Mecp2*$^{tm1.1Bird}$ mice, identifying two distinct patterns in goal-directed behavior closely associated with performance regression in behavioral tasks (Mykins, Bridges, et al., 2023). Accordingly, to the research, initially showing impaired performance in the pup-retrieval task, female mice were categorized into two distinct phenotypes: (I) those that demonstrated improved reaching efficiency comparable to WT mice and (II) those that exhibited a decline in efficiency. In light of this heterogeneity that arises from the differential loss of MeCP2 and its potential impact on circuitry aspects, our initial approach involved assessing the heterogeneity within our samples of female *Mecp2*$^{tm1.1Bird}$ mice (hereinafter referred as *Mecp2*$^{+/-}$) based on both anatomical criteria and expression patterns correlated with MeCP2 immunoreactivity.

Considering that previous reports have described that RTT mice display a reduced cortical thickness and smaller brain size (Fukuda et al., 2005; Kishi & Macklis, 2004; Mossner et al., 2020), we decided to perform an anatomical analysis of our areas of interest (**Figure 6A**). In general, genotype comparisons of 12-week-old animals did not reveal differences in size (dmPFC, WT: 2,56 mm^2 ± 0,24, *Mecp2*$^{+/-}$: 2,49 mm^2 ± 0,19, *t*-test $t_{(9)}$ = 0,492, p = 0,635; vlPFC, WT: 1,01 mm^2 ± 0,25, *Mecp2*$^{+/-}$: 1,17 mm^2 ± 0,16, *t*-test $t_{(9)}$ = 1,163, p = 0,275; vmPFC, WT: 1,07 mm^2 ± 0,07, *Mecp2*$^{+/-}$: 1,07 mm^2 ± 0,12, *t*-test $t_{(9)}$ = 0,001, p = 0,993).

Moreover, the percentage of MeCP2+ cells density across PFC subdivisions was analyzed to observe the amount of levels on the evaluated animals (**Figure 6B**). As anticipated, WT animals exhibited significantly higher levels of MeCP2 immunoreactivity than *Mecp2*$^{+/-}$ mice, although the sparse distribution unveiled that some *Mecp2*$^{+/-}$ mice displayed levels that were nearly comparable to those that of WT group (**Figure 6C**). The animals' MeCP2+ cell percentage values were normalized using z-scores to create a heatmap that visually represents differences in comparison to the WT values.

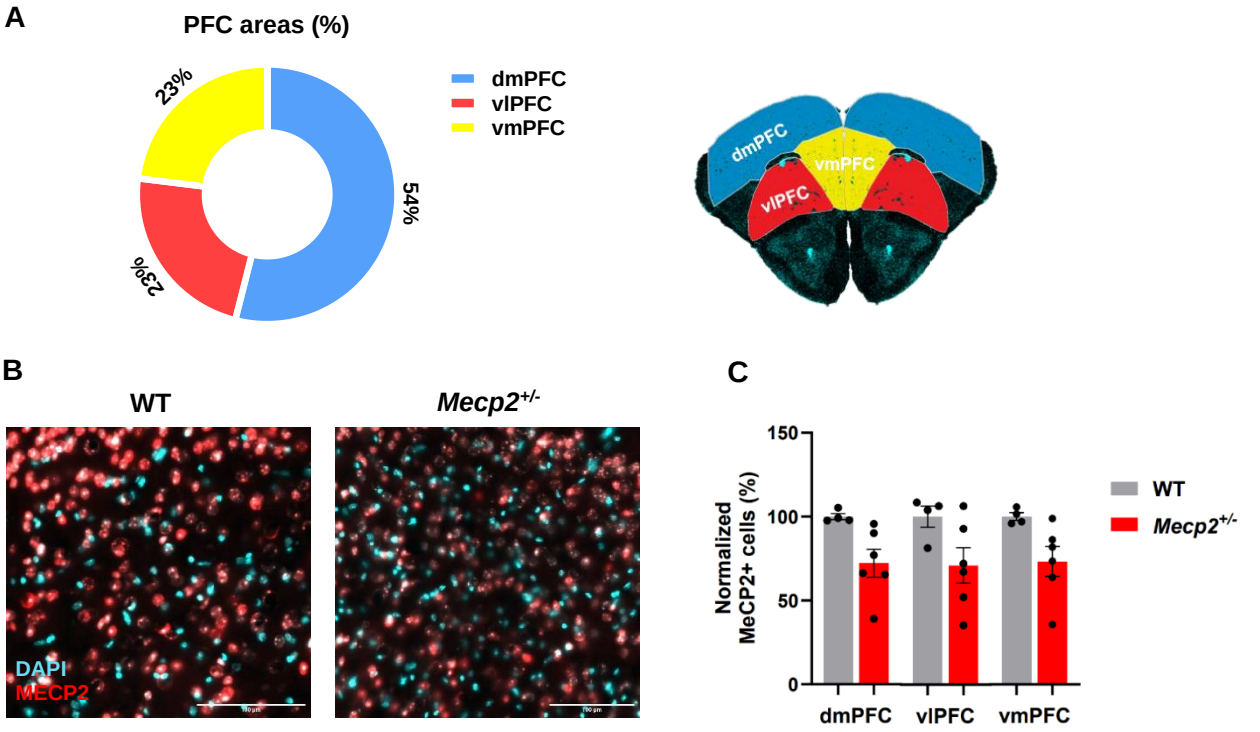


Figure 6. **PFC subdivision of *Mecp2*$^{+/-}$ mice have comparable area size percentages to WT and less MeCP2+ expression. (A)** The area percentage of subdivisions in relation to the entire prefrontal cortex. **(B)** Representative images of MeCP2 immunolabeled cells. **(C)** Histograms showing quantitative analysis of cell percentage of immunolabeled positive for MeCP2 normalized for WT values. Student's t test: *p < 0.05; **p< 0.01. Scale bar = 100 µm.

Previous studies have suggested a correlation of MeCP2 expression levels with severity of RTT-like phenotype (Archer et al., 2007). Considering the potential impact that differential MeCP2 expression could have on our IN cortical population analysis, we assessed the dual phenotypical differences through a Hierarchical Cluster Analysis based on the MeCP2+ cell density of PFC subdivisions. In **Figure 7A**, animal clusters indicate that within the same genotype, it is possible to differentiate animals by MeCP2+ cell density. Cluster 1 (C1) segregates animals with a larger deviation in mean cell percentage of MeCP2 from WT, while Cluster 2 (C2) includes animals with a smaller deviation. As a result, C1 can be associated with animals exhibiting cells with the highest rates of MeCP2 loss, while C2 is associated with animals showing the lowest rates.

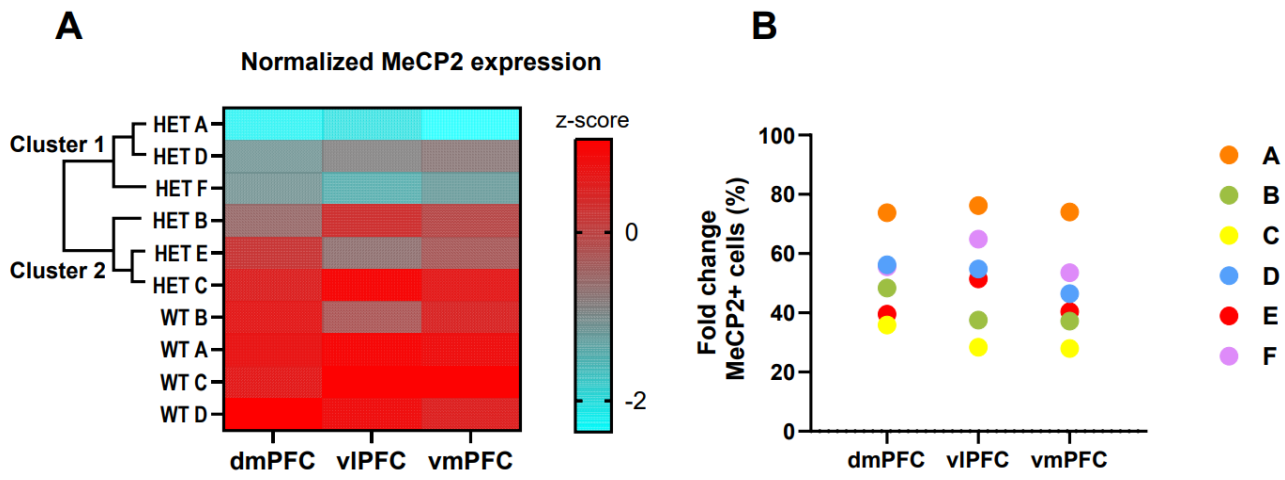


Figure 7. **Hierarchical clustering analysis of MeCP2 immunoreactivity indicates differential expression patterns in the same genotype of *Mecp2*$^{+/-}$ mice. (A)** Heat map base on z-score showing the profile of differentially MeCP2 immunolabeled cells percentage in WT and *Mecp2*$^{+/-}$ mice at P(90). Each horizontal line represents one animal and each column the analyzed area. Color legend is on the right of figure. Blue represents increased in MeCP2 immunolabeled cells, while red indicates animals with reduced MeCP2 cells relative to the geometrical means. **(B)** Dot plot representation of percentage of MeCP2 cell density fold change of females *Mecp2*$^{+/-}$ in comparison to the WT animals.

Additionally, fold changes of MeCP2 density of *Mecp2*$^{+/-}$ mice were assessed to quantify the loss rates of MeCP2 in each animal in comparison with WT. Animals of C1 exhibited the highest rates of fold change in the three divisions of the PFC (**Figure 7B**). Specially, animal *HET A* exhibited the highest rates of MeCP2 loss with a 74% decrease of MeCP2 cells density in comparison with WT animals. The other two animals, *HET D* and *HET F,* had MeCP2 cell rates that were on average 50% lower than those of the WT, as displayed in **Table 3**.

To analyze if these differential MeCP2 expression patterns could implicate in PV+ and VIP+ cell distributions in same-genotype animals, we assessed cell density comparison of IN+ labeled of C1 and C2 animals (**Figure 8 A-B**). No statistical differences were observed in the cell density of PV+ and VIP+ cells distributions when we compare animals that exhibit different levels of MeCP2 loss. However, as shown in the fold changes percentage (**Table3**), the animal samples display a highly heterogeneous levels of MeCP2 expression that could be underlying the absence of quantifiable differences in IN cell density when scrutinizing by cluster segmentation.

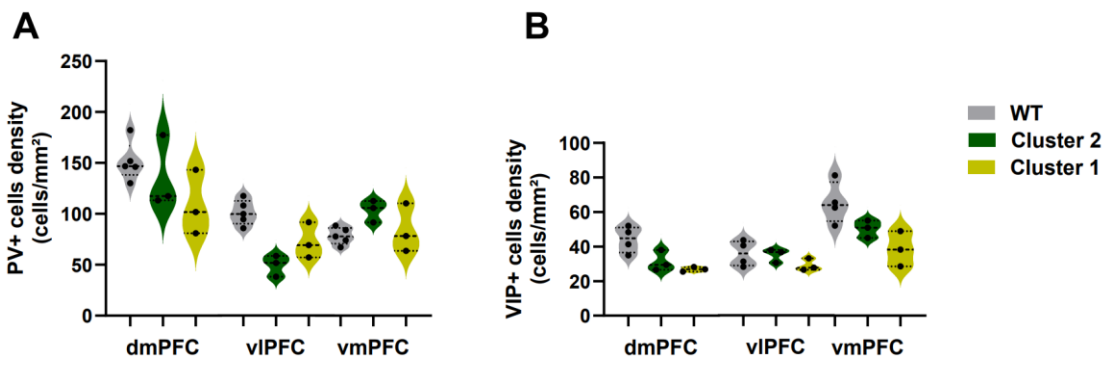


Figure 8. **Cluster groups comparison of IN+ cell density with WT (A)** Histograms showing quantitative analysis of PV+ cell density and **(B)** VIP+ IN cell density in WT and *Mecp2*$^{-/y}$ mice at P(90). Student's t test: *p < 0.05; **p< 0.01. Scale bar = 100 µm

Table 3. Report on the hierarchical clustering analysis of three PFC subregions and fold change percentage of MeCP2 density.

	Measurements	dmPFC	vlPFC	vmPFC	Descriptive statistics[1]
HET A	**Mean MeCP2/DAPI (%)**	26,219	23,775	26,000	25,330 ± 0,011
	Z-score	-2,22	0,13	-1,95	-
	Fold change (%)	73,78	76,22	74	74,667 ± 1,102
HET B	**Mean MeCP2/DAPI (%)**	51,624	62,480	62,820	58,975 ± 0,052
	Z-score	-0,32	0,42	0,11	-
	Fold change (%)	48,38	37,52	37,18	41,027 ± 5,201
HET C	**Mean MeCP2/DAPI (%)**	64,102	71,592	72,047	69,247 ± 0,036
	Z-score	0,62	0,98	0,73	-
	Fold change (%)	35,9	28,41	27,95	30,753 ± 3,644
HET D	**Mean MeCP2/DAPI (%)**	43,825	45,213	53,567	47,535 ± 0,043
	Z-score	-0,90	-0,64	-0,51	-
	Fold change (%)	56,18	54,79	46,43	52,467 ± 4,306
HET E	**Mean MeCP2/DAPI (%)**	60,438	48,558	59,637	56,211 ± 0,054
	Z-score	0,34	-0,43	-0,11	-
	Fold change (%)	39,56	51,44	40,36	43,787 ± 5,422
HET F	**Mean MeCP2/DAPI (%)**	44,415	35,091	46,499	42,002 ± 0,050
	Z-score	-0,86	-1,26	-0,99	-
	Fold change (%)	55,58	64,91	53,5	57,997 ± 4,962

2. REGION-SPECIFIC VARIATIONS OF PV+ CELL DENSITY IN SYMPTOMATIC *Mecp2*$^{-/y}$ MICE

Previous studies demonstrated an alteration in the parvalbumin (PV)-positive IN organization in the sensory-motor and auditory cortical brain regions of *Mecp2*$^{tm1.1Jae}$ null mice (Morello et al., 2018; Tomassy et al., 2014; Rupert et al., 2023). In these cortical regions, increased expression of perineuronal nets and extracellular matrix structures around GABAergic PV cells are correlated to structurally restricted plasticity (Ueno et al., 2017; Lau et al., 2020). However, observations of a general cortical hypoactivity, analysis of the mPFC of *Mecp2*$^{tm1.1Jae}$ null mice have shown no difference in PV density (Sceniak et al., 2016). Therefore, considering the relevance of the PFC to cognitive and emotional processes (Le Merre et al., 2021) and the observed motor and emotional deficits in the RTT mouse model herein used (Mykins, Bridges, et al., 2023), we sought to further characterize the impact of MeCP2 loss in key inhibitory cells across different PFC regions in the *Mecp2*$^{tm1.1Bird}$ of heterozygous female mice.

The representative images of WT and *Mecp2*$^{-/y}$ PV immunoreactive cells covering dmPFC are presented in **Figure** (**9A**). A reduction of PV+ cell was observed in *Mecp2*$^{-/y}$ mice when compared with WT littermate animals (**Figure 9B**). In contrast, an increased fluorescence intensity in the cells that were PV+ was detected (**Figure 9C**). The relative frequency distribution of PV intensity showed a curve deviation to the right side in *Mecp2*$^{-/y}$ mice, higher intensities being found when compared to control mice (**Figure 9D**). In accordance, the intensity level for each individual PV^{+}-cell within each mouse, showed different intensity profiles, where it is possible to observe an increased percentage of cells expressing high levels of PV in *Mecp2*$^{-/y}$ mice (**Figure 9E**).

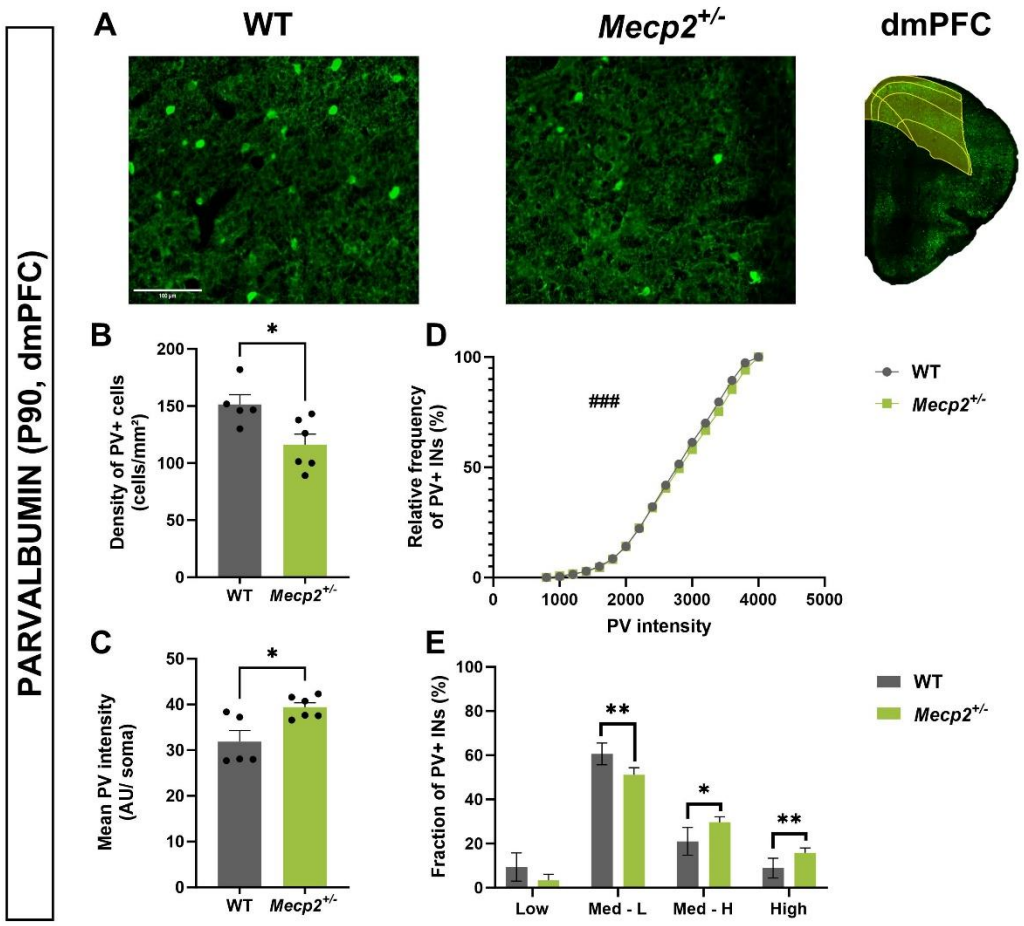


Figure 9. **Atypical high-PV expression in the dmPFC cortex of *Mecp2*$^{+/-}$. (A)** Representative images showing PV labeling in dmPFC in WT and *Mecp2*$^{+/-}$ mice at P(90). Histograms showing quantitative analysis of PV+ cell density **(B)**, PV mean fluorescence intensity **(C)**, cumulative **(D)** and binned frequency distribution of PV cells intensity **(E)** in WT and *Mecp2*$^{+/-}$ mice at P(90). Student's t test: *p < 0.05; **p< 0.01, Mann–Whitney U test for **D:** ##p < 0.01; ###p < 0.001. Scale bar = 100 µm.

In the vlPFC of *Mecp2*$^{+/-}$ mice (representative images present in **Figure 10A**), no statistical difference was observed in the density of PV+ cells when compared with WT littermate animals (**Figure 10B**), nor in the mean PV fluorescence intensity (**Figure 10C**). The relative frequency distribution of PV intensity also exhibits comparable values to WT (**Figure 10D**). Conversely, the intensity level for each individual PV+ cell within each mouse, showed different intensity profiles, a similar tendency as observed in the dmPFC, reaching it statistical significance by the reduced number of medium-low PV fractions in the *Mecp2*$^{+/-}$ mice (**Figure 10E**). The statistical report of each assessed parameter is presented in **Table 4**.

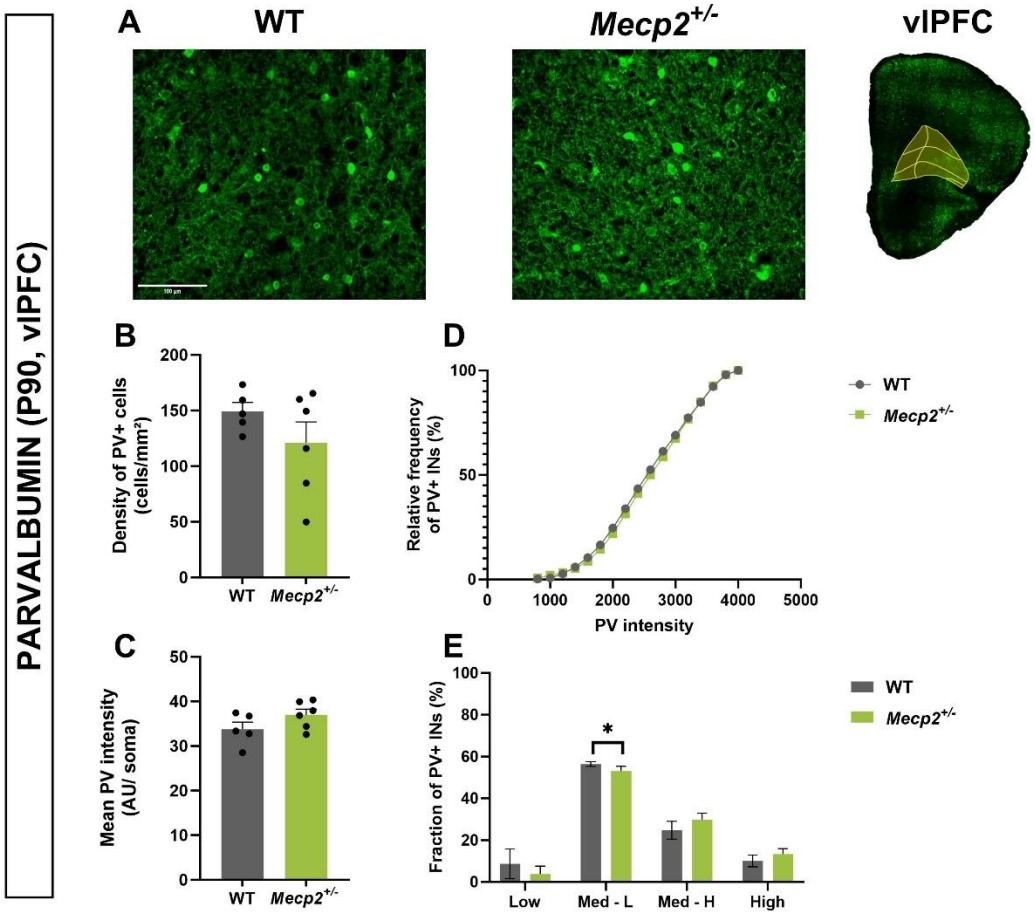


Figure 10. **PV expression in the vlPFC cortex of *Mecp2*$^{+/-}$ shows similar tendency of increase.** (A) Representative images showing PV labeling in vlPFC in WT and *Mecp2*$^{+/-}$ mice at P(90). Histograms showing quantitative analysis of PV+ cell density (B), PV mean fluorescence intensity (C), cumulative (D) and binned frequency distribution of PV cells intensity (E) in WT and *Mecp2*$^{+/-}$ mice at P(90). Student's t test: *p < 0.05; **p< 0.01, Mann–Whitney U test for D: ##p < 0.01; ###p < 0.001. Scale bar = 100 µm.

In **Figure 11A**, representative images of PV immunolabel cell in the vmPFC of *Mecp2*$^{+/-}$ mice are display. The PV+ cell density on the area exhibit values comparable to that of WT littermate animals (**Figure 11B**). However, the mean fluorescence intensity analysis showed statistical differences, with an enhancement in the *Mecp2*$^{+/-}$ (**Figure 11C**). The relative frequency distribution of PV intensity exhibited comparable values to WT (**Figure 11D**). Conversely, the intensity level for each individual PV+ cell within each mouse, showed different intensity profiles, a similar tendency to that observed in the dmPFC, not reaching statistical significance due to the reduced number of medium-low PV fractions in the *Mecp2*$^{+/-}$ mice (**Figure 11E**).

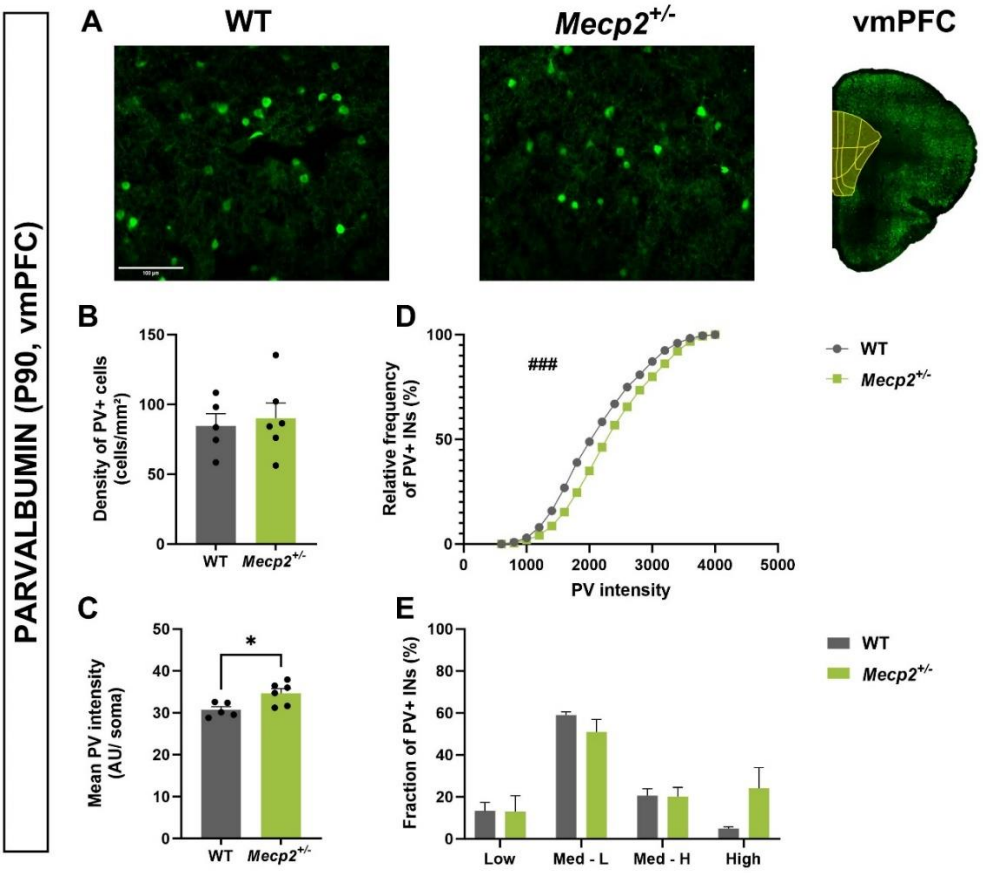


Figure 11. **Altered PV expression in the vmPFC cortex of *Mecp2*$^{+/-}$. (A)** Representative images showing PV labeling in vmPFC in WT and *Mecp2*$^{+/-}$ mice at P(90). Histograms showing quantitative analysis of PV+ cell density **(B)**, PV mean fluorescence intensity **(C)**, cumulative **(D)** and binned frequency distribution of PV cells intensity **(E)** in WT and *Mecp2*$^{+/-}$ mice at P(90). Student's t test: *p < 0.05; **p< 0.01, Mann–Whitney U test for **D:** ##p < 0.01; ###p < 0.001. Scale bar = 100 µm.

Table 4. Statistical report on the PV+ IN analysis of tree PFC subregions. The respective statistical test and significance is presented for each metric assessed.

	Measurement	Descriptive statistics[1]	Comparison	Statistical test	Significance
Fig. 9A	PV cell density	**WT:** 151,384 ± 16,998 ***Mecp2*$^{-/-}$:** 122,277 ± 34,118	WT vs *Mecp2*$^{-/-}$	Unpaired *t*-test $t_{(9)}$ = 2.77	p = 0.021
Fig. 9B	PV fluorescence intensity	**WT:** 31,885 ± 4,848 ***Mecp2*$^{-/-}$:** 39,404 ± 2,221	WT vs *Mecp2*$^{-/-}$	Unpaired t-test $t_{(9)}$ = 3.07	p = 0,013
Fig. 9C	Relative frequency of PV INs	**WT:** 2844,631; n=8513 ***Mecp2*$^{-/-}$:** 2886,112; n=7844	WT vs *Mecp2*$^{-/-}$	Mann–Whitney U test	p < 0.0001
Fig. 9D	Fraction of PV INs	**WT:** 0,090 ± 0,046 ***Mecp2*$^{-/-}$:** 0,158 ± 0,020	WT vs. *Mecp2*$^{-/-}$ (high PV)	Unpaired t-test $t_{(9)}$ = -3,306	p = 0,009
		WT: 0,210 ± 0,061 ***Mecp2*$^{-/-}$:** 0,298 ± 0,023	WT vs. *Mecp2*$^{-/-}$ (medium-high PV)	Unpaired t-test $t_{(9)}$ = -3,291	p = 0,009
		WT: 0,604 ± 0,050 ***Mecp2*$^{-/-}$:** 0,510 ± 0,034	WT vs. *Mecp2*$^{-/-}$ (medium-low PV)	Unpaired t-test $t_{(9)}$ = 3,691	p = 0,005
		WT: 0,094 ± 0,061 ***Mecp2*$^{-/-}$:** 0,037± 0,028	WT vs. *Mecp2*$^{-/-}$ (low PV)	Unpaired t-test $t_{(9)}$ = 2,080	p = 0,067
Fig. 10A	PV cell density	**WT:** 149,203 ± 16,081 ***Mecp2*$^{-/-}$:** 120,904 ± 42,233	WT vs *Mecp2*$^{-/-}$	Unpaired t - test $t_{(9)}$ = 1,28	p = 0,233
Fig. 10B	PV fluorescence intensity	**WT:** 33,762 ± 3,187 ***Mecp2*$^{-/-}$:** 37,015 ± 2,796	WT vs *Mecp2*$^{-/-}$	Unpaired t-test $t_{(9)}$ = -1,631	p = 0,137
Fig. 10C	Relative frequency of PV INs	**WT:** 2652,073; n=4120 ***Mecp2*$^{-/-}$:** 2682,866; n=3566	WT vs *Mecp2*$^{-/-}$	Mann–Whitney U test	p = 0,021
Fig. 10D	Fraction of PV INs	**WT:** 0,102 ± 0,030 ***Mecp2*$^{-/-}$:** 0,133 ± 0,024	WT vs. *Mecp2*$^{-/-}$ (high PV)	Unpaired t-test $t_{(9)}$ = -1,909	p = 0,089
		WT:0,248 ± 0,042 ***Mecp2*$^{-/-}$:** 0,298 ± 0,032	WT vs. *Mecp2*$^{-/-}$ (medium-high PV)	Unpaired t-test $t_{(9)}$ = -3,291	p = 0,050
		WT: 0,564 ± 0,013 ***Mecp2*$^{-/-}$:** 0,532 ± 0,026	WT vs. *Mecp2*$^{-/-}$ (medium-low PV)	Unpaired t-test $t_{(9)}$ = 3,691	p = 0,032
		WT: 0,088 ± 0,072 ***Mecp2*$^{-/-}$:** 0,040 ± 0,039	WT vs. *Mecp2*$^{-/-}$ (low PV)	Unpaired t-test $t_{(9)}$ = 2,080	p = 0,191
Fig. 11A	PV cell density	**WT:** 84,74 ± 19,56 ***Mecp2*$^{-/-}$:** 90,18 ± 26,75	WT vs *Mecp2*$^{-/-}$	Unpaired t-test $t_{(9)}$ = - 0,377	p = 0,715
Fig. 11B	PV fluorescence intensity	**WT:** 30,703 ± 1,536 ***Mecp2*$^{-/-}$:** 34,668 ± 2,467	WT vs *Mecp2*$^{-/-}$	Unpaired t-test $t_{(9)}$ = - 2,826	p = 0,020
Fig. 11C	Relative frequency of PV INs	**WT:** 2208,406, n=2138 ***Mecp2*$^{-/-}$:** 2427,327, n=2359	WT vs *Mecp2*$^{-/-}$	Mann–Whitney U test	p < 0.0001
Fig. 11D	Fraction of PV INs	**WT:** 0,049 ± 0,018 ***Mecp2*$^{-/-}$:** 0,242 ± 0,241	WT vs. *Mecp2*$^{-/-}$ (high PV)	Unpaired t-test $t_{(9)}$ = -1,765	p = 0,111
		WT: 0,206 ± 0,073 ***Mecp2*$^{-/-}$:** 0,201 ± 0,107	WT vs. *Mecp2*$^{-/-}$ (medium-high PV)	Unpaired t-test $t_{(9)}$ = 0,085	p = 0,934
		WT:0,590 ± 0,35 ***Mecp2*$^{-/-}$:** 0,510 ± 0,147	WT vs. *Mecp2*$^{-/-}$ (medium-low PV)	Unpaired t-test $t_{(9)}$ = 1,190	p = 0,264
		WT: 0,096 ± 0,100 ***Mecp2*$^{-/-}$:** 0,129 ± 0,186	WT vs. *Mecp2*$^{-/-}$ (low PV)	Unpaired t-test $t_{(9)}$ = -0,354	p = 0,732

[1]: In case of: Unpaired t-test (Mean ± SD); Mann–Whitney U test (Median ; n)

Examination of the vmPFC subdivision helped us to trace from each region differences in the fractions of PV+ cell with higher level of PV expression was observed on. Representative images of PV immunoreactive cells in the IL cortex are display in **Figure 12A**. Consistently with the low baseline cell density observed in the vmPFC, in the IL both genotypes exhibit uniform PV+ cell density values (**Figure 12B**). Conversely, the PV intensity analysis unveiled the most affected area within the vmPFC: the infralimbic cortex (**Figure 12C**). *Mecp2*$^{+/-}$ mice exhibited an increase of the relative frequency of PV+ cells with high levels of PV expression (**Figure 12D**), that can be better visualized by the elevated fractions of medium-high PV expression in *Mecp2*$^{+/-}$ mice in comparison with WT (**Figure 12E**).

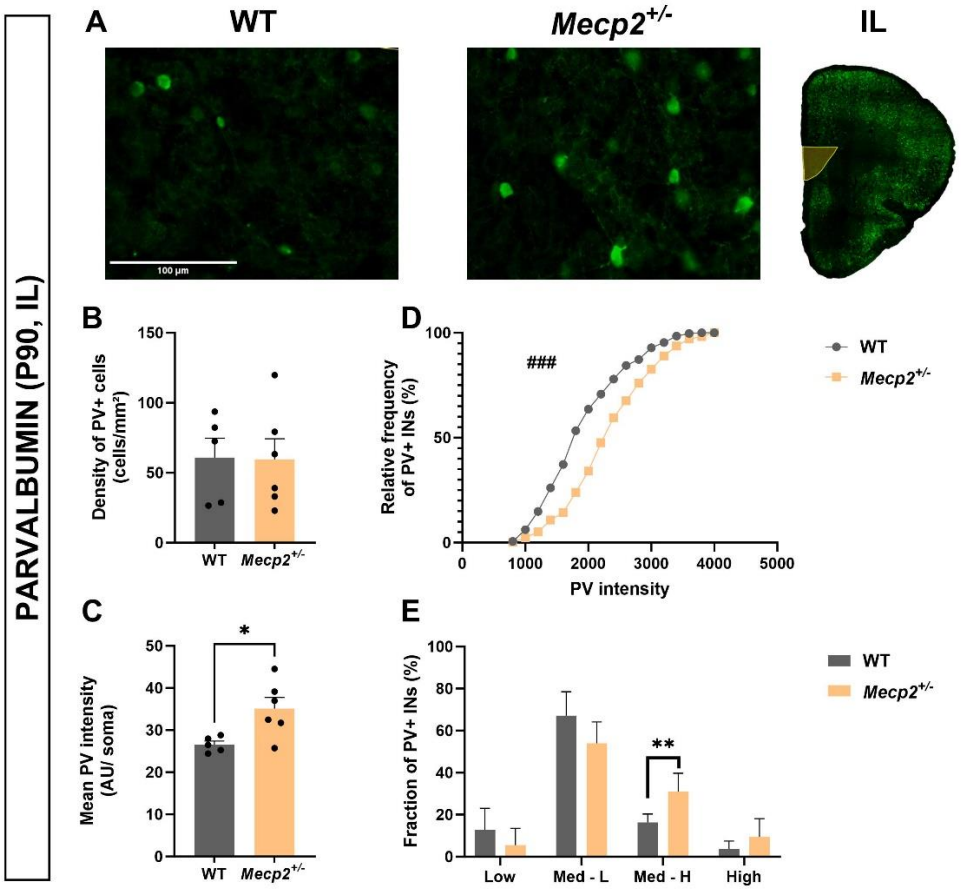


Figure 12. **Increased high PV cell fraction in the IL cortex of *Mecp2*$^{+/-}$ mice underlying the observed intensity differences within vmPFC. (A)** Representative images showing PV labeling in IL in WT and *Mecp2*$^{+/-}$ mice at P(90). Histograms showing quantitative analysis of PV+ cell density **(B)**, PV mean fluorescence intensity **(C)**, cumulative **(D)** and binned frequency distribution of PV cells intensity **(E)** in WT and *Mecp2*$^{+/-}$ mice at P(90). Student's t test: *p < 0.05; **p< 0.01, Mann–Whitney U test for **D:** ##p < 0.01; ###p < 0.001. Scale bar = 100 µm.

Within the other areas of vmPFC, no significant difference was observed in the cell density and mean intensity in m0RB **Figure 13**(**B-C**) However, relative frequency distribution in m0RB (**Figure 13D**) shows that in in *Mecp2*$^{+/-}$mice there is an enhanced percentage of cell exhibiting higher values of PV intensity, revealing some similarities with the other studied regions where a slight trend towards an increase in PV expression is observed (**Figure13E**). Similar aspects are observed in PL area. Cell density and mean intensity reveal no difference, as shown in **Figure** (**G-H**). Conversely, relative frequency shows statistical differences in the percentage of PV+ cells exhibiting higher values of intensity (**Figure I**) in *Mecp2*$^{+/-}$mice, however, cell fraction comparison shown no particular statistical difference (**Figure 13J**). The statistical report is displayed in **Table 5**.

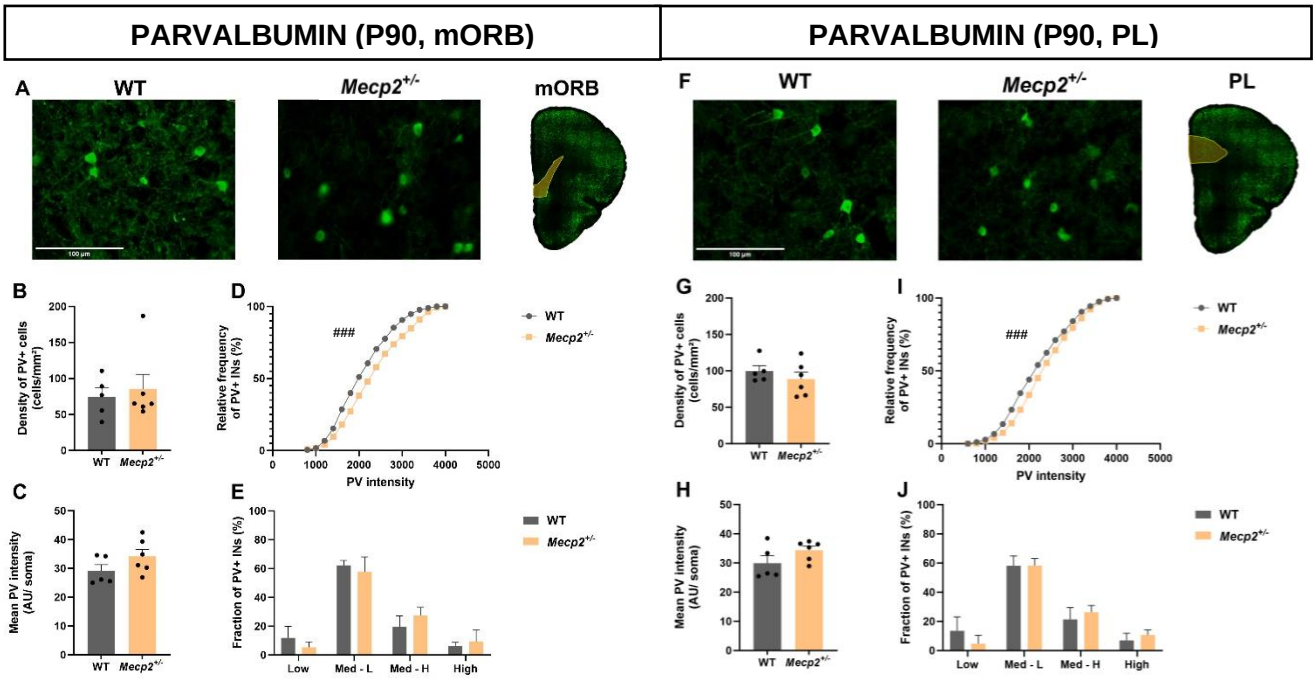


Figure 13. *Mecp2*$^{+/-}$ have an overall slight enhance in high PV cell fraction in the mORB and PL cortex. **(A)** Representative images showing PV labeling in mORB in WT and *Mecp2*$^{+/-}$ mice at P(90). Histograms showing quantitative analysis of PV+ cell density **(B)**, PV mean fluorescence intensity **(C)**, cumulative **(D)** and binned frequency distribution of PV cells intensity **(E)** in WT and *Mecp2*$^{+/-}$ mice at P(90). **(F)** Representative images showing PV labeling in PL in WT and *Mecp2*$^{+/-}$ mice at P(90). Histograms showing quantitative analysis of PV+ cell density **(G)**, PV mean fluorescence intensity **(H)**, cumulative **(I)** and binned frequency distribution of PV cells intensity **(J)** in WT and *Mecp2*$^{+/-}$ mice at P(90). Student's t test: *p < 0.05; **p< 0.01, Mann–Whitney U test for **D:** ##p < 0.01; ###p < 0.001. Scale bar = 100 µm.

Table 5. Statistical report on the PV+ IN analysis of vmPFC divisions. The respective statistical test and significance is presented for each metric assessed.

	Measurement	Descriptive statistics[1]	Comparison	Statistical test[1]	Significance
Fig. 12A	PV cell density	**WT:** 60,76 ± 27,865 ***Mecp2*$^{-/y}$:** 59,588 ± 32,875	WT vs *Mecp2*$^{-/y}$	Unpaired *t*- test $t_{(9)}$ = 0,057	p = 0,956
Fig. 12B	PV fluorescence intensity	**WT:** 26,595 ± 1,628 ***Mecp2*$^{-/y}$:** 35,101 ± 5,985	WT vs *Mecp2*$^{-/y}$	Unpaired *t*- test $t_{(9)}$ = -2,790	p = 0,021
Fig. 12C	Relative frequency of PV INs	**WT:** 1981,634; n=323 ***Mecp2*$^{-/y}$:** 2395,612 ; n=335	WT vs *Mecp2*$^{-/y}$	Mann–Whitney U test	p < 0.0001
Fig. 12D	Fraction of PV INs	**WT:** 0,037 ± 0,037 ***Mecp2*$^{-/y}$:** 0,0940 ± 0,087	WT vs. *Mecp2*$^{-/y}$ (High PV)	Unpaired *t*- test $t_{(9)}$ = -1,350	p = 0,210
		WT: 0,163 ± 0,040 ***Mecp2*$^{-/y}$:** 0,311 ± 0,086	WT vs. *Mecp2*$^{-/y}$ (Medium-high PV)	Unpaired *t*- test $t_{(9)}$ = -3,501	p = 0,007
		WT: 0,671 ± 0,114 ***Mecp2*$^{-/y}$:** 0,539 ± 0,102	WT vs. *Mecp2*$^{-/y}$ (Medium-low PV)	Unpaired *t*- test $t_{(9)}$ = 2,023	p = 0,074
		WT: 0,128 ± 0,102 ***Mecp2*$^{-/y}$:** 0,056 ± 0,080	WT vs. *Mecp2*$^{-/y}$ (Low PV)	Unpaired *t*- test $t_{(9)}$ = 1,326	p = 0,217
Fig. 13A	PV cell density	**WT:** 74,337 ± 24,902 ***Mecp2*$^{-/y}$:** 85,186 ± 46,055	WT vs *Mecp2*$^{-/y}$	Unpaired *t*- test $t_{(9)}$ = 0,883	p = 0,400
Fig. 13B	PV fluorescence intensity	**WT:** 29,117 ± 4,363 ***Mecp2*$^{-/y}$:** 34,192 ± 5,366	WT vs *Mecp2*$^{-/y}$	Unpaired *t*- test $t_{(9)}$ = -1,536	p = 0,159
Fig. 13C	Relative frequency of PV INs	**WT:** 2162,163; n=578 ***Mecp2*$^{-/y}$:** 2406,324; n=732	WT vs *Mecp2*$^{-/y}$	Mann–Whitney U test	p < 0.0001
Fig. 13D	Fraction of PV INs	**WT:** 0,062 ± 0,026 ***Mecp2*$^{-/y}$:** 0,095 ± 0,078	WT vs. *Mecp2*$^{-/y}$ (High PV)	Unpaired *t*- test $t_{(9)}$ = -0,889	p = 0,397
		WT: 0,196 ± 0,075 ***Mecp2*$^{-/y}$:** 0,273 ± 0,058	WT vs. *Mecp2*$^{-/y}$ (Medium-high PV)	Unpaired *t*- test $t_{(9)}$ = -1,937	p = 0,085
		WT: 0,623 ± 0,034 ***Mecp2*$^{-/y}$:** 0,579 ± 0,102	WT vs. *Mecp2*$^{-/y}$ (Medium-low PV)	Unpaired *t*- test $t_{(9)}$ = 0,916	p =0,383
		WT: 0,119 ± 0,081 ***Mecp2*$^{-/y}$:** 0,053 ± 0,038	WT vs. *Mecp2*$^{-/y}$ (Low PV)	Unpaired *t*- test $t_{(9)}$ = 1,784	p = 0,108
Fig. 13G	PV cell density	**WT:** 99,713 ± 14,737 ***Mecp2*$^{-/y}$:** 88,692 ± 21,373	WT vs *Mecp2*$^{-/y}$	Unpaired *t*- test $t_{(9)}$ = -0,427	p = 0,679
Fig. 13H	PV fluorescence intensity	**WT:** 29,943 ± 5,147 ***Mecp2*$^{-/y}$:** 34,366 ± 3,106	WT vs *Mecp2*$^{-/y}$	Unpaired *t*- test $t_{(9)}$ = -1,588	0,147
Fig. 13I	Relative frequency of PV INs	**WT:** 2289,932; n=1239 ***Mecp2*$^{-/y}$:** 2447,403 ± n=1294	WT vs *Mecp2*$^{-/y}$	Mann–Whitney U test	p < 0.0001
Fig. 13J	Fraction of PV INs	**WT:** 0,069 ± 0,050 ***Mecp2*$^{-/y}$:** 0,107±0,035	WT vs. *Mecp2*$^{-/y}$ (High PV)	Unpaired *t*- test $t_{(9)}$ = -1,468	p = 0,176
		WT: 0,213 ± 0,082 ***Mecp2*$^{-/y}$:** 0,263 ± 0,046	WT vs. *Mecp2*$^{-/y}$ (Medium-high PV)	Unpaired *t*- test $t_{(9)}$ = -1,275	p = 0,234
		WT: 0,582 ± 0,66 ***Mecp2*$^{-/y}$:** 0,583 ± 0,048	WT vs. *Mecp2*$^{-/y}$ (Medium-low PV)	Unpaired *t*- test $t_{(9)}$ = -0,006	p = 0,995
		WT: 0,135 ± 0,096 ***Mecp2*$^{-/y}$:** 0,047± 0,057	WT vs. *Mecp2*$^{-/y}$ (Low PV)	Unpaired *t*- test $t_{(9)}$ = 1,883	p = 0,092

[1]: In case of: Unpaired t-test (Mean ± SD); Mann–Whitney U test (Median ; n)

3. DECREASED CORTICAL DENSITY OF VIP+ IN IN FEMALE *Mecp2*$^{+/-}$ MICE

Previous reports of RTT mouse models, have shown that GABAergic cortical IN populations express MeCP2 protein at approximately twice the level as observed in non-GABAergic cells (Chao et al., 2010), and revealed high levels of expression with the three major IN subtypes (Ito-Ishida et al., 2015; Mossner et al., 2020). Furthermore, selective deletion of the *Mecp2* gene within IN populations resulted in the replication of phenotypic abnormalities, particularly affecting PV+ and VIP+ populations, while the same deletion in SST+ population showed no discernible impact (Ito-Ishida et al., 2015; Mossner et al., 2020; Rupert et al., 2023). Despite being known for a sparse distribution, cortical dysfunction of the VIP+ IN population appears to play a significant role in the development of RTT and RTT-like phenotypes. On that account, we performed a density analysis of the cortical VIP+ neuronal population, which revealed a region-specific effect in *Mecp2*$^{+/-}$ mice (**Figure 14A**). Specifically, in the dmPFC and vmPFC region, there was a statistically significant decrease in VIP+ IN density compared to the at 12-week-old of WT mice (**Figure 14B**). This reduction is a distinctive feature of both areas, as no statistically significant difference is observed in the vlPFC regions, where IN density remains comparable in terms of numeric counts and homogenized sample distribution between the two phenotypes. The statistical data is presented in **Table 6**.

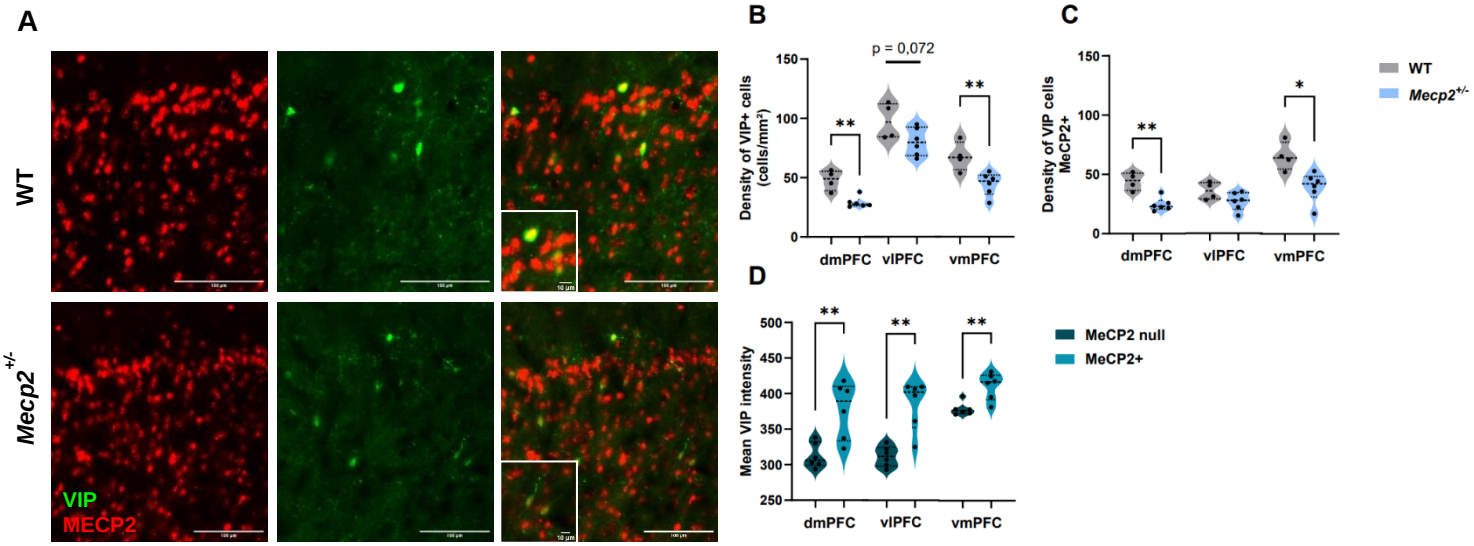


Figure 14. **MeCP2-expressing cells exhibit an increase in VIP+ immunoreactivity (A)** Representative images showing VIP and MeCP2 immunoreactivity in PFC regions **(B)** Histograms showing quantitative analysis of VIP+ cell density, **(C)** VIP+ IN co-expressing MeCP2 density in WT and *Mecp2*$^{+/-}$ mice at P(90). **(D)** Comparison analysis of mean VIP intensity of cells MeCP2 null and MeCP2 positive (+) of *Mecp2*$^{+/-}$ mice. Student's t test: *p < 0.05; **p< 0.01. Scale bar = 100 µm.

To determine the rates of MeCP2 co-expression with VIP+, we assessed the percentage of cells that were positive for both staining's. Although no statistically significant differences were observed in genotype comparisons, a consistent trend toward reduced co-expression of the two proteins is evident across all three PFC regions, specially, the dorsal and ventral medial parts (**Figure 14C**).

Table 6. Statistical report on the VIP+ IN analysis of tree PFC subregions. The respective statistical test, significance, and effect size (whenever applicable) is presented for each metric assessed.

	Measurement	Descriptive statistics[1]	Region	Comparison	Statistical test	Significance
Fig. 13B	VIP cell density	**WT:** 47,880 ± 7,433 ***Mecp2*$^{+/-}$:** 29,077 ± 4,188	dmPFC	WT vs *Mecp2*$^{+/-}$	Unpaired *t*- test $t_{(8)}$ = 4,562	p = 0,001
		WT: 39,752 ± 4,774 ***Mecp2*$^{+/-}$:** 32,094 ± 4,286	vlPFC	WT vs *Mecp2*$^{+/-}$	Unpaired *t*- test $t_{(8)}$ = 2,07	p = 0,072
		WT: 67,778 ± 10,675 ***Mecp2*$^{+/-}$:** 44,496 ± 8,817	vmPFC	WT vs *Mecp2*$^{+/-}$	Unpaired *t*- test $t_{(8)}$ = 3,36	p = 0,001
Fig. 13C	VIP cells *Mecp2*+ density	**WT:** 44,144 ± 6,525 ***Mecp2*$^{+/-}$:** 24,489 ± 5,161	dmPFC	WT vs *Mecp2*$^{+/-}$	Unpaired *t*- test $t_{(8)}$ = 4,74	p = 0,001
		WT: 35,921 ± 6,366 ***Mecp2*$^{+/-}$:** 26,956 ± 6,963	vlPFC	WT vs *Mecp2*$^{+/-}$	Unpaired *t*- test $t_{(8)}$ = 1,85	p = 0,102
		WT: 65,357 ± 10,420 ***Mecp2*$^{+/-}$:** 39,528 ± 11,384	vmPFC	WT vs *Mecp2*$^{+/-}$	Unpaired *t*- test $t_{(8)}$ = 3,251	p = 0,012
Fig. 13C	Mean VIP intensity	**MeCP2 null:** 312,605 ± 16,262 **MeCP2+:** 377,332 ± 36,130	dmPFC	MeCP2 null vs MeCP2+ cell	Unpaired *t*- test $t_{(5)}$ = 5,48	p = 0,0028
		MeCP2 null: 311,968 ± 13,203 **MeCP2+:** 385,552 ± 31,764	vlPFC	MeCP2 null vs MeCP2+ cell	Unpaired *t*- test $t_{(5)}$ = 5,87	p = 0,002
		MeCP2 null: 308,893 ± 20,126 **MeCP2+:** 86,655 ± 41,493	vmPFC	MeCP2 null vs MeCP2+ cell	Unpaired *t*- test $t_{(5)}$ = 5,31	p = 0,0032

[1]**:** (Mean ± SD)

In order to see the impact of loss of MeCP2 in VIP expression, we assessed the of mean VIP intensity of cells that had were negative for MeCP2 (MeCP2 null) and those that were positive (MeCP2+) in *Mecp2*$^{+/-}$ mice (**Figure 14D**). In all three PFC subregions, values of VIP intensity appear to be reduced in MeCP2 null cells as MeCP2+ cells exhibiting higher expression levels of VIP.

CHAPTER 5

DISCUSSION

DISCUSSION

Recent findings have unveiled MeCP2 diverse roles in brain functioning, with a strong association between the loss of this protein and cognitive deficits, including impairments in social processes (R. Z. Chen et al., 2001; McGraw et al., 2011; Nguyen et al., 2012). Evaluation of neuronal circuitry in 12-week-old male *Mecp2*$^{tm1.1Jae}$ mice have revealed a significant reduction of excitatory inputs into PN of the PFC which suggest that synaptic pathophysiology in the RTT mice model were derived by a glutamatergic hypofunction (Wood et al., 2009; Sceniak et al., 2016). In the visual cortex of *Mecp2*$^{tm1.1Bird}$ male mice, the deletion of MeCP2 in specific IN subtypes has been shown to be able to recapitulate many of the effects of global MeCP2 deletion, namely by reducing pyramidal neurons responses (Ito-Ishida et al., 2015; Banerjee et al., 2016). However, little is known about how the differential expression patterns of MeCP2 seem in (mosaic) heterozygous females can affect the local circuitry of the PFC and contribute to the overall phenotype diversity. In that perspective, the objective of this study was to characterize IN populations in different sub-regions of the PFC using 12-week-old *Mecp2*$^{tm1.1Bird}$ female mice, in our perspective to better version of the well-established mouse model of RTT (Guy et al., 2007; Santos et al., 2010; Mykins, Bridges, et al., 2023).

Consistent with the well-known mosaic patterns of MeCP2 expression (Katz et al., 2012; Ribeiro & MacDonald, 2020; Mykins, Layo-Carris, et al., 2023), we have found different MeCP2 expression patterns among individual 12-week-old *Mecp2*$^{+/-}$ mice in the different PFC regions, namely dmPFC, vlPFC and vmPFC. Considering a recent investigation about two phenotypic trait variations in the *Mecp2*$^{+/-}$ female mouse model that suggest differentially impact neuronal circuitry (Mykins, Bridges, et al., 2023), we evaluated whether this heterogeneity in our experimental setup could impact on PV+ and VIP+ IN density. Hierarchical cluster analysis identified two different clusters of animals based on MeCP2+ cell abundance, and this different pattern of MeCP2 intensity showed a trend towards an inverse correlation with the number of VIP+ cells in the three PFC subregions (i.e., animals with lower numbers of MeCP2+ cells in these regions showed higher numbers of VIP+ cells in the same regions). The same trend was not observed for PV+ cell number.

Here, we evaluated the PV+ IN population across subregions of PFC by immunofluorescence in 12-week-old female, an earlier symptomatic stage in comparison of what is observed in *Mecp2*$^{tm1.1Jae}$ model. Our analysis of the cortical PV population revealed a tendency for a decrease in numbers of PV+ cells in *Mecp2*$^{+/-}$ mice when compared to female WT mice, with a more significant impact observed in the dmPFC. The dmPFC comprises MOs and ACA, and these regions are considered to act as an association cortex of sensory inputs

into motor regions that are specialized in generate organized motor outputs (Barthas & Kwan, 2017). These control is due to their intense afferent and efferent connections with striatum and thalamus (Reep et al., 1987). On that perspective, disruption of dmPFC network is suggest having a top-down dysregulation of conscious motor information processing .

From earlier symptomatic stages until the severe stage (16-30-week-old), was reported in heterozygous female of *Mecp2*$^{tm1.1Jae}$ model an atypical increase on PV expression of cortical PV+ IN. The differences in PV levels are suggest to underly the motor impairments symptoms given the negative correlation of high faction PV cells density in the motor cortex and latency to fall (Morello et al., 2018). Subsequential analysis of mean staining intensity of PV+ cells revealed, within cells that did express PV, a pattern of increased expression of this calcium binding protein in *Mecp2*$^{+/-}$ mice. Given that different levels of PV expression in cortical IN are recognized as a molecular hallmark of PV+ IN plasticity, which is indicative of motor learning, it has been hypothesized that higher PV expression is inversely correlated with motor performance (Donato et al., 2013). In the 12-week-old *Mecp2*$^{tm1.1Bird}$ female mice, an increased fraction of PV+ cells with higher levels of PV expression were observed in all PFC subdivisions, with a more pronounced increase in the dmPFC.

Selective PV+ IN deletion of *Lmo4*, an endogenous inhibitor of tyrosine phosphatase (PTP1B), in mice was able to induce ASD-like behavior and social interactions deficits due to PTP1B activity, which was correlated with an increased excitability of PV+ IN in ACA circuitry. Rescue of behavior was obtained by simultaneous ablation of PTP1B in *Lmo4*KO mice (Zhang et al., 2020). In 10-week-old of *Mecp2*$^{tm1.1Bird}$ mice model, pharmacological inhibition of PTP1B has suggested to disrupt symptomatic behavior both in males and females, by improving survival and improvement in rotating rod performance, respectively (Krishnan et al., 2015). These studies highlight the implications that PV+ IN dysfunction can impact on overall circuitry E/I balance and its associations to synaptic pathophysiology of RTT. Considering prior research on the role of PV cell function in mediating ASD-like behaviors, evaluation of membrane E/I within the dmPFC circuitry by immunoreactivity of vesicular glutamate transporter 1 (VGLUT1), a presynaptic marker for glutamatergic function and the vesicular GABA transporter (VGAT) could clarifying whether the overall hypofunction in PFC is a result of perisomatic over-inhibition through these fast-spiking neurons or mediated by other IN subtype.

In female *Mecp2*$^{tm1.1Jae}$ of 8-10-week-old, injection of a viral construct that selective activated PN from mPFC was able to increase neuronal activity and was associated with rescue of normal breathing patterns to WT levels (C. James Howell et al., 2017). In that perspective, identification of the main affected area within

the mPFC can clarify the primarily affected circuitry. Our analysis of vmPFC subdivisions (IL, mORB and PL) unveiled the most affected regions in terms of PV population and molecular plasticity. The increased PV intensity within PV+ cells in *Mecp2*$^{-/y}$ mice arises essentially from an increased expression of these protein in the cortical IN of IL cortex, and not of the mORB or PL. Taking a closer look at the main functional division of the vmPFC, the IL cortex has been more associated with regulations of autonomic functions, controlled by the autonomic nervous system, namely breathing, heart rate and digestion (Vertes, 2004). These results align with known features RTT in patients, also observed in *Mecp2*$^{-/y}$ mice, particularly the notable presence of breathing disturbances, such as hyperventilation, apnea, and increased variability in breath frequency, already described in this model (A. P. L. Abdala et al., 2010; A. P. Abdala et al., 2014).

Besides the abnormal phenotype observed in PV+ IN cells in this mouse model, alterations in VIP+ cells were observed in this early stage of the disease (12-week-old), especially in the dmPFC and vmPFC. The VIP+ IN have a high degree of MeCP2 expression (Mossner et al., 2020) and its considered that MeCP2 plays a significant role in the development pathway of these neurons (Chao et al., 2010). In our analysis, alterations in VIP+ cell density were observed among the three PFC subdivisions, as well as differences in the mean intensity of VIP staining in MeCP2 null cells, when compared with MeCP2+. Cells lacking MeCP2 expression exhibit a decreased level of VIP immunoreactivity, contrasting with MeCP2 expressing cells. In the *Mecp2*$^{-/y}$. In other studies, MeCP2+ cell density has been positively correlated with motor coordination capacity, namely with rotarod performance, where animals with lower number of MeCP2+ cells shown higher latency to fall from the rod (Villani et al., 2021). In this study, using the same animal model as used here, pharmacological administration of fluoxetine, a serotonin (5-HT) reuptake inhibitor, was able to rescue the levels of MeCP2+ cells in some brains regions that correlated with a better performance. This correlation was found only in the PFC and not in other brain regions such as the striatum and hippocampus. The inhibition of 5-HT has an impact on the uptake of serotonin and may be linked to a reduction in the activity of IN expressing 5-HT$_{3a}$R, primarily those that include VIP+ IN.

Differences in cortical activity have a direct influence on task performance and sensory information integration. Such process are determined by the firing rates state of PN during behavioral state transitions (Vinck et al., 2015; Tang & Higley, 2020). The modulation of firing rates is known to be indirectly regulated by VIP+ IN via inhibition of others IN, such PV+ IN and SST+ IN, mediating the disinhibition of PN (Tremblay et al., 2016; Lim et al., 2018; Llorca & Deogracias, 2022). In mice, deletion of *Mecp2* gene specifically from VIP+ IN was shown to impact cortical function, namely by increasing cortical firing rates, which, in turn,

disrupted social behavior interactions, leading to a reduction in social interactions (Mossner et al., 2020). In our research, we have observed that MeCP2 had an influence in the distribution of VIP+ cells and the expression levels of VIP within individual cells, which may underlie the disruption of network organization in the PFC. Considering this potential disruption of VIP+ IN development or functioning, general hypoactivity of mPFC cortex in *Mecp*$^{2tm1.1Jae}$ null mice (Sceniak et al., 2016) may be due to impaired circuitry disinhibition of other IN subtype.

In summary, our data suggests that *Mecp2*$^{-/y}$ of 12-week-old mice, at an early symptomatic stage, have alterations in IN density within specific subdivisions of PFC. Loss of MeCP2 impair cell distribution of both PV+ and VIP+ cells in a class specific effect. Decrease of VIP+ cells and its impaired function is likely to induce a reduction of inhibitory inputs of VIP+ cell into PV+ IN, inputs that are necessary to maintain the correct and efficient firing latency. This reduction of excitatory inputs into PV+ IN may be underlying the pathophysiology of RTT by the impact on overall population activity. Compensational behavior due to reduce population cell number could explain the prevalence of cell fraction of high-PV expression in *Mecp2*$^{-/y}$, given that the lack of inhibitory stimulus induces a shorter latency firing rate that led to a higher expression of PV. An increase in neuronal activity will impact on the expression of the calcium binding protein, given its role in enabling an faster firing and repolarization (Caillard et al., 2000). By these means, loss of MeCP2 could be mediating an impairment on VIP+ and PV+ IN with PN. The VIP+ IN dysfunction could be underlying the contradictory PV+ IN gain of function.

These *Mecp2* class-specific effects on the cortical IN populations could be related with the differential maturation of the GABAergic network(Blaesse et al., 2009), which has been hypothesized to be mediated by deficits in K+/Cl- cotransporter 2 (KCC2) function during postnatal development (Kaila et al., 2014). Recent findings have revealed, within frontal brain regions, alterations in KCC2 levels in young mice that underlie seizure susceptibility as a result of neuronal and synaptic E/I imbalance (Gigliucci et al., 2021).

Collectively, the PFC IN cellular components found to be altered at symptomatic stages in females of the *Mecp2*$^{tm1.1.BIRD}$ mouse model correlate with abnormal behaviors, such as hindlimb clasping and regressive tactile hyposensitivity, which are typically observed in this model. These results suggest that cortical neurons may play a significant role in the neurophysiology of Rett Syndrome, which patients experience a motor cortex hyperexcitability potentially originating from an excessive inhibition of specific PFC networks.

CHAPTER 6

CONCLUSION

CONCLUSION

In conclusion, this study has delved into an initial characterization of *Mecp2*$^{-/y}$ mice at an early symptomatic stage, shedding light on the possible cortical IN alterations in this model. Our findings emphasize the significance of the cortical IN population in this RTT model, as it supports the possibility of E/I imbalance within the PFC subdivisions. This work underlines the role of each PFC area associated with core aspects of cognitive functions, ranging from working memory to visceral homeostasis regulation, and the impairments observed in patients with a RTT phenotype and in RTT models, namely those affecting sensory processing, preparatory motor activity, and breathing disturbances. Through a meticulous examination of the PFC, we have uncovered insights and implications of MeCP2 expression mosaics in the IN population, specifically PV+ and VIP+, one of the molecular markers that covers the majority of GABAergic IN heterogenous population.

The result reported here demonstrate that, at the symptomatic stage of the disease, *Mecp2*$^{-/y}$ exhibit significant prefrontal cortical alterations, namely:

- **Abnormal configuration of the PV+ cortical IN population**, specifically a reduction in number and conversely, enhanced expression levels of PV in those cells that do express this protein.
- **Altered patterns of co-expression of VIP and MeCP2**, characterized by a decrease of double-positive cells in the *Mecp2*$^{-/y}$ mice.
- **Disruption the pattern of VIP expression by loss of MeCP2**, with a reduction of VIP expression in MeCP2 null cells.

This study points to the differential impact that mosaic loss of MeCP2 has on cortical GABAergic IN subtypes and suggest that the dysregulation of these neuronal populations will impact on their assembly and synaptic connectivity with other inhibitory cells. Though the descriptive nature of this work does not allow us to determine the contribution of these changes to overall IN circuitry dysfunction, our results further support the important role of the GABAergic system in the pathogenesis of RTT and the class-specific impact of loss of MeCP2, at the cell level, in the prefrontal cortex circuitry.

Finally, the insights gained from this research contribute to the ongoing quest to wards comprehension of IN cortical development and its correlation with RTT clinical features. Assessing IN morphological and physiological dimensions throughout development should enable us to further understand the mechanisms behind cortical IN impairments and therapeutically target them in the future.

REFERENCES

REFERENCES

Abdala, A. P. L., Dutschmann, M., Bissonnette, J. M., & Paton, J. F. R. (2010). Correction of respiratory disorders in a mouse model of Rett syndrome. *Proceedings of the National Academy of Sciences of the United States of America*, *107*(42), 18208–18213. https://doi.org/10.1073/pnas.1012104107

Abdala, A. P., Lioy, D. T., Garg, S. K., Knopp, S. J., Paton, J. F. R., & Bissonnette, J. M. (2014). Effect of Sarizotan, a 5-HT1a and D2-Like Receptor Agonist, on Respiration in Three Mouse Models of Rett Syndrome. *American Journal of Respiratory Cell and Molecular Biology*, *50*(6), 1031–1039. https://doi.org/10.1165/rcmb.2013-0372OC

Adkins, N. L., & Georgel, P. T. (2011). MeCP2: Structure and function. *Biochemistry and Cell Biology = Biochimie Et Biologie Cellulaire*, *89*(1), 1–11. https://doi.org/10.1139/O10-112

Amir, R. E., Van Den Veyver, I. B., Schultz, R., Malicki, D. M., Tran, C. Q., Dahle, E. J., Philippi, A., Timar, L., Percy, A. K., Motil, K. J., Lichtarge, O., O'Brian Smith, E., Glaze, D. G., & Zoghbi, H. Y. (2000). Influence of mutation type and X chromosome inactivation on Rett syndrome phenotypes. *Annals of Neurology*, *47*(5), 670–679. https://doi.org/10.1002/1531-8249(200005)47:5<670::AID-ANA20>3.0.CO;2-F

Amir, R. E., Van den Veyver, I. B., Wan, M., Tran, C. Q., Francke, U., & Zoghbi, H. Y. (1999). Rett syndrome is caused by mutations in X-linked MECP2, encoding methyl-CpG-binding protein 2. *Nature Genetics*, *23*(2), 185–188. https://doi.org/10.1038/13810

Anderson, S. A., Eisenstat, D. D., Shi, L., & Rubenstein, J. L. R. (1997). Interneuron Migration from Basal Forebrain to Neocortex: Dependence on *Dlx* Genes. *Science*, *278*(5337), 474–476. https://doi.org/10.1126/science.278.5337.474

Anderson, S. A., Marín, O., Horn, C., Jennings, K., & Rubenstein, J. L. (2001). Distinct cortical migrations from the medial and lateral ganglionic eminences. *Development (Cambridge, England)*, *128*(3), 353–363. https://doi.org/10.1242/dev.128.3.353

Archer, H., Evans, J., Leonard, H., Colvin, L., Ravine, D., Christodoulou, J., Williamson, S., Charman, T., Bailey, M. E. S., Sampson, J., de Klerk, N., & Clarke, A. (2007). Correlation between clinical severity in patients with Rett syndrome with a p.R168X or p.T158M MECP2 mutation, and the direction and degree of skewing of X-chromosome inactivation. *Journal of Medical Genetics*, *44*(2), 148–152. https://doi.org/10.1136/jmg.2006.045260

Aronoff, R., Matyas, F., Mateo, C., Ciron, C., Schneider, B., & Petersen, C. C. H. (2010). Long-range connectivity of mouse primary somatosensory barrel cortex. *European Journal of Neuroscience*, *31*(12), 2221–2233. https://doi.org/10.1111/j.1460-9568.2010.07264.x

Ascoli, G. A., Alonso-Nanclares, L., Anderson, S. A., Barrionuevo, G., Benavides-Piccione, R., Burkhalter, A., Buzsáki, G., Cauli, B., DeFelipe, J., Fairén, A., Feldmeyer, D., Fishell, G., Fregnac, Y., Freund, T. F., Gardner, D., Gardner, E. P., Goldberg, J. H., Helmstaedter, M., Hestrin, S., ... The Petilla Interneuron Nomenclature Group (PING). (2008). Petilla terminology: Nomenclature of features of GABAergic interneurons of the cerebral cortex. *Nature Reviews Neuroscience*, *9*(7), Article 7. https://doi.org/10.1038/nrn2402

Augui, S., Nora, E. P., & Heard, E. (2011). Regulation of X-chromosome inactivation by the X-inactivation centre. *Nature Reviews Genetics*, *12*(6), 429–442. https://doi.org/10.1038/nrg2987

Banerjee, A., Rikhye, R. V., Breton-Provencher, V., Tang, X., Li, C., Li, K., Runyan, C. A., Fu, Z., Jaenisch, R., & Sur, M. (2016). Jointly reduced inhibition and excitation underlies circuit-wide changes in cortical processing in Rett syndrome. *Proceedings of the National Academy of Sciences*, *113*(46). https://doi.org/10.1073/pnas.1615330113

Bankhead, P., Loughrey, M. B., Fernández, J. A., Dombrowski, Y., McArt, D. G., Dunne, P. D., McQuaid, S., Gray, R. T., Murray, L. J., Coleman, H. G., James, J. A., Salto-Tellez, M., & Hamilton, P. W. (2017). QuPath: Open source software for digital pathology image analysis. *Scientific Reports*, *7*. https://doi.org/10.1038/s41598-017-17204-5

Barthas, F., & Kwan, A. C. (2017). Secondary Motor Cortex: Where 'Sensory' Meets 'Motor' in the Rodent Frontal Cortex. *Trends in Neurosciences*, *40*(3), 181–193. https://doi.org/10.1016/j.tins.2016.11.006

Beaulieu, C. (1993). Numerical data on neocortical neurons in adult rat, with special reference to the GABA population. *Brain Research*, *609*(1–2), 284–292. https://doi.org/10.1016/0006-8993(93)90884-p

Bebbington, A., Percy, A., Christodoulou, J., Ravine, D., Ho, G., Jacoby, P., Anderson, A., Pineda, M., Ben Zeev, B., Bahi-Buisson, N., Smeets, E., & Leonard, H. (2010). Updating the profile of C-terminal MECP2 deletions in Rett syndrome. *Journal of Medical Genetics*, *47*(4), 242–248. https://doi.org/10.1136/jmg.2009.072553

Beier, K. T., Steinberg, E. E., DeLoach, K. E., Xie, S., Miyamichi, K., Schwarz, L., Gao, X. J., Kremer, E. J., Malenka, R. C., & Luo, L. (2015). Circuit Architecture of VTA Dopamine Neurons Revealed by Systematic Input-Output Mapping. *Cell*, *162*(3), 622–634. https://doi.org/10.1016/j.cell.2015.07.015

Beierlein, M., Gibson, J. R., & Connors, B. W. (2003). Two Dynamically Distinct Inhibitory Networks in Layer 4 of the Neocortex. *Journal of Neurophysiology*, *90*(5), 2987–3000. https://doi.org/10.1152/jn.00283.2003

Bennett, B. D., & Bolam, J. P. (1993). Characterization of calretinin-immunoreactive structures in the striatum of the rat. *Brain Research*, *609*(1–2), 137–148. https://doi.org/10.1016/0006-8993(93)90866-l

Berger, B., Gaspar, P., & Verney, C. (1991). Dopaminergic innervation of the cerebral cortex: Unexpected differences between rodents and primates. *Trends in Neurosciences*, *14*(1), 21–27. https://doi.org/10.1016/0166-2236(91)90179-x

Björklund, A., Divac, I., & Lindvall, O. (1978). Regional distribution of catecholamines in monkey cerebral cortex, evidence for a dopaminergic innervation of the primate prefrontal cortex. *Neuroscience Letters*, *7*(2–3), 115–119. https://doi.org/10.1016/0304-3940(78)90153-2

Blaesse, P., Airaksinen, M. S., Rivera, C., & Kaila, K. (2009). Cation-chloride cotransporters and neuronal function. *Neuron*, *61*(6), 820–838. https://doi.org/10.1016/j.neuron.2009.03.003

Bolkan, S. S., Stujenske, J. M., Parnaudeau, S., Spellman, T. J., Rauffenbart, C., Abbas, A. I., Harris, A. Z., Gordon, J. A., & Kellendonk, C. (2017). Thalamic projections sustain prefrontal activity during working memory maintenance. *Nature Neuroscience*, *20*(7), 987–996. https://doi.org/10.1038/nn.4568

Bortone, D. S., Olsen, S. R., & Scanziani, M. (2014). Translaminar Inhibitory Cells Recruited by Layer 6 Corticothalamic Neurons Suppress Visual Cortex. *Neuron*, *82*(2), 474–485. https://doi.org/10.1016/j.neuron.2014.02.021

Bortz, D. M., Feistritzer, C. M., & Grace, A. A. (2023). Medial Prefrontal Cortex to Medial Septum Pathway Activation Improves Cognitive Flexibility in Rats. *The International Journal of Neuropsychopharmacology*, *26*(6), 426–437. https://doi.org/10.1093/ijnp/pyad019

Braunschweig, D., Simcox, T., Samaco, R. C., & LaSalle, J. M. (2004). X-Chromosome inactivation ratios affect wild-type MeCP2 expression within mosaic Rett syndrome and Mecp2-/+ mouse brain. *Human Molecular Genetics*, *13*(12), 1275–1286. https://doi.org/10.1093/hmg/ddh142

Briscoe, S. D., & Ragsdale, C. W. (2018). Homology, neocortex, and the evolution of developmental mechanisms. *Science (New York, N.Y.)*, *362*(6411), 190–193. https://doi.org/10.1126/science.aau3711

Brodman, K. (1909). Vergleichende Lokalisationslehre der Grosshirnrhinde. *(Reprinted as Brodmann's 'Localisation in the Cerebral Cortex,' Translated and Edited by L. J. Garey, London: Smith-Gordon, 1994)*. https://doi.org/10.1046/j.1469-7580.2000.196304931.x

Butt, S. J. B., Fuccillo, M., Nery, S., Noctor, S., Kriegstein, A., Corbin, J. G., & Fishell, G. (2005). The Temporal and Spatial Origins of Cortical Interneurons Predict Their Physiological Subtype. *Neuron*, *48*(4), 591–604. https://doi.org/10.1016/j.neuron.2005.09.034

Butt, S. J. B., Sousa, V. H., Fuccillo, M. V., Hjerling-Leffler, J., Miyoshi, G., Kimura, S., & Fishell, G. (2008). The Requirement of Nkx2-1 in the Temporal Specification of Cortical Interneuron Subtypes. *Neuron*, *59*(5), 722–732. https://doi.org/10.1016/j.neuron.2008.07.031

C. James Howell, Michael P. Sceniak, Min Lang, Wenceslas Krakowiecki, Fatimah E. Abouelsoud, Saloni U. Lad, Heping Yu, & David M. Katz. (2017). Activation of the Medial Prefrontal Cortex Reverses Cognitive and Respiratory Symptoms in a Mouse Model of Rett Syndrome. *Eneuro*, *4*(6), ENEURO.0277-17.2017. https://doi.org/10.1523/ENEURO.0277-17.2017

Caillard, O., Moreno, H., Schwaller, B., Llano, I., Celio, M. R., & Marty, A. (2000). Role of the calcium-binding protein parvalbumin in short-term synaptic plasticity. *Proceedings of the National Academy of Sciences of the United States of America*, *97*(24), 13372–13377. https://doi.org/10.1073/pnas.230362997

Caputi, A., Rozov, A., Blatow, M., & Monyer, H. (2009). Two Calretinin-Positive GABAergic Cell Types in Layer 2/3 of the Mouse Neocortex Provide Different Forms of Inhibition. *Cerebral Cortex*, *19*(6), 1345–1359. https://doi.org/10.1093/cercor/bhn175

Catapano, L. A., Magavi, S. S., & Macklis, J. D. (2008). Neuroanatomical tracing of neuronal projections with Fluoro-Gold. *Methods in Molecular Biology (Clifton, N.J.)*, *438*, 353–359. https://doi.org/10.1007/978-1-59745-133-8_27

Cauli, B., Audinat, E., Lambolez, B., Angulo, M. C., Ropert, N., Tsuzuki, K., Hestrin, S., & Rossier, J. (1997). Molecular and physiological diversity of cortical nonpyramidal cells. *The Journal of Neuroscience: The Official Journal of the Society for Neuroscience*, *17*(10), 3894–3906. https://doi.org/10.1523/JNEUROSCI.17-10-03894.1997

Chahrour, M., & Zoghbi, H. Y. (2007). The Story of Rett Syndrome: From Clinic to Neurobiology. *Neuron*, *56*(3), 422–437. https://doi.org/10.1016/j.neuron.2007.10.001

Chameau, P., & van Hooft, J. A. (2006). Serotonin 5-HT3 receptors in the central nervous system. *Cell and Tissue Research*, *326*(2), 573–581. https://doi.org/10.1007/s00441-006-0255-8

Chao, H.-T., Chen, H., Samaco, R. C., Xue, M., Chahrour, M., Yoo, J., Neul, J. L., Gong, S., Lu, H.-C., Heintz, N., Ekker, M., Rubenstein, J. L. R., Noebels, J. L., Rosenmund, C., & Zoghbi, H. Y. (2010). Dysfunction in GABA signalling mediates autism-like stereotypies and Rett syndrome phenotypes. *Nature*, *468*(7321), 263–269. https://doi.org/10.1038/nature09582

Chen, C.-F. F., Zou, D.-J., Altomare, C. G., Xu, L., Greer, C. A., & Firestein, S. J. (2014). Nonsensory target-dependent organization of piriform cortex. *Proceedings of the National Academy of Sciences of the United States of America*, *111*(47), 16931–16936. https://doi.org/10.1073/pnas.1411266111

Chen, R. Z., Akbarian, S., Tudor, M., & Jaenisch, R. (2001). Deficiency of methyl-CpG binding protein-2 in CNS neurons results in a Rett-like phenotype in mice. *Nature Genetics*, *27*(3), 327–331. https://doi.org/10.1038/85906

Chiaruttini, N., Burri, O., Haub, P., Guiet, R., Sordet-Dessimoz, J., & Seitz, A. (2022). An Open-Source Whole Slide Image Registration Workflow at Cellular Precision Using Fiji, QuPath and Elastix. *Frontiers in Computer Science*, *3*, 780026. https://doi.org/10.3389/fcomp.2021.780026

Cowan, R. L., Wilson, C. J., Emson, P. C., & Heizmann, C. W. (1990). Parvalbumin-containing GABAergic interneurons in the rat neostriatum. *The Journal of Comparative Neurology*, *302*(2), 197–205. https://doi.org/10.1002/cne.903020202

Cruikshank, S. J., Ahmed, O. J., Stevens, T. R., Patrick, S. L., Gonzalez, A. N., Elmaleh, M., & Connors, B. W. (2012). Thalamic control of layer 1 circuits in prefrontal cortex. *The Journal of Neuroscience: The Official Journal of the Society for Neuroscience*, *32*(49), 17813–17823. https://doi.org/10.1523/JNEUROSCI.3231-12.2012

Czéh, B., Vardya, I., Varga, Z., Febbraro, F., Csabai, D., Martis, L.-S., Højgaard, K., Henningsen, K., Bouzinova, E. V., Miseta, A., Jensen, K., & Wiborg, O. (2018). Long-Term Stress Disrupts the Structural and Functional Integrity of GABAergic Neuronal Networks in the Medial Prefrontal Cortex of Rats. *Frontiers in Cellular Neuroscience*, *12*. https://www.frontiersin.org/articles/10.3389/fncel.2018.00148

Dani, V. S., Chang, Q., Maffei, A., Turrigiano, G. G., Jaenisch, R., & Nelson, S. B. (2005). Reduced cortical activity due to a shift in the balance between excitation and inhibition in a mouse model of Rett Syndrome. *Proceedings of the National Academy of Sciences of the United States of America*, *102*(35), 12560–12565. https://doi.org/10.1073/pnas.0506071102

DeFelipe, J., López-Cruz, P. L., Benavides-Piccione, R., Bielza, C., Larrañaga, P., Anderson, S., Burkhalter, A., Cauli, B., Fairén, A., Feldmeyer, D., Fishell, G., Fitzpatrick, D., Freund, T. F., González-Burgos, G., Hestrin, S., Hill, S., Hof, P. R., Huang, J., Jones, E. G., … Ascoli, G. A. (2013). New insights into the classification and nomenclature of cortical GABAergic interneurons. *Nature Reviews Neuroscience*, *14*(3), 202–216. https://doi.org/10.1038/nrn3444

Dixsaut, L., & Gräff, J. (2021). The Medial Prefrontal Cortex and Fear Memory: Dynamics, Connectivity, and Engrams. *International Journal of Molecular Sciences*, *22*(22), 12113. https://doi.org/10.3390/ijms222212113

Donato, F., Rompani, S. B., & Caroni, P. (2013). Parvalbumin-expressing basket-cell network plasticity induced by experience regulates adult learning. *Nature*, *504*(7479), 272–276. https://doi.org/10.1038/nature12866

Ehrhart, F., Coort, S. L. M., Cirillo, E., Smeets, E., Evelo, C. T., & Curfs, L. M. G. (2016). Rett syndrome – biological pathways leading from MECP2 to disorder phenotypes. *Orphanet Journal of Rare Diseases*, *11*(1), 158. https://doi.org/10.1186/s13023-016-0545-5

Essen, D. C. V., & Glasser, M. F. (2018). Parcellating Cerebral Cortex: How Invasive Animal Studies Inform Noninvasive Mapmaking in Humans. *Neuron*, *99*(4), 640–663. https://doi.org/10.1016/j.neuron.2018.07.002

Ezeonwuka, C. D., & Rastegar, M. (2014). MeCP2-Related Diseases and Animal Models. *Diseases (Basel, Switzerland)*, *2*(1), 45–70. https://doi.org/10.3390/diseases2010045

Fang, X., Butler, K. M., Abidi, F., Gass, J., Beisang, A., Feyma, T., Ryther, R. C., Standridge, S., Heydemann, P., Jones, M., Haas, R., Lieberman, D. N., Marsh, E. D., Benke, T. A., Skinner, S., Neul, J. L., Percy, A. K., Friez, M. J., & Caylor, R. C. (2022). Analysis of X-inactivation status in a Rett syndrome natural history study cohort. *Molecular Genetics & Genomic Medicine*, *10*(5), e1917. https://doi.org/10.1002/mgg3.1917

Férézou, I., Cauli, B., Hill, E. L., Rossier, J., Hamel, E., & Lambolez, B. (2002). 5-HT3 receptors mediate serotonergic fast synaptic excitation of neocortical vasoactive intestinal peptide/cholecystokinin

interneurons. *The Journal of Neuroscience: The Official Journal of the Society for Neuroscience*, *22*(17), 7389–7397. https://doi.org/10.1523/JNEUROSCI.22-17-07389.2002

Flores Gutiérrez, J., Natali, G., Giorgi, J., De Leonibus, E., & Tongiorgi, E. (2022). Mirtazapine treatment in a young female mouse model of Rett syndrome identifies time windows for the rescue of early phenotypes. *Experimental Neurology*, *353*, 114056. https://doi.org/10.1016/j.expneurol.2022.114056

Friedman, N. P., & Robbins, T. W. (2022). The role of prefrontal cortex in cognitive control and executive function. *Neuropsychopharmacology*, *47*(1), 72–89. https://doi.org/10.1038/s41386-021-01132-0

Fukuda, T., Itoh, M., Ichikawa, T., Washiyama, K., & Goto, Y. (2005). Delayed Maturation of Neuronal Architecture and Synaptogenesis in Cerebral Cortex of *Mecp2* -Deficient Mice. *Journal of Neuropathology & Experimental Neurology*, *64*(6), 537–544. https://doi.org/10.1093/jnen/64.6.537

Gabbott, P. L. A., Warner, T. A., Jays, P. R. L., Salway, P., & Busby, S. J. (2005). Prefrontal cortex in the rat: Projections to subcortical autonomic, motor, and limbic centers. *The Journal of Comparative Neurology*, *492*(2), 145–177. https://doi.org/10.1002/cne.20738

Geiger, J. R. P., Lübke, J., Roth, A., Frotscher, M., & Jonas, P. (1997). Submillisecond AMPA Receptor-Mediated Signaling at a Principal Neuron–Interneuron Synapse. *Neuron*, *18*(6), 1009–1023. https://doi.org/10.1016/S0896-6273(00)80339-6

Gelman, D., Griveau, A., Dehorter, N., Teissier, A., Varela, C., Pla, R., Pierani, A., & Marín, O. (2011). A Wide Diversity of Cortical GABAergic Interneurons Derives from the Embryonic Preoptic Area. *The Journal of Neuroscience*, *31*(46), 16570–16580. https://doi.org/10.1523/JNEUROSCI.4068-11.2011

Gigliucci, V., Teutsch, J., Woodbury-Smith, M., Luoni, M., Busnelli, M., Chini, B., & Banerjee, A. (2021). *Region-specific KCC2 rescue by rhIGF-1 and oxytocin in a mouse model of Rett syndrome* (p. 2021.09.25.460342). bioRxiv. https://doi.org/10.1101/2021.09.25.460342

Good, K. V., Vincent, J. B., & Ausió, J. (2021). MeCP2: The Genetic Driver of Rett Syndrome Epigenetics. *Frontiers in Genetics*, *12*. https://www.frontiersin.org/articles/10.3389/fgene.2021.620859

Gozlan, H., El Mestikawy, S., Pichat, L., Glowinski, J., & Hamon, M. (1983). Identification of presynaptic serotonin autoreceptors using a new ligand: 3H-PAT. *Nature*, *305*(5930), 140–142. https://doi.org/10.1038/305140a0

Grosso, S., Brogna, A., Bazzotti, S., Renieri, A., Morgese, G., & Balestri, P. (2007). Seizures and electroencephalographic findings in CDKL5 mutations: Case report and review. *Brain and Development*, *29*(4), 239–242. https://doi.org/10.1016/j.braindev.2006.09.001

Guy, J., Gan, J., Selfridge, J., Cobb, S., & Bird, A. (2007). Reversal of neurological defects in a mouse model of Rett syndrome. *Science (New York, N.Y.)*, *315*(5815), 1143–1147. https://doi.org/10.1126/science.1138389

Guy, J., Hendrich, B., Holmes, M., Martin, J. E., & Bird, A. (2001). A mouse Mecp2-null mutation causes neurological symptoms that mimic Rett syndrome. *Nature Genetics*, *27*(3), 322–326. https://doi.org/10.1038/85899

Hagberg, B. (2005). Rett Syndrome: Long-Term Clinical Follow-Up Experiences Over Four Decades. *Journal of Child Neurology*, *20*(9), 722–727. https://doi.org/10.1177/08830738050200090401

Hagberg, B., Aicardi, J., Dias, K., & Ramos, O. (1983). A progressive syndrome of autism, dementia, ataxia, and loss of purposeful hand use in girls: Rett's syndrome: report of 35 cases. *Annals of Neurology*, *14*(4), 471–479. https://doi.org/10.1002/ana.410140412

Han, S., Tai, C., Jones, C. J., Scheuer, T., & Catterall, W. A. (2014). Enhancement of Inhibitory Neurotransmission by GABA A Receptors Having α 2,3 -Subunits Ameliorates Behavioral Deficits in a Mouse Model of Autism. *Neuron*, *81*(6), 1282–1289. https://doi.org/10.1016/j.neuron.2014.01.016

Harvey, P. D. (2019). Domains of cognition and their assessment. *Dialogues in Clinical Neuroscience*, *21*(3), 227–237. https://doi.org/10.31887/DCNS.2019.21.3/pharvey

Hilscher, M. M., Leão, R. N., Edwards, S. J., Leão, K. E., & Kullander, K. (2017). Chrna2-Martinotti Cells Synchronize Layer 5 Type A Pyramidal Cells via Rebound Excitation. *PLOS Biology*, *15*(2), e2001392. https://doi.org/10.1371/journal.pbio.2001392

Hioki, H., Okamoto, S., Konno, M., Kameda, H., Sohn, J., Kuramoto, E., Fujiyama, F., & Kaneko, T. (2013). Cell Type-Specific Inhibitory Inputs to Dendritic and Somatic Compartments of Parvalbumin-Expressing Neocortical Interneuron. *Journal of Neuroscience*, *33*(2), 544–555. https://doi.org/10.1523/JNEUROSCI.2255-12.2013

Hoffbuhr, K. C., Moses, L. M., Jerdonek, M. A., Naidu, S., & Hoffman, E. P. (2002). Associations between MECP2 mutations, x-chromosome inactivation, and phenotype. *Mental Retardation and Developmental Disabilities Research Reviews*, *8*(2), 99–105. https://doi.org/10.1002/mrdd.10026

Holmes, A., & Wellman, C. L. (2009). Stress-induced prefrontal reorganization and executive dysfunction in rodents. *Neuroscience and Biobehavioral Reviews*, *33*(6), 773–783. https://doi.org/10.1016/j.neubiorev.2008.11.005

Hoover, W. B., & Vertes, R. P. (2007). Anatomical analysis of afferent projections to the medial prefrontal cortex in the rat. *Brain Structure and Function*, *212*(2), 149–179. https://doi.org/10.1007/s00429-007-0150-4

Hu, H., Gan, J., & Jonas, P. (2014). Fast-spiking, parvalbumin⁺ GABAergic interneurons: From cellular design to microcircuit function. *Science*, *345*(6196), 1255263. https://doi.org/10.1126/science.1255263

Ip, J. P. K., Mellios, N., & Sur, M. (2018). Rett syndrome: Insights into genetic, molecular and circuit mechanisms. *Nature Reviews Neuroscience*, *19*(6), 368–382. https://doi.org/10.1038/s41583-018-0006-3

Ito-Ishida, A., Ure, K., Chen, H., Swann, J. W., & Zoghbi, H. Y. (2015). Loss of MeCP2 in Parvalbumin-and Somatostatin-Expressing Neurons in Mice Leads to Distinct Rett Syndrome-like Phenotypes. *Neuron*, *88*(4), 651–658. https://doi.org/10.1016/j.neuron.2015.10.029

Jones, P. L., Veenstra, G. J., Wade, P. A., Vermaak, D., Kass, S. U., Landsberger, N., Strouboulis, J., & Wolffe, A. P. (1998). Methylated DNA and MeCP2 recruit histone deacetylase to repress transcription. *Nature Genetics*, *19*(2), 187–191. https://doi.org/10.1038/561

Jung, K., Chang, M., Steinecke, A., Burke, B., Choi, Y., Oisi, Y., Fitzpatrick, D., Taniguchi, H., & Kwon, H.-B. (2023). An adaptive behavioral control motif mediated by cortical axo-axonic inhibition. *Nature Neuroscience*, *26*(8), Article 8. https://doi.org/10.1038/s41593-023-01380-x

Jung, M., & Pfeifer, G. P. (2013). CpG Islands. In S. Maloy & K. Hughes (Eds.), *Brenner's Encyclopedia of Genetics (Second Edition)* (pp. 205–207). Academic Press. https://doi.org/10.1016/B978-0-12-374984-0.00349-1

Kaila, K., Price, T. J., Payne, J. A., Puskarjov, M., & Voipio, J. (2014). Cation-chloride cotransporters in neuronal development, plasticity and disease. *Nature Reviews. Neuroscience*, *15*(10), 637–654. https://doi.org/10.1038/nrn3819

Kamigaki, T. (2019). Prefrontal circuit organization for executive control. *Neuroscience Research*, *140*, 23–36. https://doi.org/10.1016/j.neures.2018.08.017

Katz, D. M., Berger-Sweeney, J. E., Eubanks, J. H., Justice, M. J., Neul, J. L., Pozzo-Miller, L., Blue, M. E., Christian, D., Crawley, J. N., Giustetto, M., Guy, J., Howell, C. J., Kron, M., Nelson, S. B., Samaco, R. C., Schaevitz, L. R., St. Hillaire-Clarke, C., Young, J. L., Zoghbi, H. Y., & Mamounas, L. A. (2012). Preclinical research in Rett syndrome: Setting the foundation for translational success. *Disease Models & Mechanisms*, *5*(6), 733–745. https://doi.org/10.1242/dmm.011007

Kawaguchi, Y. (1993). Physiological, morphological, and histochemical characterization of three classes of interneurons in rat neostriatum. *The Journal of Neuroscience: The Official Journal of the Society for Neuroscience*, *13*(11), 4908–4923. https://doi.org/10.1523/JNEUROSCI.13-11-04908.1993

Kawaguchi, Y., & Kubota, Y. (1993). Correlation of physiological subgroupings of nonpyramidal cells with parvalbumin- and calbindinD28k-immunoreactive neurons in layer V of rat frontal cortex. *Journal of Neurophysiology*, *70*(1), 387–396. https://doi.org/10.1152/jn.1993.70.1.387

Kessaris, N., Magno, L., Rubin, A. N., & Oliveira, M. G. (2014). Genetic programs controlling cortical interneuron fate. *Current Opinion in Neurobiology*, *26*(100), 79–87. https://doi.org/10.1016/j.conb.2013.12.012

Kishi, N., & Macklis, J. D. (2004). MECP2 is progressively expressed in post-migratory neurons and is involved in neuronal maturation rather than cell fate decisions. *Molecular and Cellular Neuroscience*, *27*(3), 306–321. https://doi.org/10.1016/j.mcn.2004.07.006

Kishi, N., & Macklis, J. D. (2005). Dissecting MECP2 Function in the Central Nervous System. *Journal of Child Neurology*, *20*(9), 753–759. https://doi.org/10.1177/08830738050200091001

Kriener, B., Hu, H., & Vervaeke, K. (2022). Parvalbumin interneuron dendrites enhance gamma oscillations. *Cell Reports*, *39*(11), 110948. https://doi.org/10.1016/j.celrep.2022.110948

Krishnan, N., Krishnan, K., Connors, C. R., Choy, M. S., Page, R., Peti, W., Van Aelst, L., Shea, S. D., & Tonks, N. K. (2015). PTP1B inhibition suggests a therapeutic strategy for Rett syndrome. *The Journal of Clinical Investigation*, *125*(8), 3163–3177. https://doi.org/10.1172/JCI80323

Kvitsiani, D., Ranade, S., Hangya, B., Taniguchi, H., Huang, J. Z., & Kepecs, A. (2013). Distinct behavioural and network correlates of two interneuron types in prefrontal cortex. *Nature*, *498*(7454), 363–366. https://doi.org/10.1038/nature12176

Kyle, S. M., Vashi, N., & Justice, M. J. (2018). Rett syndrome: A neurological disorder with metabolic components. *Open Biology*, *8*(2), 170216. https://doi.org/10.1098/rsob.170216

Lau, B. Y. B., Layo, D. E., Emery, B., Everett, M., Kumar, A., Stevenson, P., Reynolds, K. G., Cherosky, A., Bowyer, S.-A. H., Roth, S., Fisher, D. G., McCord, R. P., & Krishnan, K. (2020). Lateralized Expression of Cortical Perineuronal Nets during Maternal Experience is Dependent on MECP2. *eNeuro*, *7*(3), ENEURO.0500-19.2020. https://doi.org/10.1523/ENEURO.0500-19.2020

Lavdas, A. A., Grigoriou, M., Pachnis, V., & Parnavelas, J. G. (1999). The Medial Ganglionic Eminence Gives Rise to a Population of Early Neurons in the Developing Cerebral Cortex. *The Journal of Neuroscience*, *19*(18), 7881–7888. https://doi.org/10.1523/JNEUROSCI.19-18-07881.1999

Le Merre, P., Ährlund-Richter, S., & Carlén, M. (2021). The mouse prefrontal cortex: Unity in diversity. *Neuron*, *109*(12), 1925–1944. https://doi.org/10.1016/j.neuron.2021.03.035

Lee, S., Hjerling-Leffler, J., Zagha, E., Fishell, G., & Rudy, B. (2010). The Largest Group of Superficial Neocortical GABAergic Interneurons Expresses Ionotropic Serotonin Receptors. *Journal of Neuroscience*, *30*(50), 16796–16808. https://doi.org/10.1523/JNEUROSCI.1869-10.2010

Leonard, C. M. (1969). The prefrontal cortex of the rat. I. cortical projection of the mediodorsal nucleus. II. efferent connections. *Brain Research*, *12*(2), 321–343. https://doi.org/10.1016/0006-8993(69)90003-1

Leonard, C. M. (2016). Finding prefrontal cortex in the rat. *Brain Research*, *1645*, 1–3. https://doi.org/10.1016/j.brainres.2016.02.002

Letinic, K., Zoncu, R., & Rakic, P. (2002). Origin of GABAergic neurons in the human neocortex. *Nature*, *417*(6889), 645–649. https://doi.org/10.1038/nature00779

Lewis, D. A., Volk, D. W., & Hashimoto, T. (2004). Selective alterations in prefrontal cortical GABA neurotransmission in schizophrenia: A novel target for the treatment of working memory dysfunction. *Psychopharmacology*, *174*(1), 143–150. https://doi.org/10.1007/s00213-003-1673-x

Lewis, J. D., Meehan, R. R., Henzel, W. J., Maurer-Fogy, I., Jeppesen, P., Klein, F., & Bird, A. (1992). Purification, sequence, and cellular localization of a novel chromosomal protein that binds to methylated DNA. *Cell*, *69*(6), 905–914. https://doi.org/10.1016/0092-8674(92)90610-o

Li, W. (2022). Excitation and Inhibition Imbalance in Rett Syndrome. *Frontiers in Neuroscience*, *16*, 825063. https://doi.org/10.3389/fnins.2022.825063

Liguz-Lecznar, M., Dobrzanski, G., & Kossut, M. (2022). Somatostatin and Somatostatin-Containing Interneurons—From Plasticity to Pathology. *Biomolecules*, *12*(2), 312. https://doi.org/10.3390/biom12020312

Lim, L., Mi, D., Llorca, A., & Marín, O. (2018). Development and Functional Diversification of Cortical Interneurons. *Neuron*, *100*(2), 294–313. https://doi.org/10.1016/j.neuron.2018.10.009

Liu, X., Bautista, J., Liu, E., & Zikopoulos, B. (2020). Imbalance of laminar-specific excitatory and inhibitory circuits of the orbitofrontal cortex in autism. *Molecular Autism*, *11*(1), 83. https://doi.org/10.1186/s13229-020-00390-x

Llorca, A., & Deogracias, R. (2022). Origin, Development, and Synaptogenesis of Cortical Interneurons. *Frontiers in Neuroscience*, *16*, 929469. https://doi.org/10.3389/fnins.2022.929469

Lodato, S., & Arlotta, P. (2015). Generating Neuronal Diversity in the Mammalian Cerebral Cortex. *Annual Review of Cell and Developmental Biology*, *31*, 699–720. https://doi.org/10.1146/annurev-cellbio-100814-125353

Lopes, F., Barbosa, M., Ameur, A., Soares, G., De Sá, J., Dias, A. I., Oliveira, G., Cabral, P., Temudo, T., Calado, E., Cruz, I. F., Vieira, J. P., Oliveira, R., Esteves, S., Sauer, S., Jonasson, I., Syvänen, A.-C., Gyllensten, U., Pinto, D., & Maciel, P. (2016). Identification of novel genetic causes of Rett syndrome- *like* phenotypes. *Journal of Medical Genetics*, *53*(3), 190–199. https://doi.org/10.1136/jmedgenet-2015-103568

Lui, J. H., Hansen, D. V., & Kriegstein, A. R. (2011). Development and Evolution of the Human Neocortex. *Cell*, *146*(1), 18–36. https://doi.org/10.1016/j.cell.2011.06.030

Ma, Y., Hu, H., Berrebi, A. S., Mathers, P. H., & Agmon, A. (2006). Distinct Subtypes of Somatostatin-Containing Neocortical Interneurons Revealed in Transgenic Mice. *The Journal of Neuroscience*, *26*(19), 5069–5082. https://doi.org/10.1523/JNEUROSCI.0661-06.2006

Manes, F., Sahakian, B., Clark, L., Rogers, R., Antoun, N., Aitken, M., & Robbins, T. (2002). Decision-making processes following damage to the prefrontal cortex. *Brain: A Journal of Neurology*, *125*(Pt 3), 624–639. https://doi.org/10.1093/brain/awf049

Marie Carlén. (2017). What constitutes the prefrontal cortex? *Science*, *482*(October), 478–482.

Marín, O. (2012). Interneuron dysfunction in psychiatric disorders. *Nature Reviews Neuroscience*, *13*(2), Article 2. https://doi.org/10.1038/nrn3155

Martínez de Paz, A., Khajavi, L., Martin, H., Claveria-Gimeno, R., Tom Dieck, S., Cheema, M. S., Sanchez-Mut, J. V., Moksa, M. M., Carles, A., Brodie, N. I., Sheikh, T. I., Freeman, M. E., Petrotchenko, E. V., Borchers, C. H., Schuman, E. M., Zytnicki, M., Velazquez-Campoy, A., Abian, O., Hirst, M., … Ausió, J.

(2019). MeCP2-E1 isoform is a dynamically expressed, weakly DNA-bound protein with different protein and DNA interactions compared to MeCP2-E2. *Epigenetics & Chromatin*, *12*(1), 63. https://doi.org/10.1186/s13072-019-0298-1

Matagne, V., Borloz, E., Ehinger, Y., Saidi, L., Villard, L., & Roux, J.-C. (2021). Severe offtarget effects following intravenous delivery of AAV9-MECP2 in a female mouse model of Rett syndrome. *Neurobiology of Disease*, *149*, 105235. https://doi.org/10.1016/j.nbd.2020.105235

Mátyás, F., Lee, J., Shin, H.-S., & Acsády, L. (2014). The fear circuit of the mouse forebrain: Connections between the mediodorsal thalamus, frontal cortices and basolateral amygdala. *The European Journal of Neuroscience*, *39*(11), 1810–1823. https://doi.org/10.1111/ejn.12610

May, D., Kponee-Shovein, K., Mahendran, M., Downes, N., Sheng, K., Lefebvre, P., & Cheng, W. Y. (2023). Epidemiology and patient journey of Rett syndrome in the United States: A real-world evidence study. *BMC Neurology*, *23*, 141. https://doi.org/10.1186/s12883-023-03181-y

McGraw, C. M., Samaco, R. C., & Zoghbi, H. Y. (2011). Adult neural function requires MeCP2. *Science (New York, N.Y.)*, *333*(6039), 186. https://doi.org/10.1126/science.1206593

Meehan, R. R., Lewis, J. D., & Bird, A. P. (1992). Characterization of MeCP2, a vertebrate DNA binding protein with affinity for methylated DNA. *Nucleic Acids Research*, *20*(19), 5085–5092.

Mencarelli, M. A., Spanhol-Rosseto, A., Artuso, R., Rondinella, D., Filippis, R. D., Bahi-Buisson, N., Nectoux, J., Rubinsztajn, R., Bienvenu, T., Moncla, A., Chabrol, B., Villard, L., Krumina, Z., Armstrong, J., Roche, A., Pineda, M., Gak, E., Mari, F., Ariani, F., & Renieri, A. (2010). Novel FOXG1 mutations associated with the congenital variant of Rett syndrome. *Journal of Medical Genetics*, *47*(1), 49–53. https://doi.org/10.1136/jmg.2009.067884

Miller, E. K., & Cohen, J. D. (2001). An Integrative Theory of Prefrontal Cortex Function. *Annual Review of Neuroscience*, *24*(1), 167–202. https://doi.org/10.1146/annurev.neuro.24.1.167

Molnár, Z., Clowry, G. J., Šestan, N., Alzu'bi, A., Bakken, T., Hevner, R. F., Hüppi, P. S., Kostović, I., Rakic, P., Anton, E. S., Edwards, D., Garcez, P., Hoerder-Suabedissen, A., & Kriegstein, A. (2019). New insights into the development of the human cerebral cortex. *Journal of Anatomy*, *235*(3), 432–451. https://doi.org/10.1111/joa.13055

Molyneaux, B. J., Arlotta, P., Menezes, J. R. L., & Macklis, J. D. (2007). Neuronal subtype specification in the cerebral cortex. *Nature Reviews Neuroscience*, *8*(6), Article 6. https://doi.org/10.1038/nrn2151

Morello, N., Schina, R., Pilotto, F., Phillips, M., Melani, R., Plicato, O., Pizzorusso, T., Pozzo-Miller, L., & Giustetto, M. (2018). Loss of *Mecp2* Causes Atypical Synaptic and Molecular Plasticity of Parvalbumin-Expressing Interneurons Reflecting Rett Syndrome–Like Sensorimotor Defects. *Eneuro*, *5*(5), ENEURO.0086-18.2018. https://doi.org/10.1523/ENEURO.0086-18.2018

Mori, K., Manabe, H., Narikiyo, K., & Onisawa, N. (2013). Olfactory consciousness and gamma oscillation couplings across the olfactory bulb, olfactory cortex, and orbitofrontal cortex. *Frontiers in Psychology*, *4*, 743. https://doi.org/10.3389/fpsyg.2013.00743

Mossner, J. M., Batista-Brito, R., Pant, R., & Cardin, J. A. (2020). Developmental loss of MeCP2 from VIP interneurons impairs cortical function and behavior. *eLife*, *9*, e55639. https://doi.org/10.7554/eLife.55639

Mountcastle, V. (1997). The columnar organization of the neocortex. *Brain*, *120*(4), 701–722. https://doi.org/10.1093/brain/120.4.701

Muñoz, W., Tremblay, R., Levenstein, D., & Rudy, B. (2017). Layer-specific modulation of neocortical dendritic inhibition during active wakefulness. *Science (New York, N.Y.)*, *355*(6328), 954–959. https://doi.org/10.1126/science.aag2599

Mykins, M., Bridges, B., Jo, A., & Krishnan, K. (2023). *Multidimensional analysis of a social behavior identifies regression and phenotypic heterogeneity in a female mouse model for Rett syndrom*. https://doi.org/10.1101/2023.06.05.543804

Mykins, M., Layo-Carris, D., Dunn, L. R., Skinner, D. W., McBryar, A. H., Perez, S., Shultz, T. R., Willems, A., Lau, B. Y. B., Hong, T., & Krishnan, K. (2023). Wild-type MECP2 expression coincides with age-dependent sensory phenotypes in a female mouse model for Rett syndrome. *Journal of Neuroscience Research*, *101*(8), 1236–1258. https://doi.org/10.1002/jnr.25190

Nan, X., Campoy, F. J., & Bird, A. (1997). MeCP2 Is a Transcriptional Repressor with Abundant Binding Sites in Genomic Chromatin. *Cell*, *88*(4), 471–481. https://doi.org/10.1016/S0092-8674(00)81887-5

Navawongse, R., & Eichenbaum, H. (2013). Distinct Pathways for Rule-Based Retrieval and Spatial Mapping of Memory Representations in Hippocampal Neurons. *The Journal of Neuroscience*, *33*(3), 1002–1013. https://doi.org/10.1523/JNEUROSCI.3891-12.2013

Nery, S., Fishell, G., & Corbin, J. G. (2002). The caudal ganglionic eminence is a source of distinct cortical and subcortical cell populations. *Nature Neuroscience*, *5*(12), 1279–1287. https://doi.org/10.1038/nn971

Neul, J. L., Kaufmann, W. E., Glaze, D. G., Christodoulou, J., Clarke, A. J., Bahi-Buisson, N., Leonard, H., Bailey, M. E. S., Schanen, N. C., Zappella, M., Renieri, A., Huppke, P., Percy, A. K., & RettSearch Consortium. (2010). Rett syndrome: Revised diagnostic criteria and nomenclature. *Annals of Neurology*, *68*(6), 944–950. https://doi.org/10.1002/ana.22124

Nguyen, M. V. C., Du, F., Felice, C. A., Shan, X., Nigam, A., Mandel, G., Robinson, J. K., & Ballas, N. (2012). MeCP2 Is Critical for Maintaining Mature Neuronal Networks and Global Brain Anatomy during Late Stages of Postnatal Brain Development and in the Mature Adult Brain. *Journal of Neuroscience*, *32*(29), 10021–10034. https://doi.org/10.1523/JNEUROSCI.1316-12.2012

Nigro, M. J., Hashikawa-Yamasaki, Y., & Rudy, B. (2018). Diversity and Connectivity of Layer 5 Somatostatin-Expressing Interneurons in the Mouse Barrel Cortex. *The Journal of Neuroscience*, *38*(7), 1622–1633. https://doi.org/10.1523/JNEUROSCI.2415-17.2017

Ongur, D. (2000). The Organization of Networks within the Orbital and Medial Prefrontal Cortex of Rats, Monkeys and Humans. *Cerebral Cortex*, *10*(3), 206–219. https://doi.org/10.1093/cercor/10.3.206

Parent, M. A., Wang, L., Su, J., Netoff, T., & Yuan, L.-L. (2010). Identification of the Hippocampal Input to Medial Prefrontal Cortex In Vitro. *Cerebral Cortex*, *20*(2), 393–403. https://doi.org/10.1093/cercor/bhp108

Paul, A., Crow, M., Raudales, R., He, M., Gillis, J., & Huang, Z. J. (2017). Transcriptional Architecture of Synaptic Communication Delineates GABAergic Neuron Identity. *Cell*, *171*(3), 522-539.e20. https://doi.org/10.1016/j.cell.2017.08.032

Petriti, U., Dudman, D. C., Scosyrev, E., & Lopez-Leon, S. (2023). Global prevalence of Rett syndrome: Systematic review and meta-analysis. *Systematic Reviews*, *12*(1), 5. https://doi.org/10.1186/s13643-023-02169-6

Phillips, M. L., Robinson, H. A., & Pozzo-Miller, L. (2019). Ventral hippocampal projections to the medial prefrontal cortex regulate social memory. *eLife*, *8*, e44182. https://doi.org/10.7554/eLife.44182

Pohlkamp, T., Dávid, C., Cauli, B., Gallopin, T., Bouché, E., Karagiannis, A., May, P., Herz, J., Frotscher, M., Staiger, J. F., & Bock, H. H. (2014). Characterization and Distribution of Reelin-Positive Interneuron Subtypes in the Rat Barrel Cortex. *Cerebral Cortex (New York, NY)*, *24*(11), 3046–3058. https://doi.org/10.1093/cercor/bht161

Porter, J. T., Cauli, B., Staiger, J. F., Lambolez, B., Rossier, J., & Audinat, E. (1998). Properties of bipolar VIPergic interneurons and their excitation by pyramidal neurons in the rat neocortex. *The European Journal of Neuroscience*, *10*(12), 3617–3628. https://doi.org/10.1046/j.1460-9568.1998.00367.x

Preuss, T. M. (1995). Do Rats Have Prefrontal Cortex? The Rose-Woolsey-Akert Program Reconsidered. *Journal of Cognitive Neuroscience*, *7*(1), 1–24. https://doi.org/10.1162/jocn.1995.7.1.1

Prönneke, A., Scheuer, B., Wagener, R. J., Möck, M., Witte, M., & Staiger, J. F. (2015). Characterizing VIP Neurons in the Barrel Cortex of VIPcre/tdTomato Mice Reveals Layer-Specific Differences. *Cerebral Cortex (New York, N.Y.: 1991)*, *25*(12), 4854–4868. https://doi.org/10.1093/cercor/bhv202

Rae, C. L., Hughes, L. E., Anderson, M. C., & Rowe, J. B. (2015). The Prefrontal Cortex Achieves Inhibitory Control by Facilitating Subcortical Motor Pathway Connectivity. *The Journal of Neuroscience*, *35*(2), 786–794. https://doi.org/10.1523/JNEUROSCI.3093-13.2015

Rakic, P. (2009). Evolution of the neocortex: A perspective from developmental biology. *Nature Reviews Neuroscience*, *10*(10), 724–735. https://doi.org/10.1038/nrn2719

Reep, R. L., Corwin, J. V., Hashimoto, A., & Watson, R. T. (1987). Efferent connections of the rostral portion of medial agranular cortex in rats. *Brain Research Bulletin*, *19*(2), 203–221. https://doi.org/10.1016/0361-9230(87)90086-4

Rett, A. (1966). [On a unusual brain atrophy syndrome in hyperammonemia in childhood]. *Wiener Medizinische Wochenschrift (1946)*, *116*(37), 723–726.

Ribeiro, M. C., & MacDonald, J. L. (2020). Sex differences in Mecp2-mutant Rett syndrome model mice and the impact of cellular mosaicism on phenotype development. *Brain Research*, *1729*, 146644. https://doi.org/10.1016/j.brainres.2019.146644

Rose, J. E., & Woolsey, C. N. (1948). The orbitofrontal cortex and its connections with the mediodorsal nucleus in rabbit, sheep and cat. *Research Publications - Association for Research in Nervous and Mental Disease*, *27 (1 vol.)*, 210–232.

Rossi, A. F., Pessoa, L., Desimone, R., & Ungerleider, L. G. (2009). The prefrontal cortex and the executive control of attention. *Experimental Brain Research*, *192*(3), 489–497. https://doi.org/10.1007/s00221-008-1642-z

Roze, E., Cochen, V., Sangla, S., Bienvenu, T., Roubergue, A., Leu-Semenescu, S., & Vidaihet, M. (2007). Rett syndrome: An overlooked diagnosis in women with stereotypic hand movements, psychomotor retardation, Parkinsonism, and dystonia? *Movement Disorders*, *22*(3), 387–389. https://doi.org/10.1002/mds.21276

Rozov, A., Jerecic, J., Sakmann, B., & Burnashev, N. (2001). AMPA Receptor Channels with Long-Lasting Desensitization in Bipolar Interneurons Contribute to Synaptic Depression in a Novel Feedback Circuit in Layer 2/3 of Rat Neocortex. *The Journal of Neuroscience*, *21*(20), 8062–8071. https://doi.org/10.1523/JNEUROSCI.21-20-08062.2001

Rubenstein, J. L. R., & Merzenich, M. M. (2003). Model of autism: Increased ratio of excitation/inhibition in key neural systems. *Genes, Brain, and Behavior*, *2*(5), 255–267. https://doi.org/10.1034/j.1601-183x.2003.00037.x

Rupert, D. D., Pagliaro, A., Choe, J., & Shea, S. D. (2023). Selective deletion of Methyl CpG binding protein 2 from parvalbumin interneurons in the auditory cortex delays the onset of maternal retrieval in mice. *bioRxiv*, 2023.01.30.526321. https://doi.org/10.1101/2023.01.30.526321

Rymar, V. V., & Sadikot, A. F. (2007). Laminar fate of cortical GABAergic interneurons is dependent on both birthdate and phenotype. *The Journal of Comparative Neurology*, *501*(3), 369–380. https://doi.org/10.1002/cne.21250

Samaco, R. C., McGraw, C. M., Ward, C. S., Sun, Y., Neul, J. L., & Zoghbi, H. Y. (2013). Female Mecp2(+/-) mice display robust behavioral deficits on two different genetic backgrounds providing a framework for pre-clinical studies. *Human Molecular Genetics*, *22*(1), 96–109. https://doi.org/10.1093/hmg/dds406

Santos, M., Summavielle, T., Teixeira-Castro, A., Silva-Fernandes, A., Duarte-Silva, S., Marques, F., Martins, L., Dierssen, M., Oliveira, P., Sousa, N., & Maciel, P. (2010). Monoamine deficits in the brain of methyl-CpG binding protein 2 null mice suggest the involvement of the cerebral cortex in early stages of Rett syndrome. *Neuroscience*, *170*(2), 453–467. https://doi.org/10.1016/j.neuroscience.2010.07.010

Santos, M., Temudo, T., Kay, T., Carrilho, I., Medeira, A., Cabral, H., Gomes, R., Lourencço, M. T., Venâncio, M., Calado, E., Moreira, A., Oliveira, G., & Maciel, P. (2009). Mutations in the *MECP2* Gene Are Not a Major Cause of Rett Syndrome-Like or Related Neurodevelopmental Phenotype in Male Patients. *Journal of Child Neurology*, *24*(1), 49–55. https://doi.org/10.1177/0883073808321043

Saunders, C. J., Minassian, B. E., Chow, E. W. C., Zhao, W., & Vincent, J. B. (2009). Novel exon 1 mutations in MECP2 implicate isoform MeCP2_e1 in classical Rett syndrome. *American Journal of Medical Genetics Part A*, *149A*(5), 1019–1023. https://doi.org/10.1002/ajmg.a.32776

Scala, F., Kobak, D., Shan, S., Bernaerts, Y., Laturnus, S., Cadwell, C. R., Hartmanis, L., Froudarakis, E., Castro, J. R., Tan, Z. H., Papadopoulos, S., Patel, S. S., Sandberg, R., Berens, P., Jiang, X., & Tolias, A. S. (2019). Layer 4 of mouse neocortex differs in cell types and circuit organization between sensory areas. *Nature Communications*, *10*(1), Article 1. https://doi.org/10.1038/s41467-019-12058-z

Sceniak, M. P., Lang, M., Enomoto, A. C., James Howell, C., Hermes, D. J., & Katz, D. M. (2016). Mechanisms of Functional Hypoconnectivity in the Medial Prefrontal Cortex of *Mecp2* Null Mice. *Cerebral Cortex*, *26*(5), 1938–1956. https://doi.org/10.1093/cercor/bhv002

Schindelin, J., Arganda-Carreras, I., Frise, E., Kaynig, V., Longair, M., Pietzsch, T., Preibisch, S., Rueden, C., Saalfeld, S., Schmid, B., Tinevez, J.-Y., White, D. J., Hartenstein, V., Eliceiri, K., Tomancak, P., & Cardona, A. (2012). Fiji—An Open Source platform for biological image analysis. *Nature Methods*, *9*(7), 10.1038/nmeth.2019. https://doi.org/10.1038/nmeth.2019

Schneider-Mizell, C. M., Bodor, A. L., Collman, F., Brittain, D., Bleckert, A., Dorkenwald, S., Turner, N. L., Macrina, T., Lee, K., Lu, R., Wu, J., Zhuang, J., Nandi, A., Hu, B., Buchanan, J., Takeno, M. M., Torres, R., Mahalingam, G., Bumbarger, D. J., … Costa, N. M. da. (2021). Structure and function of axo-axonic inhibition. *eLife*, *10*, e73783. https://doi.org/10.7554/eLife.73783

Schubert, D., Martens, G. J. M., & Kolk, S. M. (2015). Molecular underpinnings of prefrontal cortex development in rodents provide insights into the etiology of neurodevelopmental disorders. *Molecular Psychiatry*, *20*(7), 795–809. https://doi.org/10.1038/mp.2014.147

Selimbeyoglu, A., Kim, C. K., Inoue, M., Lee, S. Y., Hong, A. S. O., Kauvar, I., Ramakrishnan, C., Fenno, L. E., Davidson, T. J., Wright, M., & Deisseroth, K. (2017). Modulation of prefrontal cortex excitation/inhibition balance rescues social behavior in *CNTNAP2*-deficient mice. *Science Translational Medicine*, *9*(401), eaah6733. https://doi.org/10.1126/scitranslmed.aah6733

Silberberg, G., & Markram, H. (2007). Disynaptic inhibition between neocortical pyramidal cells mediated by Martinotti cells. *Neuron*, *53*(5), 735–746. https://doi.org/10.1016/j.neuron.2007.02.012

Sirianni, N., Naidu, S., Pereira, J., Pillotto, R. F., & Hoffman, E. P. (1998). Rett Syndrome: Confirmation of X-Linked Dominant Inheritance, and Localization of the Gene to Xq28. *The American Journal of Human Genetics*, *63*(5), 1552–1557. https://doi.org/10.1086/302105

Sohal, V. S., & Rubenstein, J. L. R. (2019). Excitation-inhibition balance as a framework for investigating mechanisms in neuropsychiatric disorders. *Molecular Psychiatry*, *24*(9), 1248–1257. https://doi.org/10.1038/s41380-019-0426-0

Somogyi, P., Freund, T. F., & Cowey, A. (1982). The axo-axonic interneuron in the cerebral cortex of the rat, cat and monkey. *Neuroscience*, *7*(11), 2577–2607. https://doi.org/10.1016/0306-4522(82)90086-0

Spiga, O., Gardini, S., Rossi, N., Cicaloni, V., Pettini, F., Niccolai, N., & Santucci, A. (2019). Structural investigation of Rett-inducing MeCP2 mutations. *Genes & Diseases*, *6*(1), 31–34. https://doi.org/10.1016/j.gendis.2018.09.005

Squire, L., Darwin, B., & Bloom, F. (2008). *Fundamental neuroscience* (3rd ed). Elsevier - Academic press.

Stoner, R., Chow, M. L., Boyle, M. P., Sunkin, S. M., Mouton, P. R., Roy, S., Wynshaw-Boris, A., Colamarino, S. A., Lein, E. S., & Courchesne, E. (2014). Patches of disorganization in the neocortex of children with autism. *The New England Journal of Medicine*, *370*(13), 1209–1219. https://doi.org/10.1056/NEJMoa1307491

Stuss, D. P., Cheema, M., Ng, M. K., Martinez De Paz, A., Williamson, B., Missiaen, K., Cosman, J. D., McPhee, D., Esteller, M., Hendzel, M., Delaney, K., & Ausio, J. (2013). Impaired in vivo binding of MeCP2 to chromatin in the absence of its DNA methyl-binding domain. *Nucleic Acids Research*, *41*(9), 4888–4900. https://doi.org/10.1093/nar/gkt213

Takagi, H., Mizuta, H., Matsuda, T., Inagaki, S., Tateishi, K., & Hamaoka, T. (1984). The occurrence of cholecystokinin-like immunoreactive neurons in the rat neostriatum: Light and electron microscopic analysis. *Brain Research*, *309*(2), 341–345. https://doi.org/10.1016/0006-8993(84)90601-2

Tang, L., & Higley, M. J. (2020). Layer 5 Circuits in V1 Differentially Control Visuomotor Behavior. *Neuron*, *105*(2), 346-354.e5. https://doi.org/10.1016/j.neuron.2019.10.014

Taniguchi, H., Lu, J., & Huang, Z. J. (2013). The Spatial and Temporal Origin of Chandelier Cells in Mouse Neocortex. *Science (New York, N.Y.)*, *339*(6115), 70–74. https://doi.org/10.1126/science.1227622

Theriault, E., & Landis, D. M. (1987). Morphology of striatal neurons containing VIP-like immunoreactivity. *The Journal of Comparative Neurology*, *256*(1), 1–13. https://doi.org/10.1002/cne.902560102

Tomassy, G. S., Morello, N., Calcagno, E., & Giustetto, M. (2014). Developmental abnormalities of cortical interneurons precede symptoms onset in a mouse model of Rett syndrome. *Journal of Neurochemistry*, *131*(1), 115–127. https://doi.org/10.1111/jnc.12803

Trappe, R., Laccone, F., Cobilanschi, J., Meins, M., Huppke, P., Hanefeld, F., & Engel, W. (2001). MECP2 mutations in sporadic cases of Rett syndrome are almost exclusively of paternal origin. *American Journal of Human Genetics*, *68*(5), 1093–1101. https://doi.org/10.1086/320109

Tremblay, R., Lee, S., & Rudy, B. (2016). GABAergic Interneurons in the Neocortex: From Cellular Properties to Circuits. *Neuron*, *91*(2), 260–292. https://doi.org/10.1016/j.neuron.2016.06.033

Tropea, D., Giacometti, E., Wilson, N. R., Beard, C., McCurry, C., Fu, D. D., Flannery, R., Jaenisch, R., & Sur, M. (2009). Partial reversal of Rett Syndrome-like symptoms in MeCP2 mutant mice. *Proceedings of the National Academy of Sciences of the United States of America*, *106*(6), 2029–2034. https://doi.org/10.1073/pnas.0812394106

Trutzer, I. M., García-Cabezas, M. Á., & Zikopoulos, B. (2019). Postnatal development and maturation of layer 1 in the lateral prefrontal cortex and its disruption in autism. *Acta Neuropathologica Communications*, *7*(1), 40. https://doi.org/10.1186/s40478-019-0684-8

Ueno, H., Suemitsu, S., Okamoto, M., Matsumoto, Y., & Ishihara, T. (2017). Sensory experience-dependent formation of perineuronal nets and expression of Cat-315 immunoreactive components in the mouse

somatosensory cortex. *Neuroscience*, *355*, 161–174. https://doi.org/10.1016/j.neuroscience.2017.04.041

Urbinati, C., Cosentino, L., Germinario, E. A. P., Valenti, D., Vigli, D., Ricceri, L., Laviola, G., Fiorentini, C., Vacca, R. A., Fabbri, A., & De Filippis, B. (2021). Treatment with the Bacterial Toxin CNF1 Selectively Rescues Cognitive and Brain Mitochondrial Deficits in a Female Mouse Model of Rett Syndrome Carrying a MeCP2-Null Mutation. *International Journal of Molecular Sciences*, *22*(13), 6739. https://doi.org/10.3390/ijms22136739

Urbinati, C., Lanzillotta, C., Cosentino, L., Valenti, D., Quattrini, M. C., Di Crescenzo, L., Prestia, F., Pietraforte, D., Perluigi, M., Di Domenico, F., Vacca, R. A., & De Filippis, B. (2023). Chronic treatment with the anti-diabetic drug metformin rescues impaired brain mitochondrial activity and selectively ameliorates defective cognitive flexibility in a female mouse model of Rett syndrome. *Neuropharmacology*, *224*, 109350. https://doi.org/10.1016/j.neuropharm.2022.109350

Van Eden, C. G., Lamme, V. a. F., & Uylings, H. B. M. (1992). Heterotopic Cortical Afferents to the Medial Prefrontal Cortex in the Rat. A Combined Retrograde and Anterograde Tracer Study. *The European Journal of Neuroscience*, *4*(1), 77–97. https://doi.org/10.1111/j.1460-9568.1992.tb00111.x

Vertes, R. P. (2004). Differential projections of the infralimbic and prelimbic cortex in the rat. *Synapse (New York, N.Y.)*, *51*(1), 32–58. https://doi.org/10.1002/syn.10279

Villani, C., Carli, M., Castaldo, A. M., Sacchetti, G., & Invernizzi, R. W. (2021). Fluoxetine increases brain MeCP2 immuno-positive cells in a female Mecp2 heterozygous mouse model of Rett syndrome through endogenous serotonin. *Scientific Reports*, *11*, 14690. https://doi.org/10.1038/s41598-021-94156-x

Vincent, S. R., Johansson, O., Hökfelt, T., Skirboll, L., Elde, R. P., Terenius, L., Kimmel, J., & Goldstein, M. (1983). NADPH-diaphorase: A selective histochemical marker for striatal neurons containing both somatostatin- and avian pancreatic polypeptide (APP)-like immunoreactivities. *The Journal of Comparative Neurology*, *217*(3), 252–263. https://doi.org/10.1002/cne.902170303

Vinck, M., Batista-Brito, R., Knoblich, U., & Cardin, J. A. (2015). Arousal and Locomotion Make Distinct Contributions to Cortical Activity Patterns and Visual Encoding. *Neuron*, *86*(3), 740–754. https://doi.org/10.1016/j.neuron.2015.03.028

Vuillet, J., Kerkerian, L., Salin, P., & Nieoullon, A. (1989). Ultrastructural features of NPY-containing neurons in the rat striatum. *Brain Research*, *477*(1–2), 241–251. https://doi.org/10.1016/0006-8993(89)91412-1

Wan, M., Lee, S. S. J., Zhang, X., Houwink-Manville, I., Song, H.-R., Amir, R. E., Budden, S., Naidu, S., Pereira, J. L. P., Lo, I. F. M., Zoghbi, H. Y., Schanen, N. C., & Francke, U. (1999). Rett Syndrome and Beyond: Recurrent Spontaneous and Familial MECP2 Mutations at CpG Hotspots. *The American Journal of Human Genetics*, *65*(6), 1520–1529. https://doi.org/10.1086/302690

Wang, Q., Ding, S.-L., Li, Y., Royall, J., Feng, D., Lesnar, P., Graddis, N., Naeemi, M., Facer, B., Ho, A., Dolbeare, T., Blanchard, B., Dee, N., Wakeman, W., Hirokawa, K. E., Szafer, A., Sunkin, S. M., Oh, S. W., Bernard, A., … Ng, L. (2020). The Allen Mouse Brain Common Coordinate Framework: A 3D Reference Atlas. *Cell*, *181*(4), 936-953.e20. https://doi.org/10.1016/j.cell.2020.04.007

Wichterle, H., Turnbull, D. H., Nery, S., Fishell, G., & Alvarez-Buylla, A. (2001). In utero fate mapping reveals distinct migratory pathways and fates of neurons born in the mammalian basal forebrain. *Development*, *128*(19), 3759–3771. https://doi.org/10.1242/dev.128.19.3759

Wilson, C. R. E., Gaffan, D., Browning, P. G. F., & Baxter, M. G. (2010). Functional localization within the prefrontal cortex: Missing the forest for the trees? *Trends in Neurosciences*, *33*(12), 533–540. https://doi.org/10.1016/j.tins.2010.08.001

Winkowski, D. E., Nagode, D. A., Donaldson, K. J., Yin, P., Shamma, S. A., Fritz, J. B., & Kanold, P. O. (2018). Orbitofrontal Cortex Neurons Respond to Sound and Activate Primary Auditory Cortex Neurons. *Cerebral Cortex (New York, NY)*, *28*(3), 868–879. https://doi.org/10.1093/cercor/bhw409

Wise, S. P. (2008). Forward Frontal Fields: Phylogeny and Fundamental Function. *Trends in Neurosciences*, *31*(12), 599–608. https://doi.org/10.1016/j.tins.2008.08.008

Wonders, C. P., & Anderson, S. A. (2006). The origin and specification of cortical interneurons. *Nature Reviews. Neuroscience*, *7*(9), 687–696. https://doi.org/10.1038/nrn1954

Wood, L., Gray, N. W., Zhou, Z., Greenberg, M. E., & Shepherd, G. M. G. (2009). Synaptic circuit abnormalities of motor-frontal layer 2/3 pyramidal neurons in an RNA interference model of methyl-CpG-binding protein 2 deficiency. *The Journal of Neuroscience: The Official Journal of the Society for Neuroscience*, *29*(40), 12440–12448. https://doi.org/10.1523/JNEUROSCI.3321-09.2009

Xu, Q., Guo, L., Moore, H., Waclaw, R. R., Campbell, K., & Anderson, S. A. (2010). Sonic hedgehog signaling confers ventral telencephalic progenitors with distinct cortical interneuron fates. *Neuron*, *65*(3), 328–340. https://doi.org/10.1016/j.neuron.2010.01.004

Yan, Z., & Rein, B. (2022). Mechanisms of Synaptic Transmission Dysregulation in the Prefrontal Cortex: Pathophysiological Implications. *Molecular Psychiatry*, *27*(1), 445–465. https://doi.org/10.1038/s41380-021-01092-3

Yang, S.-K., Parkington, H. C., Blake, A. D., Keating, D. J., & Chen, C. (2005). Somatostatin Increases Voltage-Gated K+ Currents in GH3 Cells through Activation of Multiple Somatostatin Receptors. *Endocrinology*, *146*(11), 4975–4984. https://doi.org/10.1210/en.2005-0696

Yizhar, O., Fenno, L. E., Prigge, M., Schneider, F., Davidson, T. J., O'Shea, D. J., Sohal, V. S., Goshen, I., Finkelstein, J., Paz, J. T., Stehfest, K., Fudim, R., Ramakrishnan, C., Huguenard, J. R., Hegemann, P., & Deisseroth, K. (2011). Neocortical excitation/inhibition balance in information processing and social dysfunction. *Nature*, *477*(7363), 171–178. https://doi.org/10.1038/nature10360

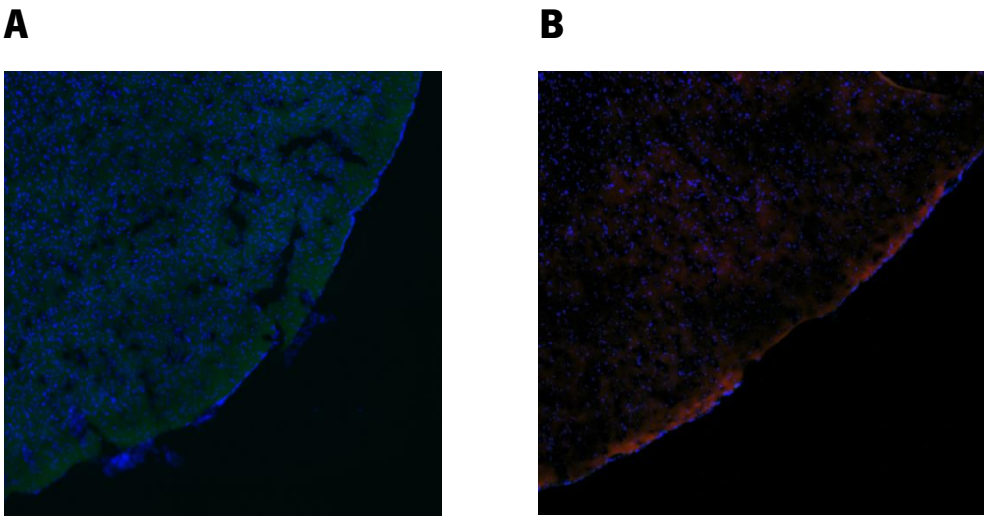
Zhang, L., Qin, Z., Ricke, K. M., Cruz, S. A., Stewart, A. F. R., & Chen, H.-H. (2020). Hyperactivated PTP1B phosphatase in parvalbumin neurons alters anterior cingulate inhibitory circuits and induces autism-like behaviors. *Nature Communications*, *11*(1), Article 1. https://doi.org/10.1038/s41467-020-14813-z

Zilberter, Y., Kaiser, K. M., & Sakmann, B. (1999). Dendritic GABA release depresses excitatory transmission between layer 2/3 pyramidal and bitufted neurons in rat neocortex. *Neuron*, *24*(4), 979–988. https://doi.org/10.1016/s0896-6273(00)81044-2

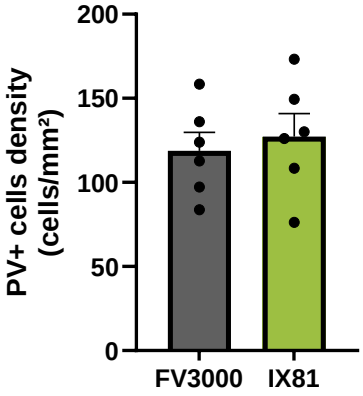
Zingg, B., Hintiryan, H., Gou, L., Song, M. Y., Bay, M., Bienkowski, M. S., Foster, N. N., Yamashita, S., Bowman, I., Toga, A. W., & Dong, H.-W. (2014). Neural Networks of the Mouse Neocortex. *Cell*, *156*(5), 1096–1111. https://doi.org/10.1016/j.cell.2014.02.023

SUPPLEMENTARY INFORMATION

SUPPLEMENTARY INFORMATION



Supplementary Figure 1. Representative images of negative control of immunofluorescence validate the assay. (A) PV and **(B)** for MeCP2 and VIP immunoassay.



Supplementary Figure 2. Analysis of confocal microscopy images has comparable values of PV+ cells from photos obtained in bright field microscope. (A) Histograms showing quantitative analysis of PV+ cell density for animals analyzed in FV3000 microscope and IX81 microscope

```
import scipy.cluster.hierarchy as sch
import matplotlib.pyplot as plt
import numpy as np


# Sample data
dmPFC_HET = [-2.22, -0.32, 0.62, -0.90, 0.34, -0.86]
vlPFC_HET = [-1.95, 0.42, 0.98, -0.64, -0.43, -1.26]
vmPFC_HET = [-2.37, 0.11, 0.73, -0.51, -0.11, -0.99]

# Create variables for each column
HET_A = [dmPFC_HET[0], vlPFC_HET[0], vmPFC_HET[0]]
HET_B = [dmPFC_HET[1], vlPFC_HET[1], vmPFC_HET[1]]
HET_C = [dmPFC_HET[2], vlPFC_HET[2], vmPFC_HET[2]]
HET_D = [dmPFC_HET[3], vlPFC_HET[3], vmPFC_HET[3]]
HET_E = [dmPFC_HET[4], vlPFC_HET[4], vmPFC_HET[4]]
HET_F = [dmPFC_HET[5], vlPFC_HET[5], vmPFC_HET[5]]

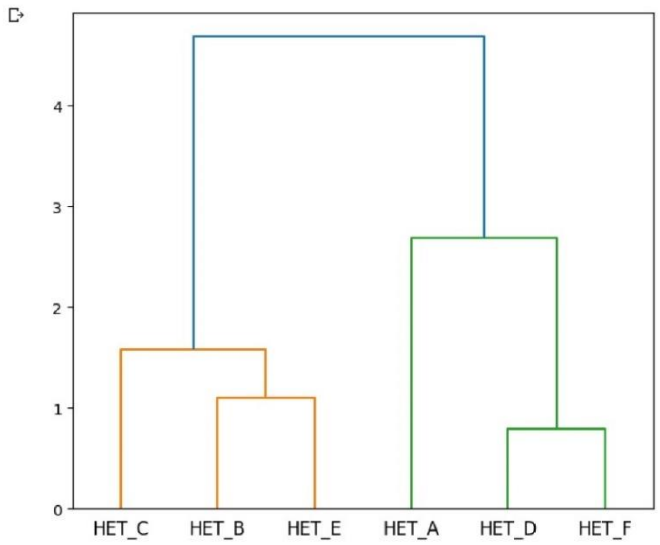
# Perform hierarchical clustering
linked = sch.linkage([HET_A, HET_B, HET_C, HET_D, HET_E, HET_F], method='ward')

# Create a figure and axis
fig, ax = plt.subplots(figsize=(7, 6))

# Plot the dendrogram
dendrogram = sch.dendrogram(linked, ax=ax, orientation='top',
                            labels=["HET_A", "HET_B", "HET_C", "HET_D",
                                    "HET_E", "HET_F"])
plt.show()
# Create a heatmap using imshow
heatmap_data = np.array([HET_A, HET_B, HET_C, HET_D, HET_E, HET_F])
ax.imshow(heatmap_data, cmap='viridis', aspect='auto')

# Set x-axis ticks and labels
new_ticks = ["HET_A", "HET_B", "HET_C", "HET_D", "HET_E", "HET_F"]
ax.set_xticks(np.arange(len(new_ticks)))
ax.set_xticklabels(new_ticks)

# Show the combined plot
plt.show()
```



Supplementary Figure 3. Hierarchical cluster output analysis based on z-score values of Mecp2 immunolabeled cells. Data Analysis with Python: A Jupyter Notebook.